Transient combustion control of internal combustion engines

Mathieu Hillion

ED n°431: ICMS - Information, Communication, Modélisation et Simulation

THESE

Pour obtenir le grade de
Docteur de l'Ecole des Mines de Paris
Spécialité "Mathématiques et Automatique"

présentée et soutenue publiquement par
Mathieu HILLION

le 3 décembre 2009

Contrôle de combustion en transitoires des moteurs à combustion interne

Directeur de Thèse: M. Nicolas PETIT

Jury

Président ..... Prof. Lars ERIKSSON
Rapporteur ..... Prof. Anna STEFANOPOULOU
Rapporteur ..... Prof. Olivier SENAME
Examinateur ..... M. Gilles CORDE
Examinateur ..... M. Jonathan CHAUVIN
Examinateur ..... Prof. Nicolas PETIT

PhD THESIS

To obtain
the Doctor's degree from l'Ecole des Mines de Paris
Speciality "Mathématiques et Automatique"

defended in public by
Mathieu HILLION

on December 3^{rd}, 2009

Transient combustion control of internal combustion engines

Thesis Advisor: M. Nicolas PETIT

Committee

Chair ..... Prof. Lars ERIKSSON
Referee ..... Prof. Anna STEFANOPOULOU
Referee ..... Prof. Olivier SENAME
Examiner ..... M. Gilles CORDE
Examiner ..... M. Jonathan CHAUVIN
Examiner ..... Prof. Nicolas PETIT

Mathieu HILLION

Centre Automatique et Systèmes, Unité Mathématiques et Systèmes, MINES ParisTech, 60 bd St Michel 75272 Paris Cedex 06, France.

IFP, 1&4 av. du Bois Préau, 92852 Rueil-Malmaison, France.

E-mail: mathieu.hillion@m4x.org

Key words. - Automotive engines, model-based control, sensitivity analysis, combustion control, combustion timing, flame propagation, cool flame, auto-ignition.
Mots clés. - Moteurs à combustion interne, commande à base de modèles, analyse de sensibilité, contrôle de combustion, propagation de flamme, flamme froide, auto-inflammation.

Friday 22nd January, 2010

Aux Miens.

Remerciements

Je voudrais en premier lieu remercier ici mes encadrants, Nicolas Petit, Jonathan Chauvin et Gilles Corde de m'avoir confié cette thèse il y a 3 ans.

Nicolas a su grâce à son écoute et ses conseils toujours précieux me guider tout au long de ces 3 années. Sa grande science est une source inépuisable.

Jonathan, dont je loue l'inébranlable passion dans notre travail, a su me pousser pendant les 3 ans de cette thèse. Je le remercie particulièrement pour sa confiance et sa constante disponibilité.

Gilles, pour avoir créé les conditions indispensables à la réalisation de ces travaux.

Je souhaite remercier les Professeurs Anna Stefanopoulou, Olivier Sename et Lars Eriksson de l'intérêt qu'ils ont porté à mon travail en acceptant de participer à mon jury.

Je remercie également Laurent Praly et Pierre Rouchon pour leurs conseils scientifiques.

Merci aux doctorants Thomas L, Emmanuel, Riccardo et Thomas C. qui m'ont épaulé durant ces années. J'avais plaisir à vous retrouver tous les jours.

Merci à tous les membres du groupe contrôle moteur de l'IFP et du CAS pour leur soutien, et pour les moments partagés à Rueil, aux Mines de Paris, à Cancùn, Seattle, Detroit ou ailleurs : Olivier, Guenaël, Philippe, Fabrice, Jérémie, Alexandre, Frédéric, Ghizlane, Hérald. Pierre-Jean, Eric, Erwan, Paul, Caroline, Florent.

Enfin, j'ai une pensée pour toute ma famille.

Transient combustion control of internal combustion engines

Formuler un problème est plus difficile
que d'en trouver la solution.
J.-Y. G.

Resume

Cette thèse traite le problème du contrôle de combustion des moteurs automobiles à combustion interne. On propose une méthode complétant les stratégies de contrôle existantes reposant sur des cartographies calibrées en régime stabilisé. Pendant les transitoires, cette méthode de contrôle utilise des variations de la variable rapide (moment d'allumage ou d'injection) pour compenser les déviations des conditions initiales des variables thermodynamiques dans les cylindres (variables lentes) par rapport à leurs valeurs optimales. Les corrections sont calculées grâce à une analyse de sensibilité d'un modèle de combustion. La stratégie de contrôle en résultant est utilisable en temps réel et, de manière intéressante, ne requiert ni capteur additionnel, ni phase de calibration supplémentaire. Plusieurs cas d'études sont exposés: un moteur essence, un moteur Diesel dilué dans un cadre d'injection monopulse puis multipulse. Des simulations ainsi que des résultats experimentaux obtenus sur banc moteurs et véhicules mettent en valeur l'interêt de la méthode proposée.

Abstract

This thesis addresses the problem of combustion control for automotive engines. A method is proposed to complement existing controllers, which use look-up tables based on steady-state operation. During transients, the new control method adjusts fast control variables (ignition or injection time) to compensate for deviations in the cylinder initial conditions from their optimal values due to the inherent slow processes involved. The necessary adjustments are determined from a sensitivity analysis of theoretical dynamic combustion models. The resulting open-loop controller is implementable in real time, and does not require any additional sensor or calibration. Several case studies are considered: spark ignition engines, and highly diluted diesel engines with mono-pulse and multi-pulse injection strategies. Simulations, test bench experiments and vehicle results stress the relevance of the approach.

Contents

Introduction: la combustion, un paradigme lent/rapide

Cette thèse traite le sujet du contrôle de combustion dans les moteurs à combustion interne pour automobiles. Le phénomène de combustion a lieu dans la chambre de combustion, entre la fermeture de la soupape d'admission et l'ouverture de la soupape d'échappement. Il dure entre 5 et 50 ms suivant le moteur. La combustion est directement responsable de la production de couple et des émissions de bruit et de polluants.

Ces dernières années, la prise de conscience écologique a poussé de nombreux pays à légiférer pour réduire la consommation et les émissions polluantes. L'industrie automobile est donc forcée de développer des moteurs plus efficaces et plus propres. En conséquence, les moteurs d'automobiles deviennent de plus en plus complexes. Par exemple, des systèmes de post-traitement permettent de nettoyer les gaz d'échappement de ses résidus de combustion indésirables. En parallèle, l'accent a été mis pour développer des modes de combustion plus propres et plus efficaces. Parmi les idées les plus significatives, on peut citer la réduction de la taille des moteurs, la suralimentation, la dilution de l'air admis par des gaz brûlés et les trains de soupapes à commande variable. Pour mettre en œuvre ces systèmes complexes, des systèmes de contrôle sophistiqués sont embarqués dans les véhicules. Ceux-ci s'occupent du contrôle des processus dominants: le remplissage des cylindres en air (boucle d'air), l'injection de carburant (boucle de fuel), et l'allumage du mélange (boucle d'allumage, uniquement sur moteur à allumage commandé). Les constantes de temps en présence vont de 1 s (boucle d'air), à 10 ms (boucles de carburant et d'allumage).

La combustion est un phénomène très largement étudié. Plusieurs aspects de la combustion peuvent être examinés en considérant la relation entre la position vilebrequin (mesurée en degré vilebrequin) et une sélection de propriétés mesurables. Le *phasage de la combustion* $\mathrm{CA_X}$, définie comme l'angle vilebrequin auquel $X\%$ du carburant a été brûlé par la combustion, est couramment utilisé. Très classiquement, trois phasages de combustion peuvent être considérés: un près du début de la combustion ($\mathrm{CA_{10}}$ ou $\mathrm{CA_{20}}$), un pour le milieu de la combustion ($\mathrm{CA_{50}}$), et un près de la fin ($\mathrm{CA_{90}}$). Ces trois indicateurs permettent de qualifier le déroulement de la combustion. Expérimentalement, on peut en

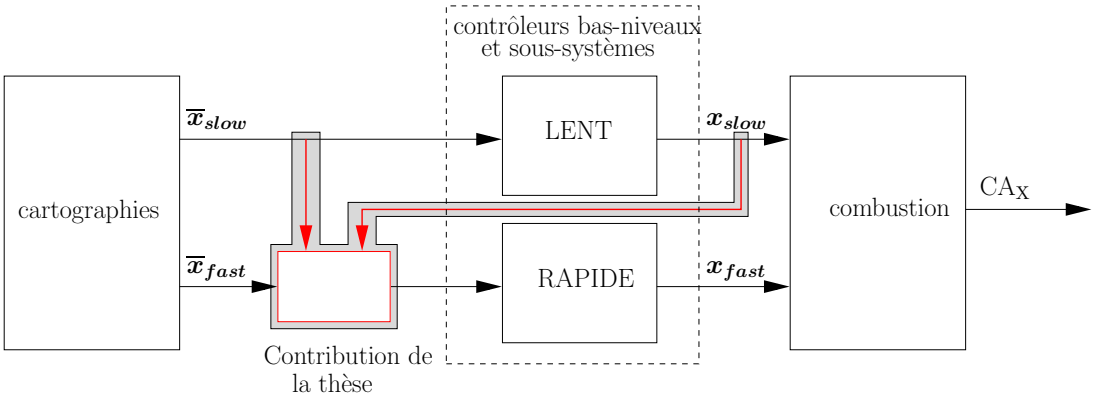

Figure 1: *La combustion est alimentée en parallèle par un système dynamique rapide et un système dynamique lent. Les différentes variables (de la boucle d'air, de carburant ou d'allumage) sont contrôlées en utilisant des cartographies statiques en supposant le fonctionnement en stabilisé.* $\boldsymbol{x}_{\boldsymbol{slow}}$*: variables lentes,* x_{fast}*: variables rapides,* $\overline{\boldsymbol{x}}_{\boldsymbol{slow}}$ *et* $\overline{x}_{fast}$*: les valeurs de stabilisé suivie par* $\boldsymbol{x}_{\boldsymbol{slow}}$ *et* x_{fast}*,* CA_X*: objectif de contrôle. Chaque variable a son régulateur bas-niveau assurant le suivi des valeurs de stabilisé. La méthode de contrôle proposée (en rouge) compense la lenteur des paramètres* $\boldsymbol{x}_{\boldsymbol{slow}}$ *en agissant sur les variables* x_{fast}*.*

effet prouver qu'ils sont très corrélés avec la production de couple, de polluants et de bruit. En conséquence, ces indicateurs doivent être contrôlés de manière optimale. C'est ce qu'on appelle *le contrôle de combustion.*

Le contrôle de combustion est classiquement réalisé de manière statique en boucle ouverte (en supposant que le moteur est en phase stabilisé) Des cartographies statiques sont en effet calibrées en stabilisé sur un banc moteur pour déterminer un compromis optimal entre les différents effets du positionnement des phasages de combustion CA_X (production de couple, de polluants et de bruit). En ne considérant que les phases stabilisées, on limite le temps de calibration, mais on néglige dangereusement les phases transitoires. Ces transitoires ne peuvent pas être vus comme une suite d'équilibres quasi-statiques. Malheureusement, les cycles de références (le cycle américain (FTP [66]) ou le cycle européen (NEDC [17])) ainsi que les conditions d'utilisation sur route engendrent des transitoires.

En phases transitoires, les phasages CA_X s'écartent de leurs valeurs optimales déterminées pour les phases stabilisées. Comme on va le voir maintenant, ceci peut être attribué à des différences dans les dynamiques des différents sous-systèmes composant le moteur.

La combustion dépend de nombreuses variables: *les conditions thermodynamiques dans la chambre* (pression (P_{cyl}), temperature (T_{cyl})), *la composition du mélange* (masse d'air (m_{air}), masse de fuel (M_f), et masse de gaz brûlés

(m_{bg})), et *le phasage de la combustion* (qui est contrôlé par l'injection de carburant dans les moteurs CI et par l'allumage dans les moteurs SI). Les deux premières catégories définissent *ce qui brûle*, pendant que la dernière définit *comment le mélange brûle*. Dans les structures de contrôle classiques, ces variables sont prises en compte de manière indépendante par des contrôleurs bas-niveaux. Cette séparation de traitement est motivée par sa simplicité, par sa facilité de calibration et de manière générale par le besoin naturel de découplage. Cependant, deux ensembles de variables devraient être considérés sur la base de leur réponse dynamique.

- Les variables lentes ($\boldsymbol{x_{slow}}$). Les masses de gaz et les températures sont gouvernées par des processus intrinsèquement lents comme la propagation des gaz (dans les tuyaux), les contraintes des actionneurs (comme celle des trains de soupapes variables) ou les échanges thermiques. Ces variables, parmi d'autres, ont une dynamique lente (avec un temps de réponse typique de 1 s) et ne peuvent pas être accélérées.

- Les variables rapides (x_{fast}). L'allumage et l'instant d'injection sont des variables sans dynamique. Elles peuvent être changées librement d'un cycle moteur à l'autre.

Dans ce manuscrit, la combustion est présentée comme la combinaison d'un processus lent et d'un processus rapide, ce à quoi on se réfèrera par la suite comme *paradigme lent/rapide*. Le schéma général qui en découle est présenté en Figure 1. Des contrôleurs indépendants garantissent que $\boldsymbol{x_{slow}}$ et x_{fast} suivent leurs valeurs de stabilisés $\overline{\boldsymbol{x}}_{\boldsymbol{slow}}$ et $\overline{x}_{fast}$, elles même stoquées dans des cartographies statiques. Cependant, comme ces variables ont des dynamiques différentes, elles deviennent incohérentes durant les transitoires. Les phasages de combustion $\{\mathrm{CA_X}\}_{0\leq X\leq 100}$ s'écartent alors très largement de leurs valeurs optimales à chaque transitoire.

Parmi tous les phasages de combustion possibles ($\{\mathrm{CA_X}\}_{0\leq X\leq 100}$), on en choisit un particulier. Pour des raisons de concision, on le notera également $\mathrm{CA_X}$ (qui est donc désormais un scalaire, par exemple $\mathrm{CA_{10}}$ ou $\mathrm{CA_{50}}$).

Il est intéressant de constater à ce stade que les écarts pendant le temps d'établissement du vecteur de paramètres lents $\boldsymbol{x_{slow}}$ peuvent être complètement compensés à l'aide de la variable scalaire x_{fast}. Plus précisément, comme la phase de calibration a mené à une combustion et donc des phasages de combustion optimaux (notés $\overline{\mathrm{CA}}_\mathrm{X}$), on propose de modifier la stratégie de régulation de la variable de rapide pour assurer que le phasage de combustion suit exactement sa valeur optimum même pendant les transitoires. Si le phasage de combustion choisi $\mathrm{CA_X}$ est égal à sa valeur optimale $\overline{\mathrm{CA}}_\mathrm{X}$, le phénomène global de combustion sera plus proche du comportement optimal. On revendique alors que grâce à cette stratégie de contrôle, la production de couple, et les émissions de polluants et de bruit en transitoire seront alors aussi près que possible de leurs valeurs optimales résultant du compromis initial en stabilisé.

Pour déterminer la nouvelle stratégie de régulation de la variable x_{fast} on utilise un modèle phénoménologique de la combustion. Ce modèle est composé d'une séquence de systèmes différentiels dont les instants de transition sont définis par des équations statiques sur l'état des systèmes. Les écarts des variables $\boldsymbol{x_{slow}}$ à leurs valeurs optimales sont représentés comme des offsets dans les conditions initiales, ce qui nous permet de formuler et de résoudre un problème d'atteinte d'une cible par compensation des valeurs initiales.

Ce type de contrôle basé sur un modèle complète directement l'approche classique par cartographie statique. De manière intéressante, cette approche *ne nécessite aucun capteur dans la chambre de combustion*, et ainsi correspond à une pré-compensation dynamique en boucle ouverte. La méthode de contrôle présentée ici se compose de calculs effectués hors ligne ainsi que de simples calculs en ligne utilisant les cartographies statiques déjà existantes et les équations du modèle de combustion. Aucune calibration supplémentaire est donc nécessaire.

Dans cette thèse, on traite le problème du contrôle de combustion à la fois pour les moteurs à allumage commandé et pour les moteurs à allumage par compression. Le manuscrit est organisé comme suit. Le chapitre 1 apporte le contexte général sur les moteurs ainsi que nos motivations pour considérer le problème de contrôle de combustion comme un paradigme lent/rapide. Les différentes architectures de contrôle ainsi que la dichotomie lent/rapide pour chaque moteur y sont également présentées. Dans le chapitre 2, on propose une stratégie de contrôle générale répondant au problème posé et la compare à l'état de l'art. Une formulation générale des modèles de combustion permet d'obtenir une stratégie de synthèse du contrôleur proposé. Finalement, les chapitres 3 et 4 donnent des cas d'étude sur les moteurs à allumage commandé et à allumage par compression respectivement. De nombreux résultats de simulation et expérimentaux sont discutés, soulignant ainsi la pertinence et le succès de la méthode proposée.

Introduction : combustion, a slow/fast paradigm

The subject of this thesis is controlling the combustion process in automotive internal combustion engines. This phenomenon takes place inside the combustion chamber, between the moments when the intake valve closes and the exhaust valve opens, and lasts from 5 ms to 50 ms, depending on the engine. Combustion is directly responsible for torque production, polluting emissions, and noise.

In recent decades, ecological concerns have prompted many countries to pass legislation aimed at reducing vehicle pollution and consumption. These developments have spurred the automotive industry to develop cleaner and more efficient engines. As a result, automotive engines have also become much more complex. For example, they incorporate after-treatment systems to clean up the exhaust, removing the undesired residuals of combustion. At the same time, a strong emphasis has been placed on developing cleaner and more efficient combustion modes. Some of the most innovative ideas in this sphere have involved downsizing, turbo-charging, charge diluting with exhaust gases, and variable valve actuation. To handle this complexity, sophisticated control systems are now embedded in the vehicles. These systems mostly take care of the dominant processes: feeding the cylinder with air (airpath), feeding the cylinder with fuel (fuelpath), and ignition (ignitionpath, only in spark ignited engines). The three dynamics under consideration have settling times ranging from 1 s (airpath) to 10 ms (fuelpath/ignitionpath).

Yet, the combustion dynamics itself has been largely overlooked. Several aspects of combustion can be profitably examined by considering the relationship between piston movement measured in crankangle degrees (CA) and a selection of measurable properties. The *combustion phasing* $\mathrm{CA_X}$, defined as the crankangle that results after consuming $X\%$ of the fuel in each cycle, is commonly used in this context. Classically, three combustion phasings are considered: one near the beginning of the combustion cycle ($\mathrm{CA_{10}}$, or $\mathrm{CA_{20}}$), one for the middle ($\mathrm{CA_{50}}$), and one near the end ($\mathrm{CA_{90}}$). The three indicators together provide an image of the combustion process. Experimentally, it can be shown that they are closely correlated with pollutant emissions, noise and torque production. For this reason, the values of $\mathrm{CA_X}$ must be optimally controlled. This topic is named *combustion*

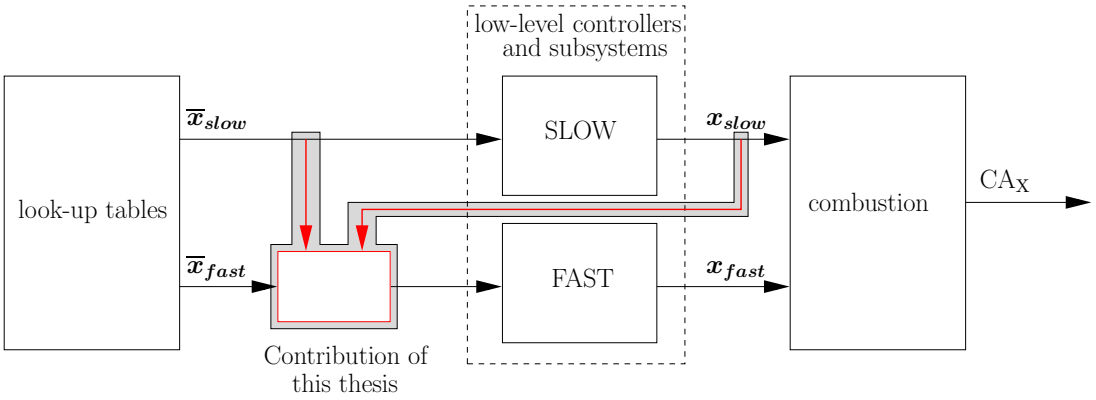

Figure 2: *Combustion as the output of parallel slow and fast dynamical systems. The control variables (airpath, fuelpath, ignitionpath) are fed by look-up tables assuming steady-state operation.* $\boldsymbol{x}_{\boldsymbol{slow}}$*: slow variables,* x_{fast}*: fast variables,* $\overline{\boldsymbol{x}}_{\boldsymbol{slow}}$ *and* $\overline{x}_{fast}$*: the tracked setpoints of* $\boldsymbol{x}_{\boldsymbol{slow}}$ *and* x_{fast}*,* CA_X*: control target. Each variable has an individual low-level controller. The proposed control methodology (red line) compensates for sluggishness in the* $\boldsymbol{x}_{\boldsymbol{slow}}$ *variables by acting on the* x_{fast} *variables.*

control.

Combustion control is usually achieved with a static, open-loop method (assuming steady-state operation). Accurate look-up tables are calculated for the steady-state using reference test benches in order to determine an optimal trade-off between the various effects of CA_X (torque production, pollutant emissions, noise). Addressing only steady-states limits the calibration effort, but the resulting look-up tables do not account for sharp transients. These transients cannot be represented as a quasi-static sequence of equilibria. Unfortunately, transients are frequently encountered in reference cycles (e.g. the American driving cycle (FTP, see [66]) or the New European Driving Cycle (NEDC, see [17])) and under real road conditions. When transients occur, the CA_X variables will systematically drift away from the optimal values determined for steady operation. As will now be shown, this effect can be attributed to differences in the settling times of the various subsystems constituting the engine.

Combustion is dependent on numerous variables: *thermodynamic conditions in the chamber* (pressure (P_{cyl}), temperature (T_{cyl})), *composition of the mixture* (air mass (m_{air}), fuel mass (M_f), and burned gases mass (m_{bg})), and *combustion phasing* (which is governed by fuel injection timing in CI engines and by a spark in SI engines). The first two categories define *what is burned*, while the last one determines *how it is burned*. In all classical engine control setups, these variables are managed by individual low-level controllers. This separation is motivated by the need for simplicity, ease of tuning, and a general preference for decoupling strategies. However, two separate sets of variables should be distinguished on the

basis of their dynamic response.

- Slow variables ($\boldsymbol{x_{slow}}$). Gas masses and temperatures are the result of inherently slow processes such as gas propagation (through pipes), actuator constraints (such as variable valve actuation), and thermal exchange. These variables, among others, have slow dynamics (with typical settling times of 1 s) and cannot be accelerated.

- Fast variables (x_{fast}). The ignition and injection times, for example, are variables that do not depend on macroscopic dynamics. They can be freely varied from one engine cycle to the next.

This research represents combustion as a combination of slow and fast processes, referred to hereafter as the *slow/fast paradigm*. The general scheme of the combustion process is shown in Figure 2. Independent controllers guarantee that both $\boldsymbol{x_{slow}}$ and x_{fast} track their desired steady-state values $\overline{\boldsymbol{x}}_{\boldsymbol{slow}}$ and $\overline{x}_{fast}$, which are stored in static look-up tables. Since the actual values become inconsistent during transients, however, the combustion phasings $\{\mathrm{CA_X}\}_{0\leq X\leq 100}$ acquire large deviations from their desired behavior whenever transients occur.

Among the possible combustion phasings ($\{\mathrm{CA_X}\}_{0\leq X\leq 100}$), we pick a single variable of particular interest. For brevity, we denote it $\mathrm{CA_X}$ (this is now a scalar, e.g. $\mathrm{CA_{10}}$ or $\mathrm{CA_{50}}$).

Interestingly, changes in the scalar variable x_{fast} can compensate for sluggishness and offsets during the settling time of the vector $\boldsymbol{x_{slow}}$. More precisely, since the calibrated look-up tables lead to optimum combustion and optimum values for the combustion phasings $\overline{\mathrm{CA_X}}$, we propose modifying the fast variable control strategy to ensure that the combustion phasing exactly tracks its optimum value during transients in spite of lag in the slow variables. If the chosen combustion phasing $\mathrm{CA_X}$ can be made equal to its optimum value $\overline{\mathrm{CA_X}}$, the whole combustion process will be closer to its optimum behavior during a transient. Indeed, we claim that under this control scheme torque production, pollution and noise will be as close as possible to their optimal trade-off values defined in the steady-state.

To determine which control actions should be performed on the x_{fast} variable, we use a phenomenological model of the combustion process. The model is a set of differential systems solved over variable time intervals implicitly defined by varying boundary conditions. Temporal tracking errors in the $\boldsymbol{x_{slow}}$ variables are represented as offsets in the initial conditions, allowing us to formulate and solve a target reaching problem.

This type of model-based control complements the static look-up tables. Interestingly, this approach *does not require any in-cylinder sensor*, and therefore corresponds to a dynamic open-loop control. The method presented here significantly improves the transient control of combustion through a combination of simple off-line computations and real-time on-line computations making use of the look-up tables that already exist. No additional calibration is required.

In this thesis, we address the combustion control problem for both Spark Ignited (SI) and Compression Ignition (CI) engines. The manuscript is organized as follows. In Chapter 1, we provide the necessary background on SI and CI engines along with our motivations for addressing combustion phasing control by means of the slow/fast paradigm. We also describe existing control architectures and sort the variables involved in combustion into slow and fast subsets. In Chapter 2, we propose a general control strategy and compare its principles against the state of the art. A general formulation of compression/combustion models is proposed and used to derive a general controller synthesis. Finally, Chapters 3, and 4 give case studies of SI and CI engines respectively. Numerous simulations and experimental results are discussed, stressing the success and relevance of this approach.

Notations and acronyms

Acronyms

BGR	Burned Gas Ratio
CA	Crankangle
CA_X	Crankangle at which X% of fuel mass is burnt
CAI	Controlled Auto-Ignition (engine)
CI	Compression Ignition (engine)
CO	Carbon Monoxide
ecf	End of Cool Flame
ECE	Urban driving cycle
EGR	Exhaust Gas Recirculation
EUDC	Extra-Urban Driving Cycle
FAR	Fuel to Air Ratio
FTP	Federal Test Procedure
HC	Unburned Hydrocarbons
HCCI	Homogeneous Charge Compression Ignition (engine)
HP EGR	High Pressure Exhaust Gas Recirculation
IC	Internal Combustion (engine)
IMEP	Indicated Mean Effective Pressure
ivc	Intake Valve Closure
KIM	Knock Integral Model
LP EGR	Low Pressure Exhaust Gas Recirculation
MFB	Mass Fraction of Burned fuel, ranges from 0 to 1
NADI	Narrow Angle Direct Injection
NEDC	New European Driving Cycle
NO_x	Nitrogen Oxides
ROHR	Rate Of Heat Released
SI	Spark Ignition (engine)
sit	Spark Ignition Timing
soc	Start Of Combustion
soi	Start Of Injection
TDC	Top Dead Center
VCR	Variable Compression Ratio

VVA	Variable Valve Actuation
VVT	Variable Valve Timing

Function regularity classes

C^0	continuous functions
C^1	continuously differentiable functions
$C^0 \cap C^1_{pc}$	continuous and piecewise continuously differentiable functions

General Notations

In the manuscript, *vectors are in bold lowercase* and *matrices in bold uppercase*. Scalars are either lower- or uppercase non-bold. A variable with an overline $\overline{x}$ is the reference variable corresponding to the variable x.

Symbol	Quantity	Unit
θ	Crankangle	°CA
θ_{TDC}	top dead center crankangle	°CA
$V(\theta)$	Cylinder volume	m^3
$P(\theta)$	Cylinder pressure	Pa
$T(\theta)$	Cylinder temperature	K
X	In-cylinder burned gas ratio (BGR)	-
T^w	Cylinder wall temperature	K
T^w_{ivc}	Cylinder wall temperature at *ivc*	K
V_{ivc}	In-cylinder volume at *ivc*	m^3
P_{ivc}	Cylinder pressure at *ivc*	Pa
T_{ivc}	Cylinder temperature at *ivc*	K
ϕ	Fuel/air ratio	-
ϕ_s	Stoichiometric fuel/air ratio	-
θ_{inj}	Injection crankangle	°CA
θ_{soc}	Start of combustion crankangle	°CA
γ	Ratio of specific heat	-
T_q	Torque	Nm
N_e	Engine speed	rpm
$\boldsymbol{x_{slow}}$	Slow variables	*
x_{fast}	Fast variable	*
x_{load}	Entry of the fast variable look-up table	*
$\boldsymbol{p_{ivc}}$	Airpath driven in-cylinder conditions at *ivc*	*
$\boldsymbol{p_{ivc}}$	In-cylinder conditions at *ivc*	*
$\mathcal{M}$	Formal model giving the CA_X	°CA
$\epsilon_{\mathcal{M}}$	Formal modeling error of the model $\mathcal{M}$	°CA

Symbol	Quantity	Unit
$\boldsymbol{\alpha}$	Proposed correction gain	*
h_c	Heat transfer coefficient	
Q_{LHV}	Fuel low heating value	J/kg
η_{vol}	Volumetric efficiency	-

Notations for the SI engine case study

Symb.	quantity	Unit
θ_{sit}	*sit* crankangle	°CA
V_{fl}^{min}	Minimal flame volume (initiation of the flame)	m^3
$T_u(\theta)$	Unburned zone temperature	K
M_{ivc}	In-cylinder total mass of gas at *ivc* (air & burned gas)	-
m_{air}	Aspirated air mass	kg
m_{air}^{est}	Estimated aspirated air mass	kg
M_f	Injected fuel mass	kg
x_f	MFB	-
ρ_u	Unburned zone density	kg/m^3
Y_u	Unburned zone fuel mass fraction	-
U	Laminar burning speed	m/s
U_0	Laminar burning speed at ambient conditions	m/s
W_t	Turbulent wrinkling	-
A	Piston head surface	m^2
S_{fl}	Flame surface area	m^2
S_{geo}	Geometric flame surface area (without wrinkling)	m^2
T_{amb}	Ambient temperature	°K
P_{amb}	Ambient pressure	Pa
α	Constant appearing in the laminar burning speed	-
β	Constant appearing in the laminar burning speed	-
V_u	Unburned zone volume	m^3
M_u	Mass of the gases in the unburned zone	kg
k	Density of turbulent kinetic energy	Js/kg
f_{wall}	Wall destruction term of the flame propagation	J
E_{kin}	Kinetic energy associated with the tumbling	J
δ_x	Characteristic function (1 if x is true, 0 otherwise)	-
$x_{\theta_{ivc}}$	Artificial state representing θ_{ivc}	°CA
$x_{M_{ivc}}$	Artificial state representing M_{ivc}	kg
x_{tumble}	Artificial state representing N_{ivc}^{tumble}	-
x_{M_f}	Artificial state representing M_f	kg
N^{tumble}	Tumble number	-

Symb.	quantity	Unit
N_{ivc}^{tumble}	Tumble number initial value	-
N_{emp}^{tumble}	Empirical look-up table of the tumble initial value	-

Notations for the CI engine case study

Symbol	Quantity	Unit
θ_{soc}	Start of combustion crankangle	°CA
θ_{ecf}	End of the cool flame crankangle	°CA
$\mathcal{A}^{ai}$	Integrand function of the auto-ignition model (KIM)	-
$\mathcal{A}^{cf}$	Integrand function of the cool flame model (KIM)	-
$p(\theta)$	In-cylinder thermodynamic parameters vector	*
P_{int}	Intake manifold pressure	Pa
T_{int}	Intake manifold temperature	°K
X_{int}	Intake manifold BGR	Pa
τ_{ai}	Artificial state for the evolution of the auto-ignition	-
τ_{cf}	Artificial state for the evolution of the cool flame	-
M_f	Total injected fuel mass	kg
M_f^{pilot}	Injected fuel mass during the pilot injection	kg
M_f^{main}	Injected fuel mass during the main injection	kg
M_f^{post}	Injected fuel mass during the post injection	kg

Chapter 1

A description of transient combustion control issues

There exists two main classes of automotive engines each of which generates torque by burning a blend of air, fuel, and exhaust gases. The first of these, the Compression Ignition (CI) engine, initiates combustion by compressing the gaseous fuel mixture. This class includes ordinary Diesel engines [23], Homogeneous Combustion Compression Ignition (HCCI) Diesel engines [68], and HCCI gasoline engines (also referred to as Controlled auto ignition (CAI)). The second type, the Spark Ignited (SI) engine, initiates combustion in the chamber with a correctly timed spark. This class comprises classic gasoline engines [23] and natural gas engines. Apart from these differences, both types of engines operate quite similarly and, consequently, require similar engine controls.

We now present these two classes of engines. We detail their various constituting subsystems (airpath, fuelpath, and ignition path for SI engines), along with their respective timescales and usual controllers. For each class, we sketch the usually observed transient behavior for CA_X variables, stress their flaws, and exhibit the slow/fast variables that play key roles in the in-cylinder combustion.

1.1 Background on SI engine

1.1.1 General engine structure

Internal combustion engines for which the combustion can be directly initiated by a spark are designated as SI engines. A pictorial view of the combustion chamber along with neighboring elements (the spark plug, the injector, the intake and exhaust valves, the intake and exhaust manifold, and the cylinder) is given in Figure 1.1. Details can be found in [23]. In the case of four strokes engines, the engine functioning timeline is the following:

1. Intake phase (cylinder filling): the intake valve opens and the fresh air enters the cylinder while the piston goes down. This phase lasts until the intake valve closes (this particular time is called *ivc*: intake valve closing). If available, Variable Valve Actuation (VVA) may modify the breathing of the engine (by impacting on the opening and closing of the intake and exhaust valves). This permits to re-aspirate some of the preceding combustion burned gases from the exhaust line. The fuel is injected during this phase.

2. Compression phase: the piston goes up and compresses the aspirated air, burned gases and fuel.

3. Combustion phase: the spark plug generates a spark that initiates the combustion of the blend of air/burned gases/fuel. A flame propagates in the chamber freeing the fuel chemical energy. The pressure increases and pushes back the piston.

4. Exhaust phase: once the piston has completed its descent, the exhaust valve opens. The exhaust gases are then flushed out of the cylinder towards the exhaust line.

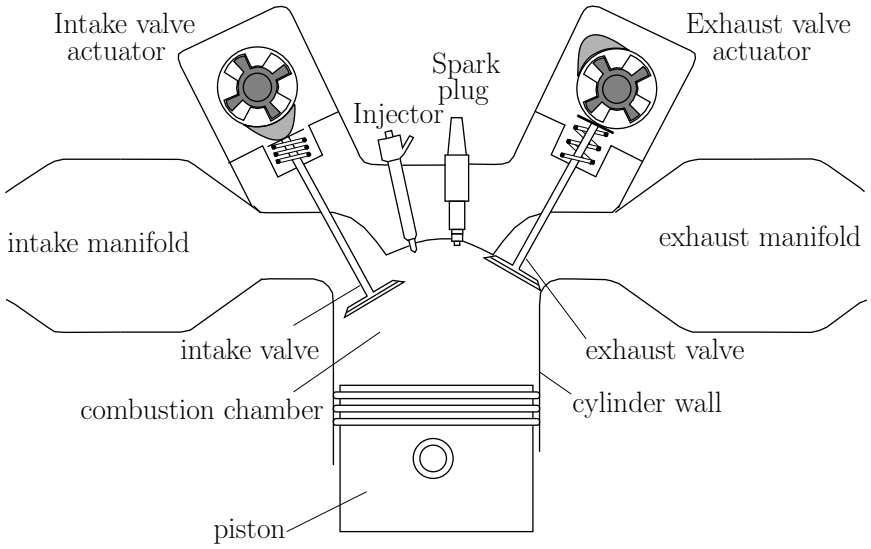

Figure 1.1: *View of the combustion chamber along with the surrounding devices.*

This timeline is pictured in Figure 1.2 where each phase is represented along with the actuators acting during them. In view of ecological concerns and to improve the engine performances, modern SI engines are equipped with turbocharger(s) and VVA. The turbocharger(s) permits to increase the engine power by increasing the pressure (and thus the aspirated air mass) in the cylinder. The VVA permits to change the intake and exhaust valves lift and their timing. In fact, VVA allows

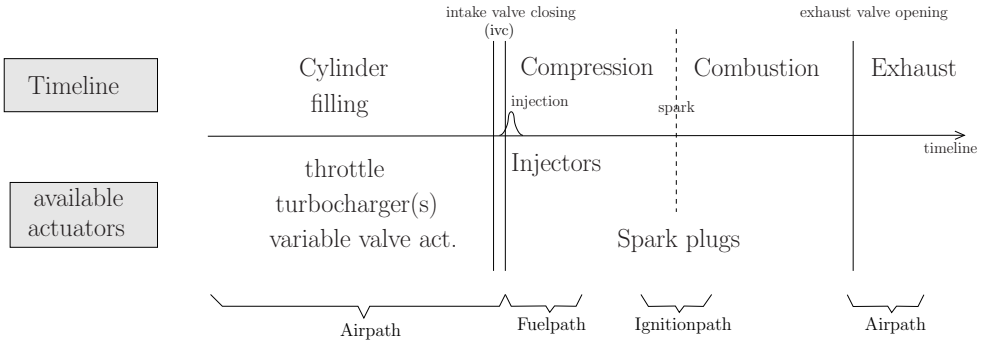

Figure 1.2: *SI engine functioning timeline. Each phase lasts 20 ms at 1500 rpm.*

exhaust gases from the preceding combustion to be re-aspirated into the cylinder and mixed with fresh air.

The general structure of a SI engine is given in Figure 1.3. It can be divided into three main subsystems. First, the *airpath* which consists of all the pipes, turbocharger(s), intake throttle, intake and exhaust manifolds, VVA systems and heat exchangers. The airpath feeds the cylinder providing appropriate thermodynamic and physical conditions. In fact, all the airpath devices act on the combustion by creating these conditions at the *ivc* moment (this moment is noted θ_{ivc}). After θ_{ivc}, the cylinder is isolated from the airpath until the exhaust phase.

Then, the *fuelpath*, which consists of the injection system, is used to inject the appropriate fuel mass into the cylinder at the appropriate time.

At last, the *ignitionpath* which consists of the spark plugs, provides a spark inside the cylinder to initiate the combustion.

After the *ivc*, the fuelpath and the ignitionpath are the only control variables to act on the combustion.

1.1.2 SI engine control

Over the years, numerous airpath controllers have been designed (see [37, 48, 62]). The task of such controller is to make the airpath feed the cylinder with the right thermodynamic properties at *ivc* with the right valve timings. Among these parameters, the air mass plays the most important role (see below the description of the fuelpath control). The main task of the airpath controller is thus to track the aspirated air mass setpoint. To this end, static maps of the values of the thermodynamic conditions at *ivc* (gathered in a vector of parameters noted $\boldsymbol{p_{ivc}}$) and of the variable valve actuator positions are used (and, among those, the *ivc* timing which plays a great role as will appear in the following). However, due to the inertia of the physical devices (hold-ups in pipes, turbochargers, variable valve actuators) and the natural saturations of the mechanical systems involved, the tracking of these setpoints cannot be rendered arbitrarily fast (the

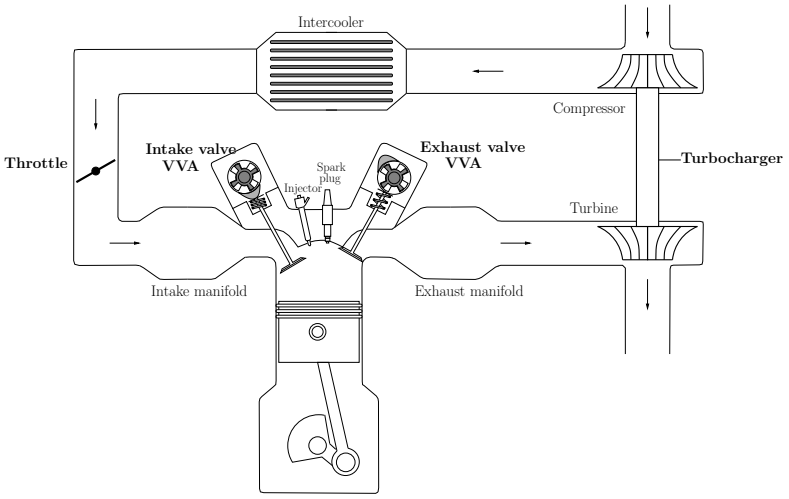

Figure 1.3: *Scheme of a general SI engine equipped with direct injection, VVA and a turbocharger.*

airpath bandwidth is approximately 1 Hz). Tracking errors may also happen due to airpath malfunctions such as natural device ageing. In fact, since the thermodynamic conditions are not a free set of variables (e.g. they are related by the ideal gas relation), it is not possible to control them independently. Thus, only a reduced set of parameters is actually controlled by the airpath controller (and thus mapped), and the other one can be computed using the static relation holding between them. In SI engines, the actually controlled variables usually include the air mass, the gas composition (BGR) and the VVA positions, while for instance, the burned gases mass can be inferred using the composition and the air mass. However, for sake of simplicity of the exposition, but without loss of generality, we consider in the following that all thermodynamic variables ($\boldsymbol{p_{ivc}}$) are controlled by the airpath.

The fuelpath controller regulates the fuel injection. To maximize the efficiency of exhaust gases after-treatment devices, the FAR (ϕ) has to be maintained as close as possible to the stoichiometric value (ϕ_s) (see [19, 65]). Accordingly, the injected fuel mass M_f is directly computed from the (estimated) value of the in-cylinder air mass m_{air}^{est} ($M_f = \phi_s m_{air}^{est}$). This estimate is usually provided by an air mass observer in the airpath controller. Feedback controllers using exhaust FAR sensors may also be considered. To maximize the mixture homogeneity, injection usually takes place during the intake phase. Fuel vaporization and mixing with air and burned gases are both completed before ignition. The injection timing has no major impact on the combustion phasing. This is the major difference between SI and CI engines. Its effect is in fact visible on pollutant formation (through the mixture homogeneity). The best control strategy results from a tradeoff. A too early injection causes the fuel to stick onto the piston head, while a too late injection reduces the available time for homogenization. We do not

want to modify this tradeoff. Consequently, controlling the injection timing in SI engines is left out of the scope of the thesis.

The torque production level does not exclusively depend on the amount of injected fuel and air mass. Spark timing, which initiates the combustion, plays a key role in the quality of the combustion (both in terms of efficiency and pollutant generation). A "global" criterion commonly used to evaluate the quality of the combustion is the middle of the combustion (CA_{50}) [15]. In fact, one considers that the engine is working at its maximal efficiency when the CA_{50} is reached at an optimal timing noted $\overline{CA}_{50}$. The role of the ignitionpath controller is thus to make the CA_{50} track the optimum value $\overline{CA}_{50}$, by adjusting the ignition time θ_{sit} according to look-up tables. Due to the overwhelming number of parameters influencing the combustion kinetics, they cannot all be used as inputs of these tables. A tradeoff is usually met by using the engine speed N_e and the drivers torque demand as entries[1]. The parameters that are not taken into account, such as the temperature of the in-cylinder gases or the BGR, are assumed to be close to their steady-state value corresponding to the tracked operating point.

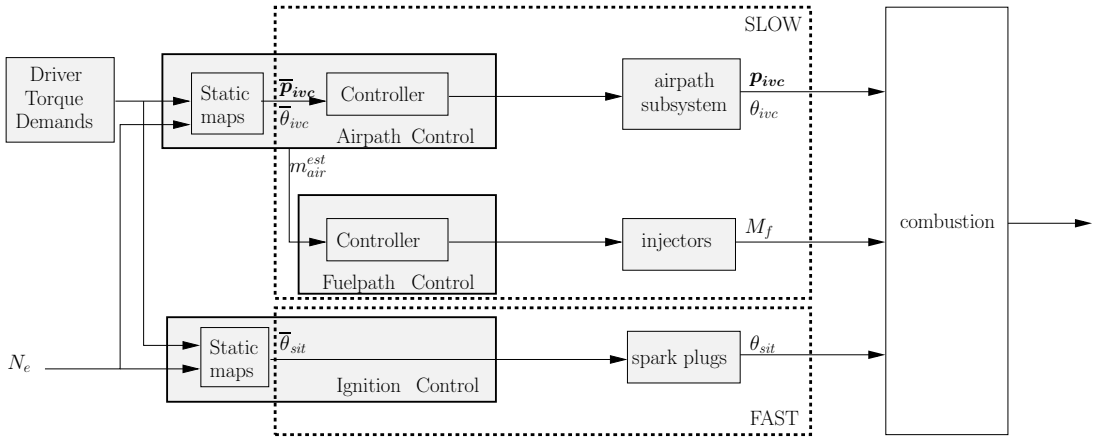

Figure 1.4: *Classic SI engine control architecture.* $\boldsymbol{p_{ivc}}$ *are the thermodynamic and physical composition in the cylinder at ivc.* $\overline{\boldsymbol{p}}_{\boldsymbol{ivc}}$ *is the steady-state mapped value of* $\boldsymbol{p_{ivc}}$*.* M_f *is the injected fuel mass.* θ_{ivc} *is the ivc timing and* $\overline{\theta}_{ivc}$*, its steady-state mapped value.* θ_{sit} *is the spark timing and* $\overline{\theta}_{sit}$*, its steady-state mapped value. The fuelpath is fed with an estimate of the in-cylinder air mass* (m_{air}^{est}) *usually provided by the airpath controller. The slow subsystem consists of the airpath and the fuelpath, while the fast subsystem is the ignitionpath.*

[1]The second usually met solution is to feed the steady-state map with the engine speed and the aspirated air mass. This is considered as an extension of the proposed branching scheme and is treated in § 2.5.2.

1.1.3 Combustion phasing transient behavior

We now describe the behavior of the presented classic controllers during transients and their impact on the combustion phenomenon. During transients, the airpath controller concentrates on the air mass control. It regulates the in-cylinder thermodynamic variables so that they track their setpoints. However, since the airpath cannot be accelerated as much as desired, there exists temporary mismatches which, in fact, negatively impact on the combustion efficiency. Mainly, the culprit is the ignitionpath controller which ignores these mismatches, and simply applies an open-loop control value $\overline{\theta}_{sit}$ for the ignition time based on look-up tables assuming in-cylinder thermodynamic variable have already reached their expected steady-state values. This issue is worsened on engines equipped with VVA. Indeed, the VVA actuators play an important disturbing role[2]. The VVA actuators changes the valves lift and their timing to create internal EGR which dilutes the air charge (and thus slows down the flame propagation [23]). Besides these beneficial effects, changing the valve lift also has an impact on the turbulence in the chamber. The flame propagation, which depends on this turbulence, is then either accelerated or slowed down. During transients, the effects of burned gases, pressure, temperature, and VVA disturbance on the flame propagation are significant. One can expect to improve the quality of the combustion (in terms of consumption) by compensating the offsets of in-cylinder thermodynamic and physical (VVA positions) parameters using the spark ignition time.

In summary, the general structure of a SI engine controller is depicted in Figure 1.4. The variables influencing the combustion can be split into two categories: the slow variables (vector) are $\boldsymbol{x_{slow}} = (\boldsymbol{p_{ivc}}, M_f, \theta_{ivc})$ and the (scalar) fast variable is $x_{fast} = \theta_{sit}$.

1.2 Background on CI engine

1.2.1 General engine structure

Internal combustion engines for which the combustion is initiated by the compression of the mixture are designated as Compression Ignited (CI) engines. The combustion chamber can be pictured as in Figure 1.1, except that there is no spark plug. In the cases of four strokes engines, the engine functioning timeline is the following:

1. Intake phase (cylinder filling): the intake valve opens and the fresh air enters the cylinder while the piston goes down. This phase lasts until the intake valve closes (*ivc*). Exhaust Gas Recirculation (EGR), if present, modifies the composition of the gases aspirated through the intake valve by

[2]Additionally, the VVA actuators can also be used to speed up the airpath dynamics, which in turn, introduces further offsets from the expected steady-state.

extracting exhaust gases in the exhaust line and mixing them with the fresh air in the intake line. If available, VVA may modify the breathing of the engine (intake and exhaust valves). This permits to re-aspirate some of the preceding combustion burned gases directly from the exhaust line through the exhaust valve).

2. Compression phase: the piston goes up and compresses the aspirated air and burned gases. The fuel is injected during this phase.

3. Combustion phase: after a delay depending on the thermodynamic and physical conditions (the so-called auto-ignition delay), the blend of air/burned gases/fuel auto-ignites. The combustion frees the fuel chemical energy. The pressure increases and pushes back the piston.

4. Exhaust phase: once the piston has completed its descent, the exhaust valve opens. The exhaust gases are then flushed out of the cylinder towards the exhaust line.

This timeline is pictured in Figure 1.5 where each phase is represented along with the various available actuators acting.

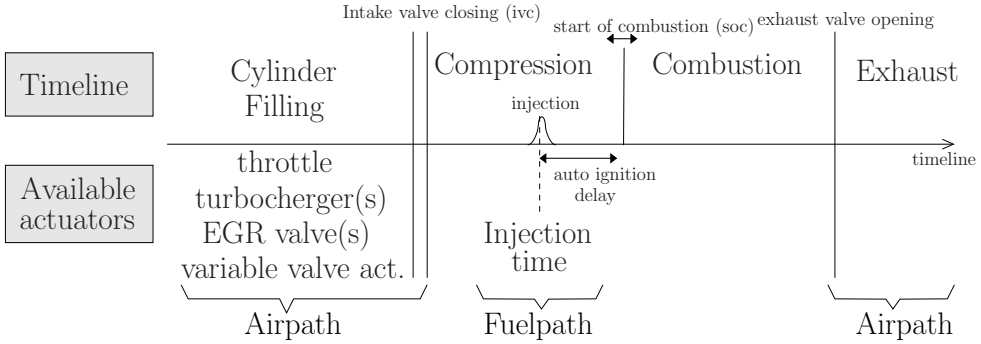

Figure 1.5: *CI engine functioning timeline. Each phase lasts 20 ms at 1500 rpm.*

The general structure of a CI engine is represented in Figure 1.6. It can be divided into two main subsystems. First, *the airpath* which consists of all the pipes, turbocharger(s), intake throttle, EGR valve(s), exhaust back pressure valve, intake and exhaust manifolds, VVA systems and heat exchangers. The airpath feeds the cylinder and provides appropriate thermodynamic and physical conditions. In fact, all the airpath devices act on the combustion by creating these conditions at the *ivc* instant. After *ivc*, the cylinder is isolated from the airpath. Secondly, *the fuelpath* which consists of the injection system. It injects the appropriate mass of fuel at the appropriate time in the chamber. After the *ivc*, the fuel injection parameters are the only control variables acting on the combustion.

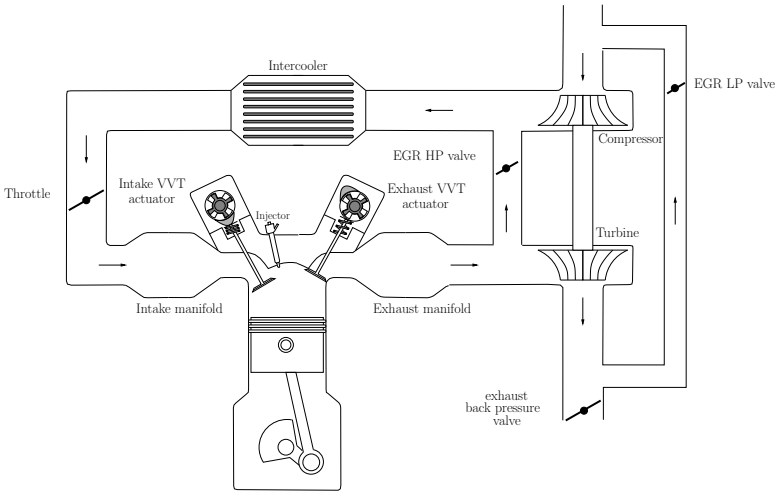

Figure 1.6: *Scheme of a general four cylinder CI engine. It is equipped with direct injection, a VVA, a low Pressure EGR (LP EGR) recirculation, a high pressure EGR (HP EGR) recirculation, an exhaust back pressure valve, an intercooler, and a turbocharger.*

1.2.2 CI engine control

As a result of this physical/temporal separation, usual CI engine controllers are classically consisting of two distinct controllers aiming at controlling each of these subsystems.

The task of the airpath controller is to make the airpath feed the cylinder with the right thermodynamic properties at *ivc* with the right valve timings (and among those the *ivc* timing θ_{ivc}). To this end, static maps of the values of the thermodynamic conditions at *ivc* (gathered in a vector $\boldsymbol{p_{ivc}}$) and of the valve timings are used. These 2D-maps usually have the drivers torque request and actual engine speed as inputs. In this thesis, it is assumed that such a properly working airpath controller is already installed on the engine, which allows reasonable tracking of the setpoints values (such controllers can be found in [9, 46, 67] and the references therein). However, due to recirculation holds-up, inertia of the physical devices (turbochargers, variable valve actuators), and actuators saturation, the tracking of these setpoints cannot be rendered arbitrarily fast (the airpath bandwidth is approximately 1 Hz). Tracking errors may also happen due to airpath malfunctions such as EGR valve clogging or natural device ageing. In fact, as in SI engines, since the thermodynamic conditions are not a free set of variables (they are, at least approximatively, related through the ideal gas law for instance), only a reduced set is actually controlled by the airpath controller (and thus mapped), while the other one can be inferred from the static relation holding between them all. In CI engines, these actually controlled variables usually include the pressure, composition, and VVA positions while for instance, the burned gases mass or the air mass can be determined using the composition

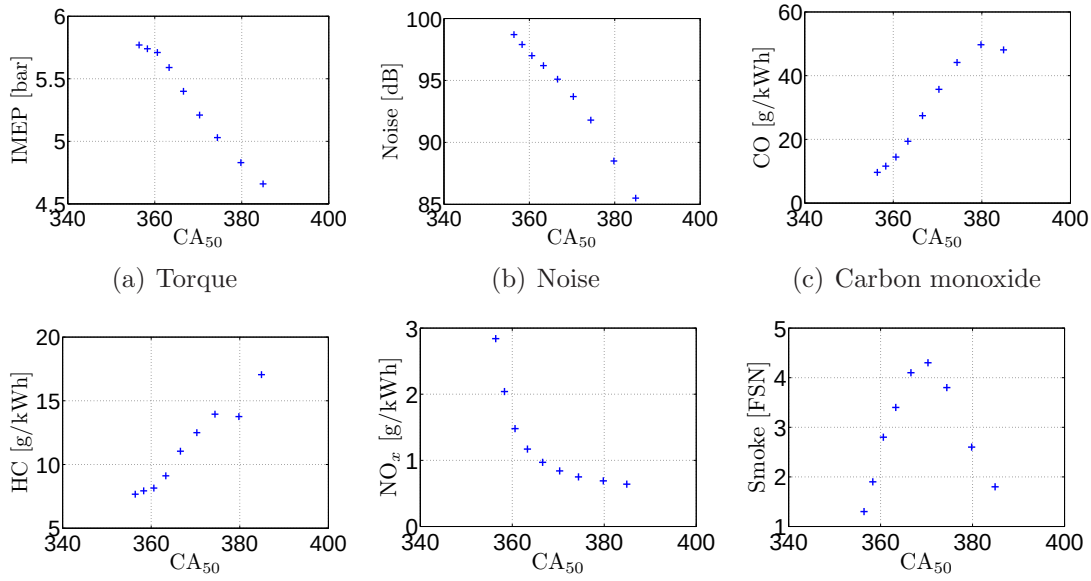

(a) Torque (b) Noise (c) Carbon monoxide

(d) Unburned hydrocarbons (e) Nitrogen oxides (f) Smoke

Figure 1.7: *Experimental results obtained for a four-cylinder CI Diesel engine (HCCI): influence of the combustion phase (represented by varying values of CA_{50}) on engine pollutants, noise, and torque production. The combustion phasings are the only parameters varying during the experiment (in fact, the injection timing is used to delay or to bring forward the whole combustion process); the Burned Gas Ratio (BGR), intake manifold pressure, intake manifold temperature, and injected fuel mass are constant.* $360°$ *CA represents the TDC.*

and the ideal gas relation. However, for sake of simplicity, in the following, we consider that all thermodynamic variables ($\boldsymbol{p_{ivc}}$) are controlled by the airpath.

On the other hand, classic fuelpath controllers are as follows. During the cylinder compression phase, fuel is injected and mixed with the compressed air and burned gas mixture. The fuel vaporizes and auto-ignites after the auto-ignition delay. Standard fuelpath control strategies focus on controlling the injected fuel mass and the injection timing. The direct injection technology enables to change these parameters from one cycle to the next. In practice, the injected fuel mass is directly computed from the driver's torque request. Therefore, this strategy cannot be changed without seriously jeopardizing the engine performance. Consequently, the fuel mass control is left as-is in the strategy we propose. By contrast, the injection timing (noted θ_{inj} for start of injection) is a direct trigger acting on the combustion phasing[3]. Classically, to control the injection timing, optimal values are determined at steady-state on experimental test-benches. These

[3]In this chapter, and, if not told otherwise in the following ones, we only consider mono-pulse injection. The discussion on multi-pulse injection is postponed until Section 4.2.

represent a tradeoff between efficiency, pollutant emissions and noise. To illustrate this, Figure 1.7 shows experimental variations of the combustion phasing created by variations of the injection timing (while all other influencing variables are kept constant). It clearly appears that the optimal value can only be an arbitrary tradeoff between torque, noise and pollutant emissions. Once determined, these optimal values are stored into 2-D look-up tables using the engine speed and the driver's torque request as inputs.

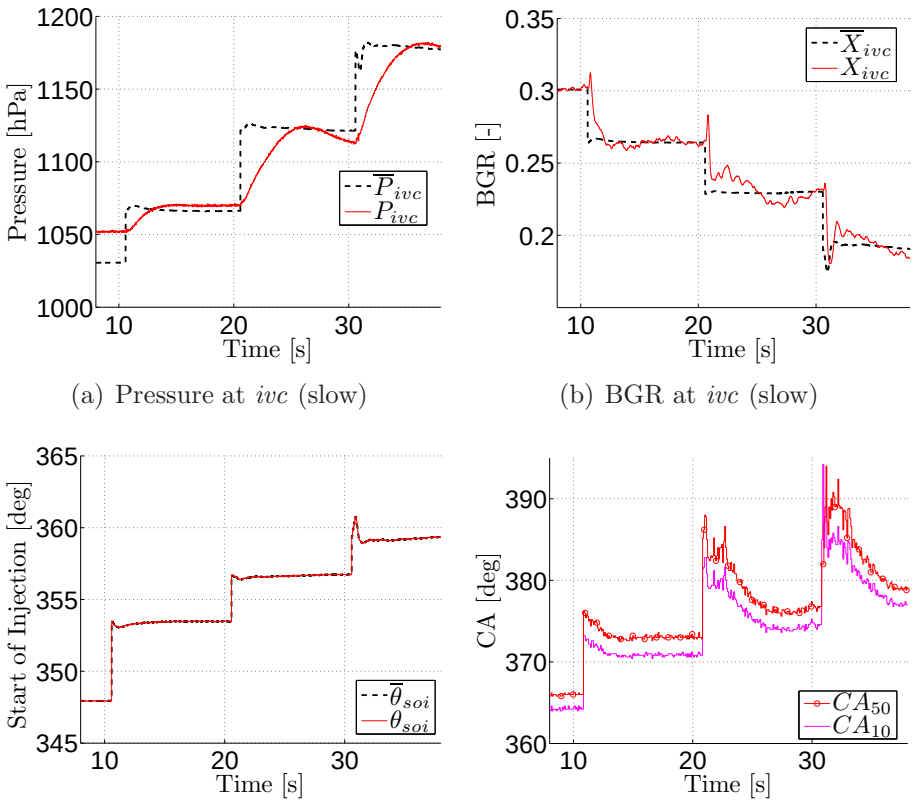

(a) Pressure at *ivc* (slow)

(b) BGR at *ivc* (slow)

(c) Start of injection (fast)

(d) Combustion phasings (CA_X)

Figure 1.8: *Experimental transient results on a 4-cylinder CI engine (HCCI) at a constant speed of 1500 rpm. Evolution of the initial thermodynamic conditions in the cylinder at ivc (pressure and temperature, both considered as slow variables), the start of injection (a fast variable) and the combustion phasing (combustion performance index). During transients, the combustion phasing CA_X features large overshoots due to the temporary mismatch between slow and fast variables. 360° CA represent the TDC. In these figures, P_{ivc} and X_{ivc} are computed according to the assumptions of § 4.1.2*

1.2.3 Combustion phasing transient behavior

During transients, due to the airpath slow dynamics, the initial thermodynamic conditions in the cylinder $\boldsymbol{p_{ivc}}$ and valve timing θ_{ivc}[4] do not match their optimal steady-state values. Since the injection timing θ_{inj} does not take into account these parameters, the fuel is injected as if the steady-state was reached. Then, the combustion does not occur at the right timing. This is clearly visible in Figure 1.8 where experimental transients obtained on a CI engine are reported. In details, the evolution of two cylinder initial conditions (pressure and BGR, which transient behavior is slow), of the injection timing (which can be changed from one cycle to the next), and the resulting combustion phasings (CA_{10} and CA_{50}) are depicted. The combustion phasing is shown to deviate away from its steady-state value during transients. Thus, the combustion phasing theoretical optimal tradeoff is not satisfied during transients.

To summarize the above discussion, the general structure of a CI engine controller is depicted in Figure 1.9. The slow (vector) variables are $\boldsymbol{x_{slow}} = (\boldsymbol{p_{ivc}}, \theta_{ivc})^T$ and the fast (scalar) variables is $x_{fast} = \theta_{inj}$.

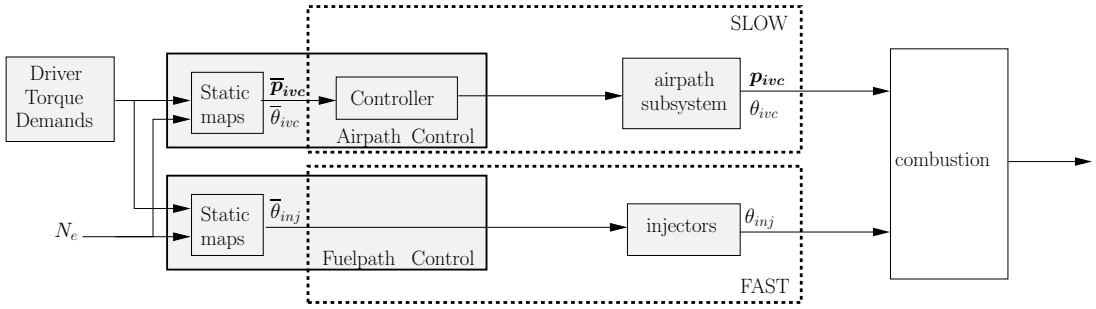

Figure 1.9: *Classic CI engine control architecture.* $\boldsymbol{p_{ivc}}$ *are the thermodynamic and physical conditions in the cylinder at ivc.* $\overline{\boldsymbol{p}}_{\boldsymbol{ivc}}$ *is the mapped steady-state value of* $\boldsymbol{p_{ivc}}$*.* θ_{ivc} *is the ivc timing and* $\overline{\theta}_{ivc}$*, its steady-state mapped value.* θ_{inj} *is the injection timing, and* $\overline{\theta}_{inj}$ *are the mapped steady-state value of* θ_{inj}*. Both the airpath and the fuelpath subsystems work in parallel without any noticeable influence on each other. One is slow, and one is fast. As a result, during transients, the combustion timing deviates from its optimum.*

1.3 Slow/fast scheme for internal combustion engines

After having presented the classic control architectures of the SI and CI engines, we now wish to underline that they both suffer from the same flaw resulting

[4]this may be due to actuator constraints, or, as in SI engines, due to a particular transient control strategy aiming at speeding up some other thermodynamic conditions transients.

in poor combustion control during transients. In both cases, we have emphasized the presence of slow and fast variables. The "slow controller" (airpath and fuel-path controllers in SI engines, airpath controller in CI engines) makes the $\boldsymbol{x_{slow}}$ variables follow their setpoint $\overline{\boldsymbol{x}}_{\boldsymbol{slow}}$. In fact, all the variables included in the vector $\boldsymbol{x_{slow}}$ are not actually controlled since there exist static relations between them (such as the ideal gas relation or the stoichiometric combustion in SI engines). However, since the static relations are fully known, we consider in the following that the whole vector $\boldsymbol{x_{slow}}$ is controlled even if only a reduced set of them is actually controlled[5]. Among the $\boldsymbol{x_{slow}}$ variables, θ_{ivc} plays a significant role since it separates the intake phase and the compression/combustion phases.

This tracking performance suffers from the relative sluggishness of the slow subsystem and exhibits offsets during transients. Consequently, the combustion phasing is degraded and exhibits over- and undershoots[6]. Interestingly, in both engines architectures, the fast variable has a strong impact on combustion phasing since it directly (in SI engines) or indirectly (through the auto-ignition delay in CI engines) controls the beginning of the combustion and thus of the whole combustion phasing. Moreover, the slow variables can be simply inferred from measurements, identification and/or observation. It follows that one can use the fast variables x_{fast} to compensate for the slow evolution of the known parameters $\boldsymbol{x_{slow}}$. This is the path we explore in this thesis. It is detailed in the next chapter.

[5]The other variables naturally converge to a vector $\overline{\boldsymbol{x}}_{\boldsymbol{slow}}$ gathering the actually mapped reference value for the smaller set of variables and reference values for the other variables that can be easily computed using the static relations.

[6]In fact, each variable in this group has its own dynamics and settling time. For instance, the process of gas filling the in-cylinder involves two of these variables (the masses of air and burned gas), so it depends on two distinct (and long) settling times. It may be possible to speed up some of the slow variables by coordinating the respective low-level controllers of these variables, at the expense of the speed of other variables such as temperature. This is actually a subject of ongoing research. Interested reader can refer to [47] for SI engines and [46] for Diesel engines.

Chapter 2

Proposed model-based combustion controller

To improve the existing controllers exposed in Chapter 1, which rely on static look-up tables under all circumstances, a control of the combustion phasing is now proposed.It will be of particular interest during transients. Let CA_X be the desired combustion phasing to control. It is considered that the calibration phase of the engine has led to the construction of steady-state maps storing optimal values $\overline{x}_{fast}$ and $\overline{\boldsymbol{x}}_{\boldsymbol{slow}}$ corresponding to an optimal combustion phasing $\overline{CA_X}$. The goal of any combustion controller is then to guarantee that, even during transients, the actual combustion phasing CA_X tracks the optimal one. To this end, two main solutions have been studied in the literature. The simplest one is to use feedback through in-cylinder measurements while the second one is to use a partially feedforward model-based control technique. After having presented them, we propose our own method.

2.1 Existing combustion timing control strategies

2.1.1 Solutions relying on in-cylinder sensors

The first class of methods uses information from in-cylinder sensors. High-frequency in-cylinder sensors enable accurate closed loop control action. The additional information from these sensors allows the reconstruction of several combustion characteristics and the utilization of them as feedback information.

Among the available sensors, in-cylinder pressure transducers are the most flexible [56]. In practice, solutions requiring such a hardware upgrade have been successfully applied to CI and SI engines. We now briefly present such solutions.

In CI engines, cylinder pressure feedback has most often been considered for Homogeneous Charge Compression Ignition (HCCI) engines. Several control actions can be considered. In [21], Haraldsson *et al.* present a closed-loop combustion control mechanism using variable compression ratio (VCR) as an actuator. Changing the compression ratio directly impacts on the rise of pressure and temperature in the cylinder, not just during compression, but also during the auto-ignition and combustion phases. Thus, VCR can be used to control CA_{50}. In [2, 54], a solution using two fuels with different combustion properties is presented. CA_{50} can be regulated by changing the recipe of the mixture to be injected. In [1, 8, 10, 55, 57], HCCI control results based on a variable valve actuation are presented. These solutions modify the charge temperature by trapping hot exhaust gases in the cylinder from one cycle to the next; the whole combustion process can thereby be delayed or advanced. In [18, 22, 69], a thermal management solution is reported. The intake manifold temperature is modified by changing the mixture of hot and cold air in the intake line. Once again, combustion, being sensitive to thermal changes, can be delayed or advanced.

In SI engines (e.g. [61, 73, 74]), closed loop controllers have been presented for the spark timing using cylinder pressure feedback.

Finally, besides pressure sensors, several other sensors have been considered to provide feedback information on the combustion. For example, accelerometers strapped onto the engine block [13, 38, 53] or crankshaft angular velocity sensors [12] have also been considered for CI Diesel engines. Ion-current sensors located in the spark plug [14, 16], crankshaft angular velocity sensors [7], and torque sensors [3] have been studied to control the spark timing of SI engines.

All these solutions can provide accurate control of combustion phasing, but also suffer from serious drawbacks [59]: they imply costly hardware (additional sensors are needed and their integration in the combustion chamber raises some technological challenges) and software (the information provided by these sensors needs high frequency treatment which is not possible in commercial-line electronic control units) upgrades and drift with time (this is notably true for cylinder pressure sensors, the most widely considered technology, since the thermodynamic conditions in the chamber are rather extreme).

2.1.2 Model-based control

Instead of using in-cylinder sensors, some authors have considered models of the engine cycle from the *ivc*, to a desired combustion phasing CA_X. The model is usually subdivided into a compression model and a combustion model. These models may be explicit (e.g., the Wiebe models [70]), implicit (e.g., the knock integral model [63]), or based on differential equations such as ratio of heat release [6, 11]). In all cases, the goal is to relate the $\boldsymbol{x_{slow}}$ and x_{fast} variables to the combustion phasing. We now detail such approaches.

Consider $\mathrm{CA_X}$, for a particular $0 \leq X \leq 100$, the desired combustion phasing. As mentioned earlier, it is presumed that the calibration phase of the engine has led to the construction of steady-state maps containing the values of $\overline{x}_{fast}$ and $\overline{\boldsymbol{x}}_{\boldsymbol{slow}}$ corresponding to an optimal combustion phasing $\overline{\mathrm{CA_X}}$. The goal of the combustion controller is to guarantee that the actual combustion phasing $\mathrm{CA_X}$ tracks the optimal one, even during transients. Assuming a very general form of additive modeling error $\epsilon_{\mathcal{M}}$, the combustion phasing is equal to

$$\mathrm{CA_X} = \mathcal{M}(\boldsymbol{x}_{\boldsymbol{slow}}, x_{fast}) + \epsilon_{\mathcal{M}}(\boldsymbol{x}_{\boldsymbol{slow}}, x_{fast}), \tag{2.1}$$

where $\mathcal{M}$ is a known model[1] of the type cited above. The goal of the modeling process (model building and calibration) is to make the modeling error $\epsilon_{\mathcal{M}}$ as small as possible. However, the more the model can be faithful to the reality, the more complex the model is to calibrate and to manipulate[2]. In fact, there is an unavoidable trade-off between simplicity of the model and faith in the reality, such that modeling errors always exist.

Model inversion

To compensate for a mismatch in the $\boldsymbol{x}_{\boldsymbol{slow}}$ variables, a very natural approach is simply to invert the model $\mathcal{M}$ and to determine a feed-forward control law for the trigger x_{fast}. The control trigger is then directly computed from the reference combustion phasing $\overline{\mathrm{CA_X}}$ under the following form:

$$x_{fast} = \mathcal{M}^{-1}(\boldsymbol{x}_{\boldsymbol{slow}}, \overline{\mathrm{CA_X}}) \tag{2.2}$$

Since combustion models are usually quite involved, they are not directly invertible. Shooting and interpolation techniques can be used to approximate their inverses. Nakayama et al. applied this solution to CI engines [52], and Hochstrasser et al. proposed it for SI engines [34]. The main drawback of this approach is that model errors propagate into the feedforward term. In detail, the resulting error in the combustion phasing can be calculated from Equations (2.1) and (2.2) as follows:

$$\begin{aligned} \mathrm{CA_X} - \overline{\mathrm{CA_X}} &= \mathcal{M}(\boldsymbol{x}_{\boldsymbol{slow}}, x_{fast}) + \epsilon_{\mathcal{M}}(\boldsymbol{x}_{\boldsymbol{slow}}, x_{fast}) - \overline{\mathrm{CA_X}} \\ &= \mathcal{M}(\boldsymbol{x}_{\boldsymbol{slow}}, \mathcal{M}^{-1}(\boldsymbol{x}_{\boldsymbol{slow}}, \overline{\mathrm{CA_X}})) \\ &\quad + \epsilon_{\mathcal{M}}(\boldsymbol{x}_{\boldsymbol{slow}}, \mathcal{M}^{-1}(\boldsymbol{x}_{\boldsymbol{slow}}, \overline{\mathrm{CA_X}})) - \overline{\mathrm{CA_X}} \\ &= \epsilon_{\mathcal{M}}(\boldsymbol{x}_{\boldsymbol{slow}}, \mathcal{M}^{-1}(\boldsymbol{x}_{\boldsymbol{slow}}, \overline{\mathrm{CA_X}})) \end{aligned} \tag{2.3}$$

The last equation is obtained from the definition of the inverse in Equation (2.2). Interestingly, even when $\boldsymbol{x}_{\boldsymbol{slow}}$ tends to $\overline{\boldsymbol{x}}_{\boldsymbol{slow}}$, this error never completely vanishes but converges to $\epsilon_{\mathcal{M}}(\overline{\boldsymbol{x}}_{\boldsymbol{slow}}, \mathcal{M}^{-1}(\overline{\boldsymbol{x}}_{\boldsymbol{slow}}, \overline{\mathrm{CA_X}})) \neq 0$. Therefore, under all

[1] This model is here written under a static equation, but may represent a dynamic (differential equation) model.

[2] In turn this raises the issues of real-time compatibility of such models as the size of the needed state in the case of differential system is increased to improve accuracy.

circumstances, the combustion phasing is different from the optimal one. This is not acceptable in practice. To circumvent this flaw, a small improvement of this method is proposed and experimentally tested in Appendix A. However, it still requires to invert the model which is usually particularly difficult. We now propose an alternative solution.

2.2 Model linearization/summary of the proposed control method

The solution summarized in the previous paragraph does not use all available information. During transients, the cylinder initial conditions and valve timing tracked setpoints $\overline{\boldsymbol{x}}_{\boldsymbol{slow}}$ are known, as are the associated control trigger setpoint values $\overline{x}_{fast}$. All these values can be used by the combustion phasing controller. They are related by the following

$$\overline{\mathrm{CA}_{\mathrm{X}}} = \mathcal{M}(\overline{\boldsymbol{x}}_{\boldsymbol{slow}}, \overline{x}_{fast}) + \epsilon_{\mathcal{M}}(\overline{\boldsymbol{x}}_{\boldsymbol{slow}}, \overline{x}_{fast}) \tag{2.4}$$

The strict equality results from a preliminary engine calibration at steady-state.

We propose to add a corrective term to the setpoint value to account for the tracking errors $\delta\boldsymbol{x}_{\boldsymbol{slow}} = \boldsymbol{x}_{\boldsymbol{slow}} - \overline{\boldsymbol{x}}_{\boldsymbol{slow}}$ between the actual airpath-driven parameters $\boldsymbol{x}_{\boldsymbol{slow}}$ and their reference values $\overline{\boldsymbol{x}}_{\boldsymbol{slow}}$. The proposed controller is

$$x_{fast} = \overline{x}_{fast} + \delta x_{fast}(\delta\boldsymbol{x}_{\boldsymbol{slow}}) \tag{2.5}$$

Dropping the unknown modeling errors, the correction is chosen to make the error between the actual combustion phasing and the reference phasing vanish. More precisely, δx_{fast} is computed to satisfy

$$0 = \mathcal{M}(\overline{\boldsymbol{x}}_{\boldsymbol{slow}} + \delta\boldsymbol{x}_{\boldsymbol{slow}}, \overline{x}_{fast} + \delta x_{fast}) - \mathcal{M}(\overline{\boldsymbol{x}}_{\boldsymbol{slow}}, \overline{x}_{fast}) \tag{2.6}$$

Due to the complexity of $\mathcal{M}$, no explicit formula for δx_{fast} can be found. Instead, this term is determined at first-order, by the sensitivity equation

$$0 = \frac{\partial \mathcal{M}}{\partial x_{fast}}(\overline{\boldsymbol{x}}_{\boldsymbol{slow}}, \overline{x}_{fast})\delta x_{fast} + \frac{\partial \mathcal{M}}{\partial \boldsymbol{x}_{\boldsymbol{slow}}}(\overline{\boldsymbol{x}}_{\boldsymbol{slow}}, \overline{x}_{fast})\delta\boldsymbol{x}_{\boldsymbol{slow}} \tag{2.7}$$

The correction term is then

$$\delta x_{fast} \triangleq -\frac{\frac{\partial \mathcal{M}}{\partial \boldsymbol{x}_{\boldsymbol{slow}}}(\overline{\boldsymbol{x}}_{\boldsymbol{slow}}, \overline{x}_{fast})}{\frac{\partial \mathcal{M}}{\partial x_{fast}}(\overline{\boldsymbol{x}}_{\boldsymbol{slow}}, \overline{x}_{fast})} \cdot \delta\boldsymbol{x}_{\boldsymbol{slow}} \tag{2.8}$$

or, equivalently, noting $\boldsymbol{\alpha}$ the gain

$$\boldsymbol{\alpha}(\overline{\boldsymbol{x}}_{\boldsymbol{slow}}, \overline{x}_{fast}) \triangleq -\frac{\frac{\partial \mathcal{M}}{\partial \boldsymbol{x}_{\boldsymbol{slow}}}(\overline{\boldsymbol{x}}_{\boldsymbol{slow}}, \overline{x}_{fast})}{\frac{\partial \mathcal{M}}{\partial x_{fast}}(\overline{\boldsymbol{x}}_{\boldsymbol{slow}}, \overline{x}_{fast})}.$$

the correction is defined as

$$\delta x_{fast} = \boldsymbol{\alpha}(\overline{\boldsymbol{x}}_{\boldsymbol{slow}}, \overline{x}_{fast})\delta \boldsymbol{x}_{\boldsymbol{slow}} \tag{2.9}$$

With the proposed strategy, the actual error is (at first order approximation)

$$\mathrm{CA_X} - \overline{\mathrm{CA_X}} = \left[\frac{\partial \epsilon_{\mathcal{M}}}{\partial \boldsymbol{x}_{\boldsymbol{slow}}} - \frac{\partial \epsilon_{\mathcal{M}}}{\partial x_{fast}} \left(\frac{\partial \mathcal{M}}{\partial x_{fast}} \right)^{-1} \frac{\partial \mathcal{M}}{\partial \boldsymbol{x}_{\boldsymbol{slow}}} \right] \delta \boldsymbol{x}_{\boldsymbol{slow}} + O(\delta {\boldsymbol{x}_{\boldsymbol{slow}}}^2) \tag{2.10}$$

where all derivative terms are evaluated about $(\overline{\boldsymbol{x}}_{\boldsymbol{slow}}, \overline{x}_{fast})$. This control strategy has several advantages. First, it does not require any feedback information; it is completely open loop. Second, the actual error vanishes when the (vector) tracking errors $\boldsymbol{\delta x}_{\boldsymbol{slow}}$ disappear. In other words, at a steady-state, the x_{fast} variable is equal to its optimal value $\overline{x}_{fast}$ and the engine operates at its optimum. Finally, the proposed controller expresses through well-known equations (the model $\mathcal{M}$), available $\boldsymbol{x}_{\boldsymbol{slow}}$ tracking errors, and the setpoints ($\overline{\boldsymbol{x}}_{\boldsymbol{slow}}$, and $\overline{x}_{fast}$).

So far, Equation (2.8) is only a formal expression; its practical form has to be deduced from a specific combustion model. In Section 2.3, we expose the general structure of such models in terms of ordinary differential equations .

For now, we wish to illustrate the application of this method to the general case of Figure 2, which we now make more precise. For this purpose, in Figure 2.1, two strategies are presented: i) the proposed strategy (dashed red) compensates for errors in the $\boldsymbol{x}_{\boldsymbol{slow}}$ variables by acting on the x_{fast} variables according to Equation (2.9), and ii) the classic strategy of in-cylinder sensor feedback (dotted blue).

2.3 Combustion modeling

The strategy developed in the previous section is based on a model of the combustion phasing (see Equation (2.1)). This model $\mathcal{M}$ relates the x_{fast} and $\boldsymbol{x}_{\boldsymbol{slow}}$ variables along with the desired combustion phasing $\mathrm{CA_X}$. Thus, it shall represent all processes appearing between the *ivc* and the $\mathrm{CA_X}$. This section exposes the most general form of such models: a series of differential systems, as will be used in the applications in Chapters 3, and 4.

Classically, two different processes compose the time interval between *ivc* and $\mathrm{CA_X}$, these are the compression phase and the combustion phase (fuel burning). Depending on which technology (SI or CI) is considered, several phenomena must be detailed in the combustion phase. In SI engines, there is usually only one phenomenon: the flame propagation. In CI engines, at least two phenomena must be considered, the auto-ignition phenomenon and the combustion phenomenon. The combustion may also be splitted into several parts such as cool flame and diffusion flame.

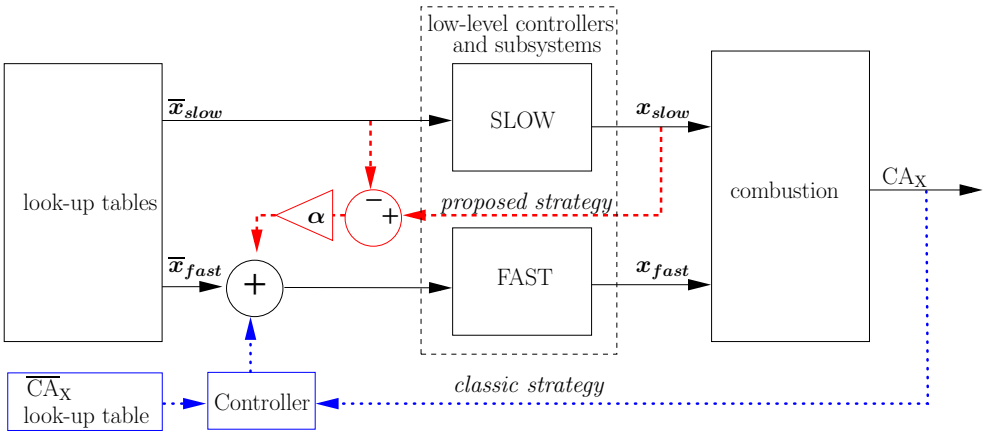

Figure 2.1: *Combustion as the output of parallel slow and fast controlled dynamical systems fed by a single look-up table assuming steady-state operation. See Figure 2 for notation. The classic feedback strategy using an in-cylinder sensor is depicted as a dotted blue line. The proposed feed-forward strategy is a dashed red line.*

2.3.1 Compression phase

During the compression phase some thermodynamic and physical parameters playing a role in the latter combustion dynamics vary. These are the in-cylinder pressure, the temperature and the composition. The most common model for the compression phase is a polytropic compression. It relates the evolution of the thermodynamic conditions to the evolution of the cylinder volume $V(\theta)$ as a function of the crankshaft angle θ. The polytropic assumption can also be dropped and wall heat losses can be considered instead. Following the Woschni correlation (with the heat transfer coefficient h_c) for wall heat losses [23], and assuming a constant wall temperature T^w during the cycle, we get

$$\begin{cases} \dfrac{dP}{d\theta} = -\gamma P \dfrac{dV(\theta)}{d\theta}\dfrac{1}{V(\theta)} - \dfrac{(\gamma-1)P}{TV(\theta)}\dfrac{h_c}{N_e}(T-T^w) \\ \dfrac{dT}{d\theta} = -(\gamma-1)T\dfrac{dV(\theta)}{d\theta}\dfrac{1}{V(\theta)} - \dfrac{(\gamma-1)}{V(\theta)}\dfrac{h_c}{N_e}(T-T^w) \\ \dfrac{dT^w}{d\theta} = 0 \\ \dfrac{dX}{d\theta} = 0 \end{cases}$$

The initial conditions at *ivc* are $P(\theta_{ivc}) = P_{ivc}$, $T(\theta_{ivc}) = T_{ivc}$, $T^w(\theta_{ivc}) = T^w_{ivc}$, $X(\theta_{ivc}) = X_{ivc}$. The wall temperature at the beginning of each cycle T^w_{ivc} can be obtained from a model [64, 71]. Very generally, numerous alternative compression

models can be expressed with ordinary differential equation of the form

$$\begin{cases} \dfrac{d\boldsymbol{y^0}}{d\theta} = \boldsymbol{f}(\boldsymbol{y^0}, \theta) \\ \boldsymbol{y^0}(\theta_{ivc}) = \boldsymbol{g}(\boldsymbol{p_{ivc}}) \end{cases} \tag{2.11}$$

where $\boldsymbol{f} \in C^1$ (continuously differentiable), and $\boldsymbol{g} \in C^1$. The reader shall notice that the constant parameters appearing in the right-hand side of the differential equation (2.11) have been introduced as extended states with trivial dynamics.

The end of the compression phase is determined by the control trigger (injection time in CI engines or ignition time in SI engines) which is a control variable.

2.3.2 Combustion phase

The combustion phase is a succession of n chemical/physical processes. As already mentioned, in CI engines, these can be auto-ignition, cool flame, and diffusion flame combustion. In SI engines, usually only one phenomenon is considered, it is the flame propagation. Each process is modeled by differential equations with a state (a finite set of variables is necessary to represent the evolution of the considered phenomenon (pressure, composition, turbulence, Mass of Fuel Burned (MFB), ...), an initial condition (which may depend on preceding phenomena), and a transition equation at which the considered process stops and the next phenomenon starts. Each phenomenon $i \in [\![1, n]\!]$ is thus modeled by the differential system i, $\frac{d\boldsymbol{y^i}}{d\theta} = \boldsymbol{f_i}(\boldsymbol{y^i}, \theta)$. The initial conditions are defined by continuity (from one system to the next) and the transitions are governed by transition equations $\boldsymbol{h}(\boldsymbol{y^i}) = 0$. For sake of generality[3], $\boldsymbol{f_i} \in C^1$, and $\boldsymbol{h^i} \in C^1$.

As will appear in the following, the proposed strategies of combustion control directly rely on the combustion model. The accuracy of the controller is thus dependent on its accuracy. The choice of the model and its calibration are keys to diminish the modeling errors. Yet, in practice, a tradeoff has to be found between the complexity of the model and its faith to reality. Extensive models involving a large number of states may be difficult to identify and calibrate, while models with too few states will often reveal simplistic and, therefore, relatively useless in the derivation of the proposed control actions. The calibration of these models is discussed in Appendix B.

2.3.3 Summary

The $\boldsymbol{x_{slow}}$ variables are split into two groups, the value $\boldsymbol{p_{ivc}}$ of the thermodynamic and physical conditions at *ivc* and the *ivc* timing θ_{ivc}: $\boldsymbol{x_{slow}} = (\boldsymbol{p_{ivc}}, \theta_{ivc})^T$. The x_{fast} variable is a temporal trigger denoted by θ_{tr}: $x_{fast} = \theta_{tr}$.

[3]This assumption will be relaxed in Section 2.5.

Gathering the previous equations of §2.3.1, and §2.3.2, the model of processes happening between *ivc* and $\mathrm{CA_X}$ is a sequence of $n+1 \geq 2$ differential systems of the form (2.11). Initial conditions (at θ_{ivc}) of the switching right-hand-side system of differential equations are depending on $\boldsymbol{p_{ivc}}$. Transitions between the differential systems are governed by the control trigger θ_{tr} for the first system, and by static relations for the other.

Gathering all the state variables into a single vector $\boldsymbol{x} = (\boldsymbol{y^0}, \boldsymbol{y^1}, ..., \boldsymbol{y^n})$ and using some trivial (zero right-hand side) dynamics where necessary, one obtains a general differential system of the form given in Figure 2.2. It is the explicit formulation of the model $\mathrm{CA_X} = \mathcal{M}(\boldsymbol{x_{slow}}, x_{fast})$ introduced in Equation (2.1) with $\boldsymbol{x_{slow}} = (\boldsymbol{p_{ivc}}, \theta_{ivc})$, and $x_{fast} = \theta_{tr}$.

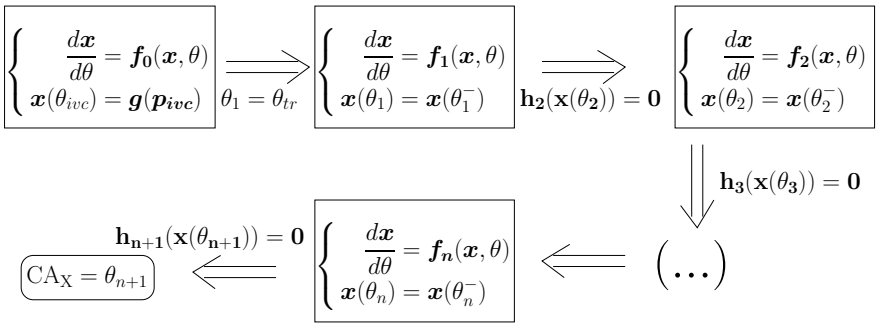

Figure 2.2: *The combustion model can be represented under the form of a sequence of differential equations with initial conditions dependent on the slow variables (for the first) of defined by continuity (for the other systems). The transitions are governed by a trigger (first transition) or by a condition on the state. This sequence is the explicit formulation of the model* $CA_X = \mathcal{M}(\boldsymbol{x_{slow}}, x_{fast})$ *used in Equation* (2.1) *where* $\boldsymbol{x_{slow}} = (\boldsymbol{p_{ivc}}, \theta_{ivc})$*, and* $x_{fast} = \theta_{tr}$*.*

2.4 Controller synthesis

We now make use of the previously presented model to determine the gain appearing in Equation (2.9). A sensitivity analysis of the model is now performed.

Since the combustion model is not expressed under an explicit input-output form as in Equation (2.1) but under the form of a sequence of differential systems with switches, one has to extend the computation of the correction (2.9) to such differential systems.

Figure 2.3 outlines the computation method. The solid black plot is the reference combustion obtained for the reference values of $\overline{\boldsymbol{x}}_{\boldsymbol{slow}} = (\overline{\boldsymbol{p}}_{\boldsymbol{ivc}}, \overline{\theta}_{ivc})^T$ and $\overline{x}_{fast} = \overline{\theta}_{tr}$. It corresponds to the reference combustion timing $\overline{\mathrm{CA_X}}$, the reference state $\overline{\boldsymbol{x}}$, and all the reference transitions timings[4] $(\{\overline{\theta}_i\}_{i \in [\![1,n+1]\!]})$ and

[4]For sake of simplicity, in the following, the intake valve closure is denoted by $\theta_0 = \theta_{ivc}$ and the control trigger by $\theta_1 = \theta_{tr}$.

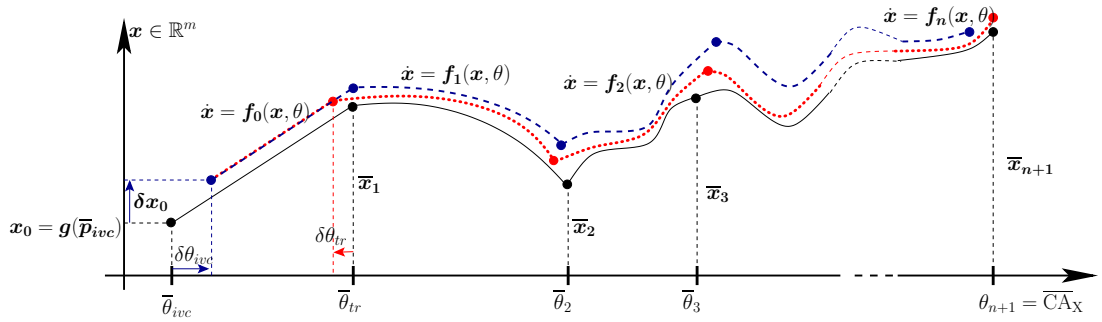

Figure 2.3: *Model of an engine cycle (compression and combustion). θ_{tr} is the control trigger, θ_{ivc} is the intake valve closure, and $\boldsymbol{p_{ivc}}$ are all necessary airpath driven parameters. Solid black plot: reference combustion, blue dashed plot: without correction, red plot: with correction, the control trigger θ_{tr} is corrected ($\delta\theta_{tr}$) to compensate for the slow parameters offsets ($\boldsymbol{\delta x_0} = \frac{\partial \boldsymbol{g}}{\partial \boldsymbol{p_{ivc}}}(\overline{\boldsymbol{p}}_{\boldsymbol{ivc}})\boldsymbol{\delta p_{ivc}}, \delta\theta_{ivc}$).*

reference values of the state at these transitions $(\{\overline{\boldsymbol{x}}_{\boldsymbol{i}}\}_{i\in[\![1,n+1]\!]})$[5]. In the presence of tracking errors $\boldsymbol{\delta x_{slow}} = (\boldsymbol{\delta p_{ivc}}, \delta\theta_{ivc})^T$, if the control trigger is not changed, then the combustion phasing is not the reference one (dashed blue plot). To counterbalance such tracking errors, a corrective term $\delta x_{fast} = \delta\theta_{tr}$ is added to have the actual combustion phasing match its reference (red plot).

Following Section 2.2, the model is linearized around the reference working point $(\overline{\boldsymbol{p}}_{\boldsymbol{ivc}}, \overline{\theta}_{ivc}, \overline{\boldsymbol{x}})$. More precisely, each differential system is properly linearized to relate initial and final offsets. Through the linearization of the transitions equations, a static relation on the final conditions offsets can be obtained. Finally, a particular combination of these equations permits the isolation of the linearized quantities of interest $(\boldsymbol{\delta p_{ivc}}, \delta\theta_{ivc}, \delta\theta_{tr}, \delta\mathrm{CA}_{\mathrm{X}})$. This gives an equation similar to Equation (2.7).

2.4.1 Propagation of offsets through one differential system

The general form of the j-th differential systems of interest is (see Figure 2.2)

$$\begin{cases} \dfrac{d\boldsymbol{x}}{d\theta} = \boldsymbol{f_j}(\boldsymbol{x}, \theta) \\ \boldsymbol{x}(\theta_j) = \boldsymbol{x_j} \end{cases} \quad j \in [\![0, n]\!] \tag{2.12}$$

which is considered on the time interval $[\theta_j, \theta_{j+1}]$ where θ_{j+1} is implicitly defined by $h_{j+1}(\boldsymbol{x}(\theta_{j+1})) = 0$ if $j > 1$ or by $\theta_1 = \theta_{tr}$. Consider that this system is initialized at $\boldsymbol{x}(\overline{\theta}_j + \delta\theta_j) = \overline{\boldsymbol{x}}_{\boldsymbol{j}} + \boldsymbol{\delta x_j}$ instead of $\boldsymbol{x}(\overline{\theta}_j) = \overline{\boldsymbol{x}}_{\boldsymbol{j}}$. This will induce offsets

[5] One has then $\overline{\boldsymbol{x}}(\overline{\theta}_i) = \overline{\boldsymbol{x}}_{\boldsymbol{i}}$.

on both $\delta\theta_{j+1}$ and $\boldsymbol{\delta x_j}$ partly defined by the switching relation $h_{j+1}(\boldsymbol{x}(\theta_{j+1})) = 0$. To find an equation relating the initial offsets $(\boldsymbol{\delta x_j}, \delta\theta_j)$ and the final offsets $(\boldsymbol{\delta x_{j+1}}, \delta\theta_{j+1})$, a sensitivity analysis is carried out using the following classic theorem (see e.g. Hale [20, thm 3.3]). This theorem permits one to find the sensitivity of a differential system to its initial conditions and/or parameters appearing in the right-hand side.

Theorem 2.4.1. *[20, thm 3.3] Let f be C^1. The application mapping the parameter $\boldsymbol{p} = (\boldsymbol{p_1}, \boldsymbol{p_2})$ to the solution $\boldsymbol{z_p}$ of the differential equation*

$$\begin{cases} \dfrac{d}{dt}\boldsymbol{z}(t) = \boldsymbol{f}(\boldsymbol{z}(t), \boldsymbol{p_1}, t) \\ \quad \boldsymbol{z}(0) = \boldsymbol{p_2} \end{cases}$$

is differentiable and its derivative in $\overline{\boldsymbol{p}} = (\overline{\boldsymbol{p}}_{\boldsymbol{1}}, \overline{\boldsymbol{p}}_{\boldsymbol{2}})$ is the application mapping $\boldsymbol{\delta p} = (\boldsymbol{\delta p_1}, \boldsymbol{\delta p_2})$ to the solution of the differential equation

$$\begin{cases} \dfrac{d}{dt}\boldsymbol{\delta z}(t) = \dfrac{\partial \boldsymbol{f}}{\partial \boldsymbol{z}}(\boldsymbol{z}_{\overline{\boldsymbol{p}}}(t), \overline{\boldsymbol{p}}_{\boldsymbol{1}}, t).\boldsymbol{\delta z}(t) + \dfrac{\partial \boldsymbol{f}}{\partial \boldsymbol{p_1}}(\boldsymbol{z}_{\overline{\boldsymbol{p}}}(t), \overline{\boldsymbol{p}}_{\boldsymbol{1}}, t).\boldsymbol{\delta p_1} \\ \quad \boldsymbol{\delta z}(0) = \boldsymbol{\delta p_2} \end{cases}$$

where $\boldsymbol{z}_{\overline{\boldsymbol{p}}}$ is the solution of the differential system

$$\begin{cases} \dfrac{d}{dt}\boldsymbol{z}(t) = \boldsymbol{f}(\boldsymbol{z}(t), \overline{\boldsymbol{p}}_{\boldsymbol{1}}, t) \\ \quad \boldsymbol{z}(0) = \overline{\boldsymbol{p}}_{\boldsymbol{2}} \end{cases}$$

The sensitivity is the solution of a linear time-varying system for which every term (but the state) is known since the linearization occurs about the reference state $\overline{\boldsymbol{z}}_{\boldsymbol{p}}$ which can be computed by integrating the differential system for $\boldsymbol{p} = \overline{\boldsymbol{p}}$.

Change of time from $\theta \in [\theta_j, \theta_{j+1}]$ to $u \in [0, 1]$

To take into account the transitions in an effective way through the differential calculus, it is convenient to get rid of the time offsets. Using the time change $\theta = \theta_j + u(\theta_{j+1} - \theta_j)$, Equation (2.12) yields

$$\begin{cases} \quad \dfrac{d\boldsymbol{x}}{du} = (\theta_{j+1} - \theta_j)\boldsymbol{f_j}(\boldsymbol{x}, \theta_j + u(\theta_{j+1} - \theta_j)) \\ \boldsymbol{x}(0) = \boldsymbol{x}_j \end{cases} \tag{2.13}$$

Sensitivity analysis

Through the previous time change, the time interval over which (2.13) is considered is now normalized to $[0, 1]$. Then, Theorem 2.4.1 is applied on the differential system (2.13) and gives the sensitivity $\boldsymbol{\delta x}$ of the state $\boldsymbol{x}$ to the offsets $(\boldsymbol{\delta x_j}, \delta\theta_j, \delta\theta_{j+1})$ about $(\overline{\boldsymbol{x}}_j, \overline{\theta}_j, \overline{\theta}_{j+1})$ as the solution of

$$\begin{cases} \dfrac{d}{du}\boldsymbol{\delta x} = \boldsymbol{A_j}(u).\boldsymbol{\delta x} + \boldsymbol{b_j}(u)\delta\theta_{j+1} + \boldsymbol{c_j}(u)\delta\theta_j \\ \boldsymbol{\delta x}(0) = \boldsymbol{\delta x}_j \end{cases} \tag{2.14}$$

where

$$\begin{aligned} \boldsymbol{A_j}(u) &= (\overline{\theta}_{j+1} - \overline{\theta}_j)\frac{\partial \boldsymbol{f_j}}{\partial \boldsymbol{x}}(\overline{\boldsymbol{x}}, \overline{\theta}_j + u(\overline{\theta}_{j+1} - \overline{\theta}_j)) \\ \boldsymbol{b_j}(u) &= \Big[\boldsymbol{f_j}(\overline{\boldsymbol{x}}, \overline{\theta}_j + u(\overline{\theta}_{j+1} - \overline{\theta}_j)) \\ &\qquad + (\overline{\theta}_{j+1} - \overline{\theta}_j)u\frac{\partial \boldsymbol{f_j}}{\partial \theta}(\overline{\boldsymbol{x}}, \overline{\theta}_j + u(\overline{\theta}_{j+1} - \overline{\theta}_j))\Big] \\ \boldsymbol{c_j}(u) &= -\Big[\boldsymbol{f_j}(\overline{\boldsymbol{x}}, \overline{\theta}_j + u(\overline{\theta}_{j+1} - \overline{\theta}_j)) \\ &\qquad + (\overline{\theta}_{j+1} - \overline{\theta}_j)(1-u)\frac{\partial \boldsymbol{f_j}}{\partial \theta}(\overline{\boldsymbol{x}}, \overline{\theta}_j + u(\overline{\theta}_{j+1} - \overline{\theta}_j))\Big] \end{aligned} \tag{2.15}$$

We recall that $\overline{\boldsymbol{x}}$ is the solution of the differential system (2.13) (in normalized time u), or, similarly of system (2.12) (in time θ) with initial conditions $\overline{\boldsymbol{x}}_j$. The sensitivity analysis, conducted on each differential systems, gives linear differential systems on the variables $(\boldsymbol{\delta x_j})_{j\in[0,n+1]}$, and $(\delta\theta_j)_{j\in[0,n+1]}$. To simplify these linear differential equations into linear *static* equations, we use the adjoint lemma.

Adjoint lemma

Let $\boldsymbol{\gamma_j}$ be the solution of the following differential system (the choice of initial or final condition being postponed)

$$\frac{d\boldsymbol{\gamma_j}}{du} = -\boldsymbol{A_j}(u)^T\boldsymbol{\gamma_j} \tag{2.16}$$

By, the adjoint lemma (see e.g. [39])

$$\boldsymbol{\gamma_j}(1)^T\boldsymbol{\delta x_{j+1}} - \boldsymbol{\gamma_j}(0)^T\boldsymbol{\delta x_j} = \int_0^1 \boldsymbol{\gamma_j}(u)^T\boldsymbol{b_j}(u)du.\delta\theta_{j+1} + \int_0^1 \boldsymbol{\gamma_j}(u)^T\boldsymbol{c_j}(u)du.\delta\theta_j \tag{2.17}$$

The static relation (2.17) which relates the initial offsets $(\boldsymbol{\delta x_j}, \delta\theta_j)$ to the final offsets $(\boldsymbol{\delta x_{j+1}}, \delta\theta_{j+1})$ expresses the propagation of the offsets through a differential system. Depending on the choice of the initial or final conditions of system (2.16), it can take various forms. This point is exploited in the following.

2.4.2 Propagation of offsets through a series of differential systems

By definition, the transition equations (h_j) regulate the transitions between two successive differential systems. Linearizing these transition yields

$$\frac{\partial h_{j+1}}{\partial \boldsymbol{x}}(\overline{\boldsymbol{x}}(\overline{\theta}_{j+1}))\boldsymbol{\delta x_{j+1}} = \mathbf{0} \tag{2.18}$$

Finally, using Equations (2.17) and (2.18), and a judicious choice of the initial state of Equations (2.16), it is possible to get rid of the intermediate unknowns $(\boldsymbol{\delta x_j})_{j\in[\![1,n+1]\!]}$. In fact, only $\boldsymbol{\delta x_0}$ is useful because it is the initial state error

$$\boldsymbol{\delta x_0} = \frac{\partial \boldsymbol{g}}{\partial \boldsymbol{p_{ivc}}}(\overline{\boldsymbol{p}}_{\boldsymbol{ivc}})\boldsymbol{\delta p_{ivc}} \tag{2.19}$$

The following algorithm can be repeated for i ranging from 1 to n to give a static relation.

Algorithm 2.4.1. *Gathering all the Equations* (2.17) *for each system* $j \in [\![0, i]\!]$ *yields*

$$\begin{cases} \boldsymbol{\gamma_0}(1)^T\boldsymbol{\delta x_1} - \boldsymbol{\gamma_0}(0)^T\boldsymbol{\delta x_0} = \displaystyle\int_0^1 \boldsymbol{\gamma_0}(u)^T\boldsymbol{b_0}(u)du.\delta\theta_1 + \int_0^1 \boldsymbol{\gamma_0}(u)^T\boldsymbol{c_0}(u)du.\delta\theta_0 \\ \boldsymbol{\gamma_1}(1)^T\boldsymbol{\delta x_2} - \boldsymbol{\gamma_1}(0)^T\boldsymbol{\delta x_1} = \displaystyle\int_0^1 \boldsymbol{\gamma_1}(u)^T\boldsymbol{b_1}(u)du.\delta\theta_2 + \int_0^1 \boldsymbol{\gamma_1}(u)^T\boldsymbol{c_1}(u)du.\delta\theta_1 \\ \qquad\qquad\qquad\qquad\qquad\qquad\qquad\qquad ... \\ \boldsymbol{\gamma_i}(1)^T\boldsymbol{\delta x_{i+1}} - \boldsymbol{\gamma_i}(0)^T\boldsymbol{\delta x_i} = \displaystyle\int_0^1 \boldsymbol{\gamma_i}(u)^T\boldsymbol{b_i}(u)du.\delta\theta_{i+1} + \int_0^1 \boldsymbol{\gamma_i}(u)^T\boldsymbol{c_i}(u)du.\delta\theta_i \end{cases}$$

The adjoint state of the system (i) is chosen to have a final condition being

$$\boldsymbol{\gamma_i}(1) = \frac{\partial h_{i+1}}{\partial \boldsymbol{x}}(\overline{\boldsymbol{x}}(\overline{\theta}_{i+1}))^T$$

The adjoint state of every system $j \in [\![0, i-1]\!]$ *is chosen to have a final condition being (by continuity)*

$$\boldsymbol{\gamma_{j+1}}(0) = \boldsymbol{\gamma_j}(1)$$

Finally, adding the $i+1$ *equations above side by side and using Equation* (2.18)*, one obtains*

$$-\boldsymbol{\gamma_0}(0)^T\frac{\partial \boldsymbol{g}}{\partial \boldsymbol{p_{ivc}}}(\overline{\boldsymbol{p}}_{\boldsymbol{ivc}})\boldsymbol{\delta p_{ivc}} = \sum_{j=0}^{i}\int_0^1 \boldsymbol{\gamma_j}(u)^T\boldsymbol{b_j}(u)du.\delta\theta_{j+1} + \sum_{j=0}^{i}\int_0^1 \boldsymbol{\gamma_j}(u)^T\boldsymbol{c_j}(u)du.\delta\theta_j \tag{2.20}$$

This algorithm, repeated for i ranging from 1 to n, gives n static equations for the $n+2$ unknowns $(\delta\theta_j)_{j\in[\![0,n+1]\!]}$. The first system initial time shift is the known intake valve closure time shift (see again Figure 2.3)

$$\delta\theta_0 = \delta\theta_{ivc} \tag{2.21}$$

and, finally, the last system final time shift is zero since it is the desired combustion phasing control error

$$\delta\theta_{n+1} = \delta\mathrm{CA_X} = 0 \tag{2.22}$$

2.4.3 The correction as the solution of a linear system

Once gathered, equations (2.20), (2.21), and (2.22) constitute the following linear system where the unknowns are gathered in the $n+2$ dimensional vector $\boldsymbol{\delta\Theta} = (\delta\theta_0, ..., \delta\theta_{n+1})^T$

$$\boldsymbol{\Xi} \cdot \boldsymbol{\delta\Theta} = \boldsymbol{E} \cdot \begin{pmatrix} \boldsymbol{\delta p_{ivc}} \\ \delta\theta_{ivc} \end{pmatrix} \tag{2.23}$$

where

$$\boldsymbol{\Xi} = \left(\begin{array}{c|c|c} 1 & 0 & 0 \\ \hline \boldsymbol{c} & \boldsymbol{\Lambda} & \boldsymbol{b} \\ \hline 0 & 0 & 1 \end{array}\right) \tag{2.24}$$

where $\boldsymbol{b}$, $\boldsymbol{c}$, $\boldsymbol{\Lambda}$, and $\boldsymbol{E}$ are vectors and matrices detailed in Appendix C.1. Here, $\boldsymbol{b}$ is of dimension $n \times 1$, $\boldsymbol{c}$ is of dimension $n \times 1$, $\boldsymbol{\Lambda}$ is of dimension $n \times n$, and $\boldsymbol{E}$ is of dimension $(n+2) \times \dim(x_{slow})$. In fact, Equation (2.23) corresponds to Equation (2.7) for the model of the cycle presented in Section 2.3. One may remark that it is not directly invertible and that the unknown of interest, namely $\delta\theta_1$, cannot be considered separately from the other timing offsets $\delta\theta_2, \delta\theta_3, ..., \delta\theta_{n+1}$. More precisely, applying our control solution not only changes the control trigger timing but also all these other transition timings. In this thesis, no particular attention is paid to these other transition timings delays, but this could be of interest.

2.4.4 Proposed solution to the control problem

To actually compute the corrective term appearing in Equation (2.9), the second component of the vector $\boldsymbol{\delta\Theta}$ has to be determined as a function of the vector $\boldsymbol{\delta x_{slow}} = (\boldsymbol{\delta p_{ivc}}, \delta\theta_{ivc})^T$. Let q be the dimension of $\boldsymbol{\delta x_{slow}}$. A sufficient and necessary condition for the existence of this corrective term is expressed in terms of the column space of matrices $\boldsymbol{E}$ and $\boldsymbol{\Xi}$

$$\boldsymbol{E}(\mathbb{R}^q) \subset \boldsymbol{\Xi}(\mathbb{R}^{n+2})$$

For this to happen, a sufficient condition is

$$\det(\boldsymbol{\Xi}) \neq 0$$

Since $\boldsymbol{\Xi}$ is a block-matrix (see Equation (2.24)), this condition is equivalent to

$$\det(\boldsymbol{\Lambda}) \neq 0$$

We assume that this condition holds. It seems to be always the case for the combustion models we studied. The link of this property with the reachability of such models is still under investigation. In general, counter examples can be found, but not in the class of combustion models (to illustrate this, Appendix C.2 gathers two simple cases where $\det(\boldsymbol{\Lambda}) = 0$ and no trigger correction δx_{fast} can be found to compensate for any $\boldsymbol{\delta x_{slow}}$). Using the invertibility of $\boldsymbol{\Lambda}$, and thus of $\boldsymbol{\Xi}$, one easily finds the control law δx_{fast} as the second component of the solution vector of Equation (2.23). In details,

$$\delta x_{fast} \triangleq \delta\theta_{tr} = \begin{pmatrix}0 & 1 & 0 & \dots & 0\end{pmatrix} \cdot \boldsymbol{\Xi}^{-1}\boldsymbol{E} \cdot \begin{pmatrix}\delta \boldsymbol{p_{ivc}} \\ \delta\theta_{ivc}\end{pmatrix} = \begin{pmatrix}0 & 1 & 0 & \dots & 0\end{pmatrix} \cdot \boldsymbol{\Xi}^{-1}\boldsymbol{E} \cdot \delta \boldsymbol{x_{slow}} \tag{2.25}$$

This is the exact synthesis of Equation (2.9) for the sequenced differential systems; in fact, the gain of this linear control law is the

$$\boldsymbol{\alpha}(\overline{\boldsymbol{x}}_{\boldsymbol{fast}}, \overline{\boldsymbol{x}}_{\boldsymbol{slow}}) \triangleq \begin{pmatrix}0 & 1 & 0 & \dots & 0\end{pmatrix} \cdot \boldsymbol{\Xi}^{-1}\boldsymbol{E} \tag{2.26}$$

2.5 Towards a more general control solution

The presented synthesis is applicable to engine control schemes fitting into the representation of Figure 2 using continuously differentiable (C^1) right-hand sides differential equations. Two natural extensions are now proposed. The first aims at reducing the smoothness requirements for the differential systems right-hand sides. The second extension develops a more general branching scheme of the slow and fast subsystems.

2.5.1 Relaxing the smoothness requirements on the differential system right-hand sides

In the modeling process, functions of class $C^0 \cap C^1_{pc}$ (continuous and piecewise continuously differentiable) can be used rather than functions of class C^1 (continuous and differentiable) as right-hand side of the differential systems. Relaxing this smoothness requirement permits to deal with combustion models having discontinuities in their derivatives. The SI propagation flame model presented in Chapter 3 is a noticeable example.

From a theoretical viewpoint, one simply has to extend Theorem 2.4.1 to functions of class $C^0 \cap C^1_{pc}$. For this purpose, now state the following theorem

Theorem 2.5.1 (Sensitivity of a differential equation with $C^0 \cap C^1_{pc}$ right-hand side)**.** *Consider the following differential system*

$$\begin{cases} \dfrac{d}{dt}\boldsymbol{z}(t) = \boldsymbol{f}(\boldsymbol{z}(t), \boldsymbol{p_1}, t) \\ \quad \boldsymbol{z}(0) = \boldsymbol{p_2} \end{cases}$$

where $\boldsymbol{f} : \Omega \to \mathbb{R}^n$ is piecewise C^1 ($C^0 \cap C^1_{pc}$) with several continuously differentiable discontinuity hypersurfaces of the type $h(\boldsymbol{x}, \boldsymbol{p_1}, t) = 0$, and Ω is an open subset of $\mathbb{R}^n \times \mathbb{R}^k \times [0, 1]$. We denote by $\boldsymbol{z_p}$ the solution corresponding to the parameter $\boldsymbol{p} = (\boldsymbol{p_1}, \boldsymbol{p_2})$.

Let $\overline{\boldsymbol{p}}$ be such that the solution $\boldsymbol{z}_{\overline{\boldsymbol{p}}}$ crosses the discontinuity hypersurfaces in the following order: $h_1(\boldsymbol{x}, \boldsymbol{p_1}, t) = 0$ at $t = \overline{t}^s_1$, $h_2(\boldsymbol{x}, \boldsymbol{p_1}, t) = 0$ at $t = \overline{t}^s_2 > \overline{t}^s_1$, ..., $h_m(\boldsymbol{x}, \boldsymbol{p_1}, t) = 0$ at $t = \overline{t}^s_m > \overline{t}^s_{m-1}$. The preceding term "crosses" means that at time $\overline{t}^s_i$, one has

$$\frac{\partial h_i}{\partial \boldsymbol{x}}(\boldsymbol{z}_{\overline{\boldsymbol{p}}}(\overline{t}^s_i), \overline{\boldsymbol{p}}_{\boldsymbol{1}}, \overline{t}^s_i).\boldsymbol{f}(\boldsymbol{z}_{\overline{\boldsymbol{p}}}(\overline{t}^s_i), \overline{\boldsymbol{p}}_{\boldsymbol{1}}, \overline{t}^s_i) + \frac{\partial h_i}{\partial t}(\boldsymbol{z}_{\overline{\boldsymbol{p}}}(\overline{t}^s_i), \overline{\boldsymbol{p}}_{\boldsymbol{1}}, \overline{t}^s_i) \neq 0 \tag{2.27}$$

This last expression can be assumed strictly positive without loss of generality.

Then,

- *there exists a neighborhood $\mathcal{V}(\overline{\boldsymbol{p}})$ of $\overline{\boldsymbol{p}}$ such that for every $\boldsymbol{p} \in \mathcal{V}(\overline{\boldsymbol{p}})$, the differential system has a unique solution $\boldsymbol{z_p}$ that crosses the discontinuity hypersurface in the exact same order as $\boldsymbol{z}_{\overline{\boldsymbol{p}}}$ does.*

- *the application $\boldsymbol{\Gamma}$*

$$\begin{aligned} \boldsymbol{\Gamma} : \mathcal{V}(\overline{\boldsymbol{p}}) &\to ([0, 1] \to \mathbb{R}^n) \\ \boldsymbol{p} &\mapsto \boldsymbol{z_p} \end{aligned}$$

  is differentiable and its derivative in $\overline{\boldsymbol{p}}$ is the application which maps $\boldsymbol{\delta p}$ to the solution of

$$\begin{cases} \dfrac{d}{dt}\boldsymbol{\delta z}(t) = \dfrac{\partial \boldsymbol{f}}{\partial \boldsymbol{z}}(\boldsymbol{z}_{\overline{\boldsymbol{p}}}(t), \overline{\boldsymbol{p}}_{\boldsymbol{1}}, t).\boldsymbol{\delta z}(t) + \dfrac{\partial \boldsymbol{f}}{\partial \boldsymbol{p_1}}(\boldsymbol{z}_{\overline{\boldsymbol{p}}}(t), \overline{\boldsymbol{p}}_{\boldsymbol{1}}, t).\boldsymbol{\delta p_1} \\ \quad \boldsymbol{\delta z}(0) = \boldsymbol{\delta p_2} \end{cases}$$

The proof is given in Appendix D. From the Systems (2.12), one simply applies the change of time $\theta = \theta_j + u(\theta_{j+1} - \theta_j)$ to obtain the system

$$\begin{cases} \dfrac{d\boldsymbol{x}}{du} = (\theta_{j+1} - \theta_j)\boldsymbol{f_j}(\boldsymbol{x}, \theta_j + u(\theta_{j+1} - \theta_j)) \triangleq \boldsymbol{f'_j}(\boldsymbol{x}, u, \boldsymbol{p}_1) \\ \boldsymbol{x}(0) = \boldsymbol{x}_j \end{cases} \tag{2.28}$$

Now, we wish to determine conditions under which Theorem 2.5.1 can be applied. The main difficulty is to prove the "crossing" assumption stated in the theorem. If $\boldsymbol{f_j} \in C^0 \cap C^1_{pc}$, so is the right-hand side $\boldsymbol{f'_j}$ of the differential system (2.28). Note h'_j (as in the theorem statement) the discontinuity hypersurfaces of $\boldsymbol{f'_j}$ and $\overline{u}_s$ the time at which the solution given for the reference parameter $\overline{\boldsymbol{p}}_{\boldsymbol{1}} = (\overline{\theta}_{j+1}, \overline{\theta}_j)$ and $\overline{p}_2 = \overline{x}_j$ reaches $h'_j(\boldsymbol{x}, u, \boldsymbol{p_1}) = 0$. With these notations, to apply the proposed theorem, one has to verify that

$$\frac{\partial h'_j}{\partial \boldsymbol{x}}(\boldsymbol{z}_{\overline{\boldsymbol{p}}}(\overline{u}_s), \overline{\boldsymbol{p}}_{\boldsymbol{1}}, \overline{u}_s).\boldsymbol{f'_j}(\boldsymbol{z}_{\overline{\boldsymbol{p}}}(\overline{u}_s), \overline{\boldsymbol{p}}_{\boldsymbol{1}}, \overline{u}_s) + \frac{\partial h'_j}{\partial u}(\boldsymbol{z}_{\overline{\boldsymbol{p}}}(\overline{u}_s), \overline{\boldsymbol{p}}_{\boldsymbol{1}}, \overline{u}_s) \neq 0 \tag{2.29}$$

Since $\boldsymbol{f'_j}$ is obtained from $\boldsymbol{f_j}$ by a scaling and homothetic gain, the discontinuity hypersurface of both functions can be deduced from each them. Thus, $\boldsymbol{h'_j}(x, u, \boldsymbol{p_1}) = 0$ is in fact obtained from a discontinuity hypersurface $\boldsymbol{h_j}(x, \theta) = 0$. Finally, using the inverse change of time ($u \to \theta$), Equation (2.29) becomes

$$\frac{\partial h_j}{\partial \boldsymbol{x}}(\boldsymbol{z}_{\overline{\boldsymbol{p}}}(\overline{\theta}_s), \overline{\theta}_s).(\overline{\theta}_{j+1} - \overline{\theta}_j)\boldsymbol{f_j}(\boldsymbol{z}_{\overline{\boldsymbol{p}}}(\overline{\theta}_s), \overline{\theta}_s) + (\overline{\theta}_{j+1} - \overline{\theta}_j)\frac{\partial h_j}{\partial \theta}(\boldsymbol{z}_{\overline{\boldsymbol{p}}}(\overline{\theta}_s), \overline{\theta}_s) \neq 0$$

which is equivalent to

$$\frac{\partial h_j}{\partial \boldsymbol{x}}(\boldsymbol{z}_{\overline{\boldsymbol{p}}}(\overline{\theta}_s), \overline{\theta}_s).\boldsymbol{f_j}(\boldsymbol{z}_{\overline{\boldsymbol{p}}}(\overline{\theta}_s), \overline{\theta}_s) + \frac{\partial h_j}{\partial \theta}(\boldsymbol{z}_{\overline{\boldsymbol{p}}}(\overline{\theta}_s), \overline{\theta}_s) \neq 0$$

To conclude, it suffices to prove that the solutions "crosses" the discontinuity hypersurfaces for each differential equation in the sequence of the studied model, to prove that Theorem 2.5.1 can be applied on the model, and that the proposed correction computation is valid. This will be used in Chapter 3.

2.5.2 Extended branching scheme of the combustion system

In Figure 2, the entries of the look-up tables driving the x_{fast} variables and the $\boldsymbol{x_{slow}}$ variables have the same entries. This is a commonly encountered situation. For instance, in the SI and CI engine control schemes presented in Figures 1.4 and 1.9, respectively, these entries are the engine speed N_e and the driver's torque request $\overline{T}_q$. This assumption can easily been relaxed to make more actual control schemes fit into our general framework.

In fact, the entries of the x_{fast} look-up tables may be the engine speed and a variable representing the load, but which is different from the one considered up to now (the driver's torque request[6]). This situation is illustrated in Figure 2.4 on a SI engine control scheme. The only difference with the one presented earlier in Figure 1.4 is that the spark ignition timing look-up table entries are the engine speed and the estimated aspirated air mass.

[6]This variable (such as the actually produced torque (if available), intake manifold pressure or the estimated air mass) is usually an airpath variable representing the engine load.

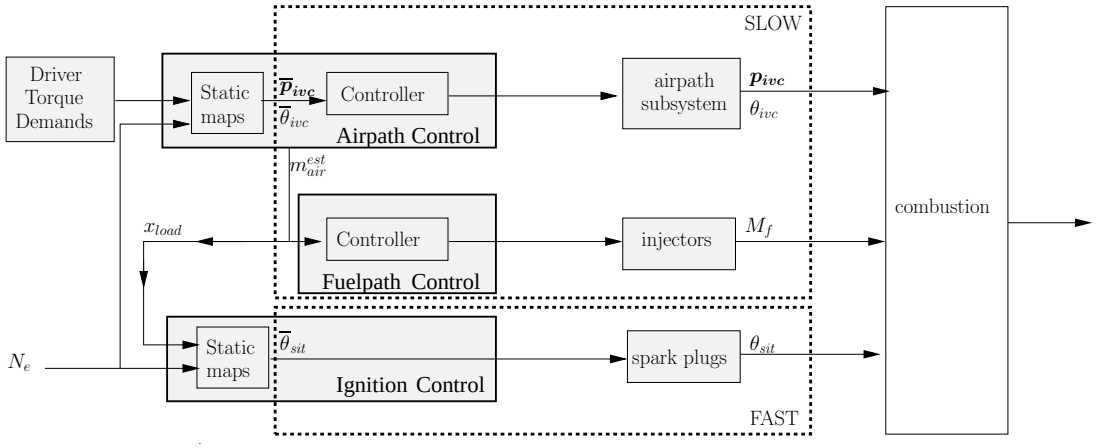

Figure 2.4: *SI engine control structure.* $\boldsymbol{p_{ivc}}$ *are the thermodynamic and physical composition in the cylinder at ivc.* $\overline{\boldsymbol{p}}_{\boldsymbol{ivc}}$ *is the steady-state mapped value of* $\boldsymbol{p_{ivc}}$*.* M_f *is the fuel mass injected.* θ_{ivc} *is the ivc timing and* $\overline{\theta}_{ivc}$*, its steady-state mapped value.* θ_{sit} *is the spark timing and* $\overline{\theta}_{sit}$*, its steady-state mapped value. The fuelpath and the ignition path are fed with an estimation of the in-cylinder air mass (*m_{air}^{est}*) usually provided by the airpath controller. The slow subsystem consists of the airpath and the fuelpath, while the fast subsystem is the ignitionpath.*

Interestingly, to account for this new branching scheme, hardly any modification in the controller synthesis needs to be performed. In fact, the only change is the point about which the linearization shall be done.

Let x_{load} be the load variable used as entry of the x_{fast} variable look-up table. It is a slow variable, such that, in the most general case, it can be a function of $\boldsymbol{x_{slow}}$, and $\overline{\boldsymbol{x}}_{\boldsymbol{slow}}$. To be as general as possible, we may add the engine speed and other variables such as the driver's torque request as well and consider that a mapping g exists such that

$$x_{load} \triangleq g(\boldsymbol{x_{slow}}, \overline{\boldsymbol{x}}_{\boldsymbol{slow}}, N_e, \overline{T}_q)$$

Now let us perform the calculus of Section 2.2 again.

In this case, the main difference is that $\overline{x}_{fast}$ and $\overline{\boldsymbol{x}}_{\boldsymbol{slow}}$ are not independent anymore. Thus, one has to account for the cross-dependencies between all variables. At steady-state, the combustion phasing is given by[7]

$$\overline{\mathrm{CA}}_{\mathrm{X}} = \mathcal{M}\left(\overline{\boldsymbol{x}}_{\boldsymbol{slow}}(N_e, \overline{T}_q), \overline{x}_{fast}(N_e, g(\overline{\boldsymbol{x}}_{\boldsymbol{slow}}, \overline{\boldsymbol{x}}_{\boldsymbol{slow}}, N_e, \overline{T}_q))\right) \tag{2.30}$$

During transients, with the correction, the combustion phasing is given by

$$\mathrm{CA}_{\mathrm{X}} = \mathcal{M}\left(\overline{\boldsymbol{x}}_{\boldsymbol{slow}}(N_e, \overline{T}_q) + \boldsymbol{\delta x_{slow}}, \overline{x}_{fast}(N_e, g(\boldsymbol{x_{slow}}, \overline{\boldsymbol{x}}_{\boldsymbol{slow}}, N_e, \overline{T}_q)) + \delta x_{fast}\right) \tag{2.31}$$

[7]As exposed in Section 2.2, the unknown modeling error are dropped in the correction calculus.

One may thus pursue the calculus developed in Section 2.2 with these expressions and find the updated correction definition

$$\delta x_{fast} = -\frac{\boldsymbol{a}}{b} \cdot \delta \boldsymbol{x_{slow}} \tag{2.32}$$

where

$$\begin{aligned}
\boldsymbol{a} = & \frac{\partial \overline{x}_{fast}}{\partial \boldsymbol{x_{load}}}(N_e, g(\overline{\boldsymbol{x}}_{\boldsymbol{slow}}, \overline{\boldsymbol{x}}_{\boldsymbol{slow}}, N_e, \overline{T}_q)) \frac{\partial g}{\partial \boldsymbol{x_{slow}}}(\overline{\boldsymbol{x}}_{\boldsymbol{slow}}, \overline{\boldsymbol{x}}_{\boldsymbol{slow}}, N_e, \overline{T}_q) \\
& + \frac{\partial \mathcal{M}}{\partial \boldsymbol{x_{slow}}}(\overline{\boldsymbol{x}}_{\boldsymbol{slow}}, \overline{x}_{fast}) \\
b = & \frac{\partial \mathcal{M}}{\partial x_{fast}}(\overline{\boldsymbol{x}}_{\boldsymbol{slow}}, \overline{x}_{fast})
\end{aligned}$$

This is a new version of Equation (2.8). One should thus update the correction derivation according to the control branching scheme. Yet, the term $\frac{\partial \overline{x}_{fast}}{\partial \boldsymbol{x_{load}}}$ which is a derivative of a look-up table could be troublesome. Rather, a change in the linearization point yields a handy simplification.

Since x_{load} is a load variable, using (N_e, x_{load}) or $(N_e, \overline{T}_q)$ as inputs of a look-up table should yield similar results. To clarify this, we assume that there is a one-to-one function $\boldsymbol{h}$ relating (N_e, x_{load}) to the variables $(N_e, \overline{T}_q)$ *when the engine is at steady-state*

$$(N_e, \overline{T}_q) = \boldsymbol{h}(N_e, x_{load}) \tag{2.33}$$

For example, if x_{load} is the driver's torque request $\overline{T}_q$, $\boldsymbol{h}$ is the identity function. If x_{load} is the actually produced torque T_q, then, since at steady-state $\overline{T}_q = T_q$, $\boldsymbol{h}$ is also the identity function. If x_{load} is the estimated aspirated air mass in the case of SI engine, then, at steady-state, it follows that the estimated air mass is the output of an airpath look-up table $MAP_{m_{air}}$ such that $m_{air}^{est} = MAP_{m_{air}}(N_e, \overline{T}_q)$ [8]. To increase the produced torque at constant engine speed, one has to increase the injected fuel and then the aspirated air mass[9]. Then, $MAP_{m_{air}}$ is one-to-one to $\overline{T}_q$, and its inverse is precisely the function $\boldsymbol{h}$. The second and third examples underline the fact that relation (2.33) only needs to be true at steady-state.

Change of the linearization point Using the function $\boldsymbol{h}$ introduced above,one can transform Equation (2.30) into

$$\overline{\mathrm{CA}}_{\mathrm{X}} = \mathcal{M}(\overline{\boldsymbol{x}}_{\boldsymbol{slow}}(\boldsymbol{h}(N_e, x_{load})), \overline{x}_{fast}(N_e, x_{load})) \tag{2.34}$$

[8] We recall that, even if the aspirated air mass is not actually controlled, it is related to the actually controlled variables by static relations. And can thus be considered as the output of a look-up table (see Section 1.3)

[9] By assumption the blend of air and fuel is stoichiometric.

Let $\breve{\boldsymbol{x}}_{\boldsymbol{slow}}(N_e, x_{load}) \triangleq \overline{\boldsymbol{x}}_{\boldsymbol{slow}}(\boldsymbol{h}(N_e, x_{load}))$. Then, Equation (2.34) writes

$$\overline{\mathrm{CA}}_{\mathrm{X}} = \mathcal{M}(\breve{\boldsymbol{x}}_{\boldsymbol{slow}}(N_e, x_{load}), \overline{x}_{fast}(N_e, x_{load})) \tag{2.35}$$

which is similar to Equation (2.4) where $\breve{\boldsymbol{x}}_{\boldsymbol{slow}}$ and x_{load} play the roles of $\overline{\boldsymbol{x}}_{\boldsymbol{slow}}$ and $\overline{T}_q$, respectively. In this situation, no cross-dependencies occurs, and one may thus finish the computation of the correction with the linearization around $\breve{\boldsymbol{x}}_{\boldsymbol{slow}}$ and $\overline{x}_{fast}$ leading to a correction

$$\delta x_{fast} \triangleq -\frac{\frac{\partial \mathcal{M}}{\partial \boldsymbol{x}_{\boldsymbol{slow}}}(\breve{\boldsymbol{x}}_{\boldsymbol{slow}}, \overline{x}_{fast})}{\frac{\partial \mathcal{M}}{\partial x_{fast}}(\breve{\boldsymbol{x}}_{\boldsymbol{slow}}, \overline{x}_{fast})} \cdot \delta \boldsymbol{x}_{\boldsymbol{slow}}, \tag{2.36}$$

where $\boldsymbol{\delta x}_{\boldsymbol{slow}} = \boldsymbol{x}_{\boldsymbol{slow}} - \breve{\boldsymbol{x}}_{\boldsymbol{slow}}$. In other words, *the only needed modification* is a change of the linearization point: Equation (2.36) is substituted to Equation (2.32) and can be compared to Equation (2.8). The correction derivation remains as-is.

Finally, one may ask whether this extension includes the branching scheme originally exposed in Chapter 1. In that case, one had $x_{load} = \overline{T}_q$ such that the function $\boldsymbol{h}$ was the identity function and that $\breve{\boldsymbol{x}}_{\boldsymbol{slow}} = \overline{\boldsymbol{x}}_{\boldsymbol{slow}}(\boldsymbol{h}(N_e, x_{load})) = \overline{\boldsymbol{x}}_{\boldsymbol{slow}}(N_e, \overline{T}_q)$. The linearization point is thus the same in both cases. However, in the general case, one may pay attention to the fact that this "new" reference variable $\breve{\boldsymbol{x}}_{\boldsymbol{slow}}$ is different (except at steady-state) from the tracked slow parameters values $\overline{\boldsymbol{x}}_{\boldsymbol{slow}}$.

2.6 Practical computations

2.6.1 Summary of the proposed method

For sake of convenience, we now summarize the procedure yielding the evaluation of the gain "α" (Equation (2.26) appearing in the control law defined in Equation (2.8). To this end, the proposed method of Section 2.4 is summarized in the following algorithm

Algorithm 2.6.1. *Construction of the corrective terms.*

1. *State the combustion model under the form of $n+1$ differential systems (as pictured in Figure 2.2). Let m be the dimension of the state $\boldsymbol{x}$.*
2. *Solve the differential systems over the whole time interval to find the reference state $\overline{\boldsymbol{x}}(\theta)$ with initial conditions being derived from $\overline{x}_{fast}$ and $\overline{\boldsymbol{x}}_{\boldsymbol{slow}}$.*
3. *Using Equations* (2.14)*, solve (numerically or by analytical integration) the $n+1$ linear differential systems of dimension m corresponding to the adjoint state and construct (matrix products) the matrix $\boldsymbol{\Xi}$ using Algorithm 2.4.1 .*
4. *Invert the $n \times n$ matrix $\boldsymbol{\Lambda}$, which directly gives the inverse of $\boldsymbol{\Xi}$.*
5. *Follow Equation* (2.25) *(matrix product) to get the corrective gain "$\boldsymbol{\alpha}$".*

2.6.2 Practical implementation

Real-time computations

In practical implementation, Algorithm 2.6.1 has to be repeated for each engine cycle because both $\overline{x}_{fast}$ and $\overline{\boldsymbol{x}}_{\boldsymbol{slow}}$ are constantly changing at every cycle and the gain "$\boldsymbol{\alpha}$" depends on it. Interestingly, although this algorithm might seem relatively time-consuming and thus non feasible in real-time, it is in fact possible to perform most of the computations off-line. In view of application, depending on the complexity of the models, two simplifications can be performed:

- If the model is simple enough, an explicit analytic expression for the gain "$\boldsymbol{\alpha}$" may be derived. In particular, this may arise from the possibility of analytical integration of the differential system representing the combustion model. This solution has been explored in [24, 28, 31], and partly used in [30].

- In a second approach, one may drastically reduce the online computation. In fact, the gain "$\boldsymbol{\alpha}$" depends on the reference parameters $\overline{x}_{fast}$ and $\overline{\boldsymbol{x}}_{\boldsymbol{slow}}$ (respectively $\breve{\boldsymbol{x}}_{\boldsymbol{slow}}$ in the case of §2.5.2). It follows from the extension presented in Section 2.5, that the values of the $\overline{\boldsymbol{x}}_{\boldsymbol{slow}}$ and of the $\overline{x}_{fast}$ depend on the same two parameters (N_e and x_{load}). Accordingly, the gain "$\boldsymbol{\alpha}$" can also be mapped in a 2D-look-up table with entries (N_e, x_{load}). The whole computation of Algorithm 2.6.1 is thus performed off-line and stored in a 2D-look-up table. Online computation of the proposed correction is thus reduced to an interpolation in a 2D-look-up table and a matrix product ($\delta x_{fast} = \boldsymbol{\alpha}(N_e, x_{load})\boldsymbol{\delta x}_{\boldsymbol{slow}}$).

The first solution is best-suited for development phases of the engine controller (when the choice of the model and the available CPU power enable this choice) while the second one can be directly implemented in commercial line engine control units since the calibration maps of the airpath and fuelpath setpoints are known and fixed.

Controller design

We now briefly summarize how the proposed corrective term is cooperating with existing controllers. The general CI engine control scheme can be upgraded with the proposed combustion controller as is depicted in Figure 2.5. This approach can be simply extended to the SI control scheme presented in Chapter 1. However, as stated in Section 2.5, the SI control features branching extensions. In details, Figure 2.6 presents the upgrade of this control scheme with the proposed correction. In both figures, the computation of the gain "$\boldsymbol{\alpha}$" has been embedded in a dark grey box.
Again, it is important to notice that

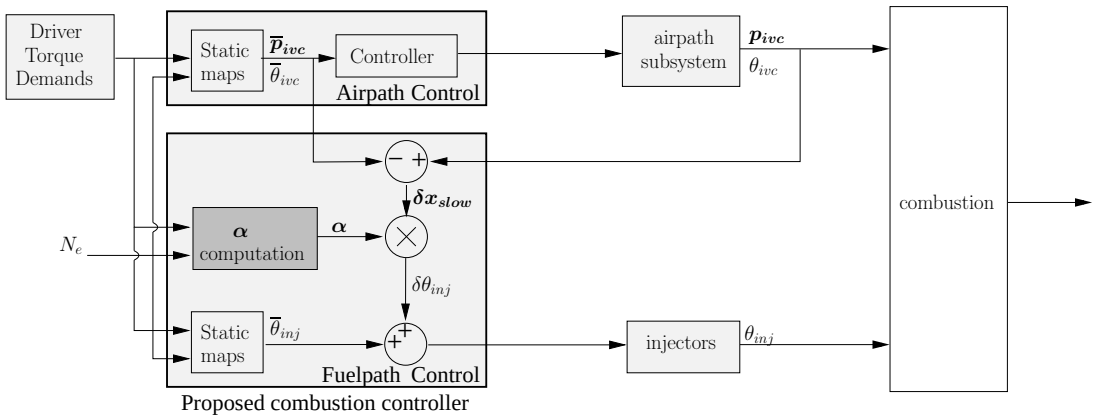

Figure 2.5: *Classic CI engine control structure complemented by the proposed combustion controller.* $\boldsymbol{p_{ivc}}$ *are the thermodynamic and physical conditions in the cylinder at ivc.* $\overline{\boldsymbol{p}}_{\boldsymbol{ivc}}$ *is the mapped steady-state value of* $\boldsymbol{p_{ivc}}$*,* θ_{ivc} *is the ivc timing and* $\overline{\theta}_{ivc}$*, its steady-state mapped value.* θ_{inj} *are the injection timing, and* $\overline{\theta}_{inj}$ *are the mapped steady-state value of* θ_{inj}*. The dark grey box implements the computation of the gain "*$\boldsymbol{\alpha}$*" of the correction.*

- no sensor nor actuator has been added in the control scheme. The proposed controller only uses sensors and actuators commonly available;
- the controller is independent from the airpath and the airpath controller structure, and does not impact on them[10];
- no other calibration than the model calibration is needed to implement the proposed strategy. The calibration effort is then strongly controlled.

2.6.3 Validation of the proposed controller

Once obtained through Algorithm 2.6.1, the controller proposed in this thesis is ready to use. Indeed, no extra-calibration (such as gain tuning) is needed apart from the model calibration. The validation of the proposed controller can thus be

[10]It is claimed that the fast subsystem controller does not have any impact on the slow subsystem. However, this is not completely true and we wish to discuss this. In fact, there exists some hardware loops such as EGR and/or turbocharger which make the airpath subsystem dependent on the exhaust thermodynamic conditions. Since the trigger chosen to control the combustion (injection timing for CI engines or ignition timing for SI engines) has a strong impact on combustion, the proposed combustion controller changes the conditions at the end of the combustion (thus during the exhaust phase), and eventually in the exhaust line, which affects the airpath subsystem.

This impact may be positive by accelerating the airpath dynamics or negative by slowing it down. This point was actually investigated, but no particular conclusion arose. Yet, we claim that the proposed controller provides corrections which are so small that this impact is negligible. To support this, one can examine the experimental results of the upcoming chapters (in particular, this point is discussed in §4.1.3).

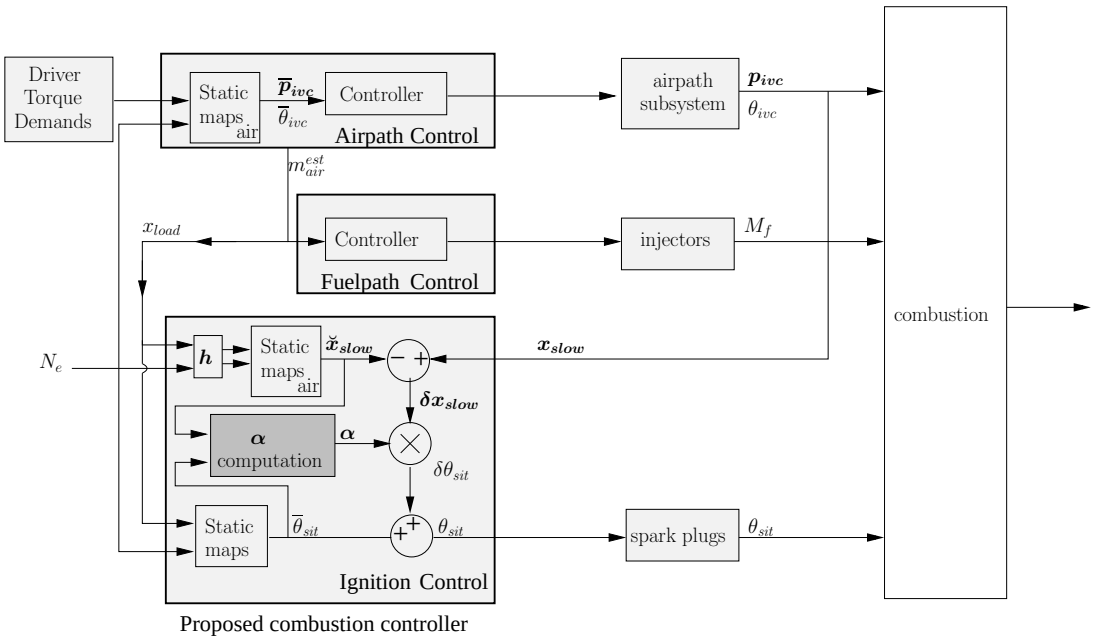

Figure 2.6: *Classic SI engine control structure complemented by the proposed combustion controller.* $\boldsymbol{p_{ivc}}$ *are the thermodynamic and physical composition in the cylinder at ivc.* $\overline{\boldsymbol{p}}_{\boldsymbol{ivc}}$ *is the steady-state mapped value of* p_{ivc}*.* θ_{ivc} *is the ivc timing and* $\overline{\theta}_{ivc}$*, its steady-state mapped value.* M_f *is the fuel mass injected.* θ_{sit} *is the spark timing and* $\overline{\theta}_{sit}$*, its steady-state mapped value. The fuelpath is fed with an estimation of the in-cylinder air mass (*m_{air}^{est}*) usually provided by the airpath controller. The slow subsystem consists of the airpath and the fuelpath, while the fast subsystem is the ignitionpath. The dark gray box implements the computation of the gain "*$\boldsymbol{\alpha}$*" of the correction.*

performed directly after the controller design. To this end, combustion phasings have to be monitored during transient operation. Appendix B gathers classic tools needed to reconstruct on-line the actual combustion phasings.

In the next two chapters, two case studies are reported in which we implement the proposed controller. In each case, the control design process is described, from the combustion modeling to the validation of the dedicated controller through simulation and experimental results.

Chapter 3

SI engine case study

In this chapter, we apply the general method we proposed in Chapter 2 for combustion control to the case of SI engines. We focus on modern SI engines which are in fact the most challenging. Typically, they are equipped with a turbocharger, direct injection, and VVT devices (see Figure 3.1). Variable Valve Timing (VVT) actuators are used in SI engines to exploit all the possibilities of direct injection and turbocharging and are of particular interest in the context of downsizing (reduction of the engine size) which has appeared as a major solution to reduce fuel consumption [43]. VVT is a particular variable Valve Actuation (VVA) system in which the valves lift profiles are not modified but only shifted in time. Beneficial effects are an additional reduction of the pumping losses and an increase of the torque performance over a range wider than the one considered on conventional (fixed valve) SI engines. Additionally, VVT systems allow an internal exhaust gas recirculation leading to a significant pollutant emissions reductions. To maximize the benefits of such technical solutions, accurate engine control is needed. Indeed, VVT and turbocharger devices extend the range of possibilities at steady-state, which in turn complexifies the transients (compared to fixed valve profile atmospheric SI engine).

As before, we assume that a functioning airpath controller is already in service (examples of such systems can be found in [48, and the reference therein]), and that the injected fuel mass is regulated to guarantee a stoichiometric combustion. The ignition timing is also assumed to be calibrated in order to have the middle of the combustion CA_{50} take place at a particular crankshaft angle which is known to yield the best efficiency (such calibration is exposed in, e.g., [15]). The (usual) branching of look-up tables is such that this case study directly fits into the extension proposed in Section 2.5. Figure 3.2 recalls the control scheme already discussed there.

The ignition timing is mapped with respect to the engine speed N_e, and the aspirated air mass. These variables are the ones impacting the most the combustion phasing. However, numerous other variables also have non negligible effects.

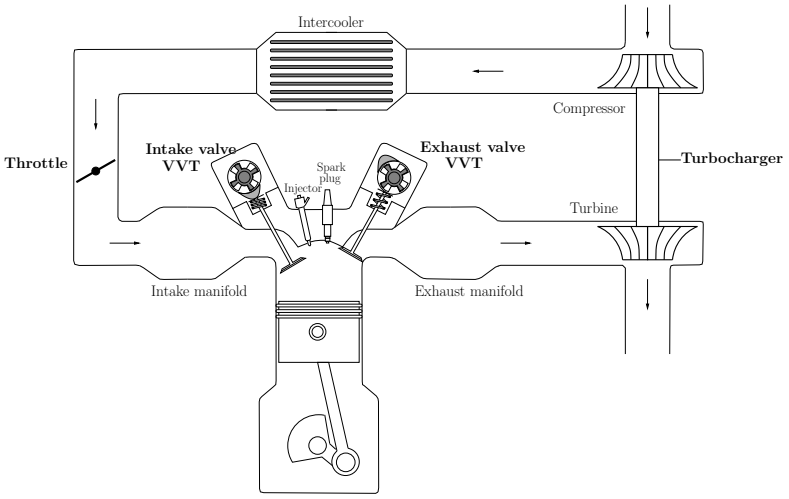

Figure 3.1: *Four cylinder SI engine with Direct injection, a turbocharger, and VVT.*

In particular, the VVT has two major effects. First, it dilutes the air charge by re-circulating burned gases, and changes the composition inside the chamber (which is represented by the BGR variable). Secondly, by shifting the valves lift profiles, the VVT changes the engine breathing and, thus, the turbulence in the chamber of the intake flow. Since, the combustion is strongly affected by the composition and the turbulence in the chamber, both variables must be accounted for in the ignition timing control.

As is stressed in Chapter 1, the produced torque is strongly affected by the temporal position of the middle of the combustion CA_{50}. In fact, the engine efficiency is optimal when the CA_{50} occurs at a particular timing noted as $\overline{\mathrm{CA}}_{50}$. Therefore, to get all the benefits of the proposed engine architecture, we focus on the middle of the combustion CA_{50}, and apply our combustion control method to have it track its optimum value $\overline{\mathrm{CA}}_{50}$. Since no look-up table of dimension greater that two can be used (for practical calibration and interpolation reasons), we propose to add a correction to the existing control scheme to account for the two discussed influencing variables (BGR and turbulence) and for other airpath driven variables such as the pressure and the temperature (these will naturally appear in the modeling part).

3.1 Combustion model

The engine setup considered in this case study is very general, and therefore, the combustion model we now detail is also very general. The correction derived from this model can be applied to any kind of SI engine at a little effort.

The engine cycle of an SI engine consists of two phases: the compression phase (from the θ_{ivc} to the ignition timing θ_{sit}) and the combustion phase (burning phase

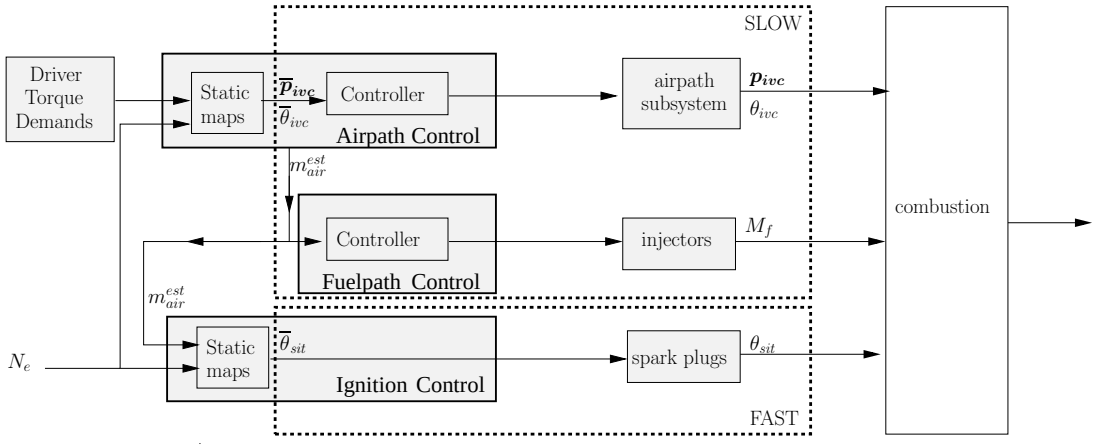

Figure 3.2: *SI engine control structure.* $\boldsymbol{p_{ivc}}$ *are the thermodynamic and physical composition in the cylinder at ivc.* $\overline{\boldsymbol{p}}_{\boldsymbol{ivc}}$ *is the steady-state mapped value of* $\boldsymbol{p_{ivc}}$*.* θ_{ivc} *is the ivc timing and* $\overline{\theta}_{ivc}$*, its steady-state mapped value.* M_f *is the fuel mass injected.* θ_{sit} *is the spark timing and* $\overline{\theta}_{sit}$*, its steady-state mapped value. The fuelpath and the ignition path are fed with an estimation of the in-cylinder air mass (*m_{air}^{est}*) usually provided by the airpath controller. The slow subsystem consists of the airpath and the fuelpath, while the fast subsystem is the ignitionpath.*

from θ_{sit} to the end of the combustion). In the exposed model, the compression phase is an isentropic compression of parameter γ. Such models have already been studied in §2.3.1. Hence, this section mostly concentrates on the combustion phase.

In SI engines, combustion is directly initiated by the spark. The combustion starts in a small region inside the cylinder (around the spark plug) and propagates through the whole chamber. The proposed combustion model is thus mainly a flame propagation model.

We now consider the flame propagation model presented in [40], which has been experimentally validated even during transients. It represents the cylinder volume as two zones (the burned zone and the unburned zone) separated by the flame front which is modeled as a thin layer (see Figure 3.3). During the combustion, the flame propagates from the burned zone towards the unburned one. The model relies on the following assumptions

- *no spatial dependencies* of the variables.
- *homogeneity* of the mixture and *pressure equilibrium* between the two zones;
- *perfect mixing* of the three gases: air, burned gases and fuel vapor;
- *stoichiometric combustion*;

The main elements appearing in the model are

- the MFB (see §3.1.1);
- the laminar burning speed of the flame front (see §3.1.2);
- the turbulent kinetic energy (see §3.1.3);
- the flame front geometry (see §3.1.4);
- the evolution of the thermodynamic states (see §3.1.6).

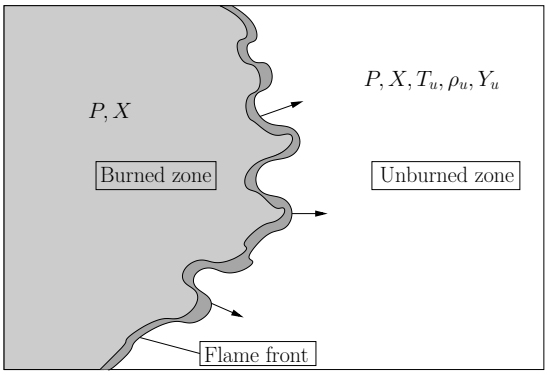

Figure 3.3: *Combustion in a SI engine combustion chamber: propagation of the flame. The flame front is represented as a thin layer (in dark grey) propagating from the burned zone (in light grey) toward the unburned zone (in white). The turbulence in the chamber wrinkles the local geometry of the flame front.*

3.1.1 Mass fraction of burned fuel x_f

The MFB, noted x_f, is defined as the ratio of the already burned fuel over the total injected fuel mass M_f. It is the most important variable in SI engine combustion modeling because it directly defines the middle of the combustion, which, by definition, is reached when $x_f = 0.5$. The dynamics of MFB is given by Equation (3.1) (see [40])

$$\frac{dx_f}{dt} = \frac{1}{M_f}.\rho_u.Y_u.U.S_{fl} \tag{3.1}$$

where M_f is the injected fuel mass, ρ_u is the mean density of the unburned gases, Y_u is the fuel mass fraction in the unburned zone, U is the laminar burning speed, and S_{fl} is the flame surface. In this equation, ρ_u and Y_u are thermodynamic conditions considered as state of the model. Their evolutions will be derived later in this chapter. We now concentrate on the laminar burning speed and on the flame surface.

3.1.2 Laminar burning speed U

The correlation of Metghalchi and Keck expresses the laminar burning speed of a flame propagating in a mixture of fresh-air burned-gases and fuel (see [23, 51])

$$U = U_0 \left(\frac{T_u}{T_{amb}}\right)^{\alpha} \left(\frac{P}{P_{amb}}\right)^{\beta} (1 - 2.1X) \tag{3.2}$$

where U_0, α and β are parameters depending on the FAR ϕ, T_u is the temperature of the unburned gases, P is the pressure in the combustion chamber, X is the Burned Gas Ratio in the cylinder (before the combustion) and P_{amb} and T_{amb} are constant parameters (normalized reference ambient pressure and temperature). Following the assumption of stoichiometric combustion, $\phi = \phi_s$ is constant, and so are U_0, α, and β. Finally, T_u , X, and P are thermodynamic conditions considered as state of the model.

3.1.3 Turbulence in the chamber

The turbulent kinetic energy mainly arises from the tumbling phenomenon observed in the chamber (because swirl motion, spray injection and squish effects can be neglected in SI engines [40]). The variations of the density of turbulent kinetic energy (noted k) are modeled by a first order differential equation driven by the tumbling energy. Formally, we have

$$\frac{dk}{d\theta} = -\frac{C_{turb}}{M_{ivc} + M_f}\frac{dE_{kin}}{d\theta} - \frac{C_{diss}}{N_e}k(\theta)$$

where C_{turb} and C_{diss} are constant positive parameters. E_{kin} is the kinetic energy associated to the tumbling which can be computed (see [40]) by assuming that the tumbling is a rotation around the longitudinal axis of the total mass of gases in the chamber considered as a cylinder (of radius R_{ad})

$$E_{kin}(\theta) = \frac{1}{2} J {N_e}^2 N^{tumble}(\theta)^2$$

The *tumbling number* N^{tumble} is a factor which is introduced to model the intake phase influence on the tumbling. It is initialized at the *ivc* as a function of the aspirated air mass m_{air} (the more air flows into the cylinder, the higher the tumble initial value is) and of the engine speed. This initial value is then stored in a steady-state look-up table $N^{tumble}_{ivc} = N^{tumble}_{emp}(m_{air}, N_e)$. After initialization, the tumble is assumed to decrease linearly until the TDC is reached

$$N^{tumble}(\theta) = N^{tumble}_{ivc} \left(\frac{\theta - \theta_{TDC}}{\theta_{IVC} - \theta_{TDC}}\right) \delta_{\theta<\theta_{TDC}}(\theta)$$

Because the rotation is performed around an horizontal axis, the inertia J is

$$J = \frac{1}{2}(M_{ivc} + M_f)R^2_{ad} = \frac{1}{8}(M_{ivc} + M_f)\frac{V(\theta)^2}{A^2}$$

Finally, with the notation $E^*_{kin} = 16A^2 \frac{E_{kin}}{(M_{ivc}+M_f){N_e}^2}$, the density of turbulent kinetic energy k is driven by the differential equation

$$\begin{cases} \dfrac{dk}{d\theta} = -\dfrac{C_{turb}{N_e}^2}{16A^2}\dfrac{dE^*_{kin}}{d\theta} - \dfrac{C_{diss}}{N_e}k(\theta) \\ E^*_{kin}(\theta) = V(\theta)^2\left(N^{tumble}_{ivc}\left(\dfrac{\theta-\theta_{TDC}}{\theta_{IVC}-\theta_{TDC}}\right)\delta_{\theta<\theta_{TDC}}(\theta)\right)^2 \\ k(\theta_{ivc}) = C_1 {N^{tumble}_{ivc}}^2 {N_e}^2 \end{cases} \tag{3.3}$$

where C_1 is a constant. Importantly, one can remark that $\frac{dE^*_{kin}}{d\theta}$ belongs to $C^0 \cap C^1_{pc}$. This implies that the right-hand side of the differential Equation (3.3) is piecewise continuously differentiable and continuous. It stresses the importance of the generalized formulation of the sensitivity result (Theorem 2.5.1) introduced in Chapter 2.

3.1.4 Flame surface S_{fl}

Following [23, 40], the flame surface is defined as the product

$$S_{fl} = S_{geo}.W_t.f_{wall} \tag{3.4}$$

where S_{geo} is the geometric surface of the flame, W_t represents the surface wrinkling, and f_{wall} is the wall destruction term. We now detail how these three variables are computed.

Geometric surface S_{geo}

The geometric surface is a macroscopic measure of the flame surface which neglects the wrinkling phenomenon. To obtain this surface, a first step is to express the surface as a function of the volume of the flame. In [40], the proposed flame geometry provides a geometrical surface which evolution is not smooth with respect to its volume. Rather, we assume the following:

- at the beginning of the combustion, the flame has a spherical shape;
- when its diameter equals the distance from the piston to the cylinder-head (defined as $V(\theta)/A$ where A is the cylinder-head area and V is the cylinder volume), the flame becomes a truncated sphere from which two spherical caps are cut-off (see Figure 3.4).

Analytically, the geometric surface is defined as a function of the flame volume V_{fl} (defined below in Equation (3.6)) and of the crankangle θ as

$$S_{geo}(V_{fl},\theta) = \begin{cases} \sqrt[3]{36\pi}.{V_{fl}}^{2/3} & \text{if } V_{fl} < \frac{\pi}{6}\left(\frac{V(\theta)}{2A}\right)^3 \\ 2\sqrt{2\pi V_{fl}\frac{V(\theta)}{2A} + \frac{4}{3}\pi^2\left(\frac{V(\theta)}{2A}\right)^4} & \text{if } V_{fl} > \frac{\pi}{6}\left(\frac{V(\theta)}{2A}\right)^3 \end{cases} \tag{3.5}$$

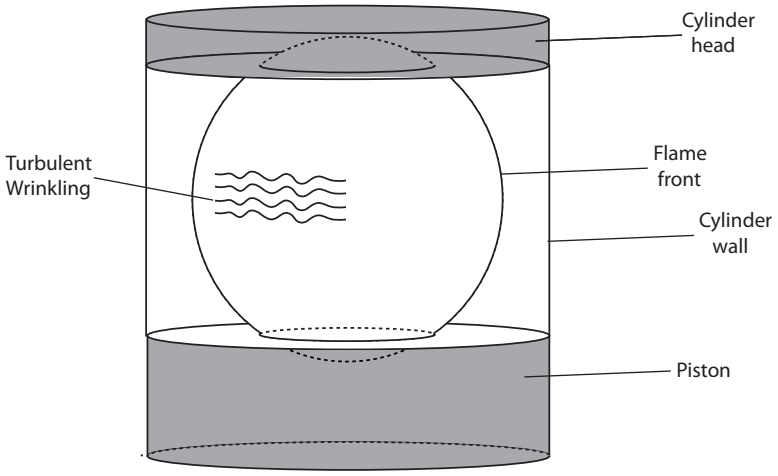

Figure 3.4: *Flame shape during propagation. Eventually, two caps are cut-off from the spherical surface.*

The function S_{geo} is a continuous function with piecewise continuous derivativess with respect to its inputs ($S_{geo} \in C^0 \cap C^1_{pc}$) depending on the engine characteristics (through the piston head surface A and the volume $V(\theta)$).

Eventually, the flame volume V_{fl} is computed from the MFB x_f and the unburned zone density ρ_u. Let V_u and M_u be the unburned zone volume and total mass, then, by definition of Y_u, and the assumption of homogeneity of the mixture, one has

$$\begin{aligned} V_{fl} &= V - V_u \\ &= V - M_u.\frac{1}{\rho_u} \\ &= V - \frac{M_f - m_f}{Y_u}\frac{1}{\rho_u} \\ &= V - \frac{M_f - m_f}{M_f}\frac{M_{ivc} + M_f}{\rho_u} \\ &= V - (1 - x_f)\frac{M_{ivc} + M_f}{\rho_u} \end{aligned} \tag{3.6}$$

To model the spark initiation of the flame (which starts in a small volume), this value is only considered when the flame volume has reached a minimal value V_{fl}^{min}; if not, the flame volume value is set to V_{fl}^{min}. The geometrical surface is thus

$$V_{fl} = S_{geo}\left(\max\left(V_{fl}^{min}, V(\theta) - (1 - x_f)\frac{M_{ivc} + M_f}{\rho_u}\right), \theta\right) \tag{3.7}$$

where S_{geo} is defined in Equation (3.5).

Wrinkling W_t

The wrinkling of the flame surface is due to the turbulent kinetic energy k. It increases the actual flame surface. At the beginning of the combustion, the flame is too small to be wrinkled, W_t is then equal to one. As the flame gets wider, W_t increases, meaning that the flame is wrinkled by the turbulent kinetic energy k. A typical model for W_t is (see [40])

$$W_t = 1 + sigm(V_{fl})\frac{\sqrt{k}}{U} \tag{3.8}$$

where $sigm$ is a scaled sigmoïd function (e.g. tanh), and U is defined in Equation (3.2). Together with Equation (3.3), Equation (3.8) forms the model for the wrinkling W_t.

Wall destruction term f_{wall}

The wall destruction term f_{wall} accounts for the reduction of the flame surface when it reaches the chamber walls. Then, f_{wall} is close to 1 during the first part of the combustion, dropping smoothly to 0 when the flame approaches the walls. In our control approach, we aim at controlling the CA_{50}. The model is not used after the CA_{50}. Thus, the simplifying assumption that the wall destruction term is 1 from the *ivc* to the CA_{50} can be considered at almost no expense

$$f_{wall} = 1 \tag{3.9}$$

In summary, the three terms defining the flame surface S_{fl} in Equation (3.4) are defined in Equations (3.5), (3.8), and Equation (3.9), respectively.

3.1.5 Flame propagation model

Note $C_2 = \frac{U_0}{{T_{amb}}^{\alpha}{P_{amb}}^{\beta}}$ and $C_3 = -\frac{C_{turb}}{16A^2}$ two constants. Once gathered, Equations (3.1), (3.2), (3.5), (3.7), (3.8), and (3.3) allow to express the flame propagation model

$$\begin{cases} \dfrac{dx_f}{d\theta} = \dfrac{1}{N_e}\dfrac{\rho_u Y_u}{M_f}\left(C_2 T_u^{\alpha} P^{\beta}(1-2.1X) + sigm(V_{fl})\sqrt{k}\right) S_{geo}(V_{fl},\theta) \\ \qquad \text{where} \quad V_{fl} = \max\left(V_{fl}^{min}, V(\theta) - (1-x_f)\dfrac{M_{ivc}+M_f}{\rho_u}\right) \\ x_f(\theta_{sit}) = 0 \end{cases} \tag{3.10}$$

$$\begin{cases} \dfrac{dk}{d\theta} = C_3 {N_e}^2 \dfrac{dE^*_{kin}}{d\theta} - \dfrac{C_{diss}}{N_e}k(\theta) \\ \qquad \text{where} \quad E^*_{kin}(\theta) = V(\theta)^2\left(N_{ivc}^{tumble}\left(\dfrac{\theta-\theta_{TDC}}{\theta_{IVC}-\theta_{TDC}}\right)\delta_{\theta<\theta_{TDC}}(\theta)\right)^2 \\ k(\theta_{ivc}) = C_1 {N_{ivc}^{tumble}}^2 {N_e}^2 \end{cases} \tag{3.11}$$

In this model, several thermodynamic states appear in the right hand sides. Their dynamics are computed in the next section.

3.1.6 thermodynamic state dynamics

The thermodynamic states under consideration are the pressure in the chamber P, the BGR X, the unburned zone temperature T_u, its density ρ_u, and its fuel mass fraction Y_u. Because of the homogeneity assumption, Y_u, and X are constant during the compression phase and the combustion phase

$$\frac{dY_u}{d\theta} = \frac{dX}{d\theta} = 0$$

During the compression phase

The isentropic compression assumption yields:

$$\begin{aligned}
\frac{dP}{d\theta} &= -\gamma P \frac{dV(\theta)}{d\theta}\frac{1}{V(\theta)} \\
\frac{dT_u}{d\theta} &= -(\gamma-1)T \frac{dV(\theta)}{d\theta}\frac{1}{V(\theta)} \\
\frac{d\rho_u}{d\theta} &= -\rho_u \frac{dV(\theta)}{d\theta}\frac{1}{V(\theta)} \\
\frac{dY_u}{d\theta} &= 0 \\
\frac{dX}{d\theta} &= 0
\end{aligned} \tag{3.12}$$

The initialization of these thermodynamic conditions at the *ivc* is

$$\begin{aligned}
P(\theta_{ivc}) &= P_{ivc} \\
T_u(\theta_{ivc}) &= T_{ivc} \\
\rho_u(\theta_{ivc}) &= \frac{M_{ivc}+M_f}{V_{ivc}} \\
Y_u(\theta_{ivc}) &= \frac{M_f}{M_{ivc}+M_f} \\
X(\theta_{ivc}) &= X_{ivc}
\end{aligned} \tag{3.13}$$

During the combustion phase

The pressure rise due to the fuel heat release is obtained from the classic relation [23]

$$V\frac{dP}{d\theta} + \gamma P \frac{dV}{d\theta} = (\gamma-1)Q_{LHV}M_f\frac{dx_f}{d\theta}, \tag{3.14}$$

where Q_{LHV} is the fuel energy per mass unit. During the combustion, the unburned zone is compressed by the expansion of the flame. Neglecting wall heating losses, and the heat exchange between the burned gases zone and the unburned gases zone leads to consider an isentropic compression of the unburned gases with the same isentropic parameter γ than during the compression phase. Then, the temperature evolution and density evolution in the unburned zone can be inferred from the pressure using the isentropic relations $T_u P^{\frac{1-\gamma}{\gamma}} = cst$, and $\rho_u / P^{1/\gamma} = cst$

$$\begin{aligned}
\frac{dP}{d\theta} &= -\gamma \frac{P}{V}\frac{dV}{d\theta} + \frac{\gamma - 1}{V} Q_{LHV} M_f \frac{dx_f}{d\theta} \\
\frac{dT_u}{d\theta} &= -(\gamma - 1)\frac{T_u}{V}\frac{dV}{d\theta} + \frac{(\gamma-1)^2}{\gamma}\frac{T_u}{PV} Q_{LHV} M_f \frac{dx_f}{d\theta} \\
\frac{d\rho_u}{d\theta} &= -\frac{\rho_u}{V}\frac{dV}{d\theta} + \frac{\gamma - 1}{\gamma}\frac{\rho_u}{PV} Q_{LHV} M_f \frac{dx_f}{d\theta} \\
\frac{dY_u}{d\theta} &= 0 \\
\frac{dX}{d\theta} &= 0
\end{aligned} \tag{3.15}$$

where $\frac{dx_f}{d\theta}$ arises from Equation (3.10).

Parameters appearing in the right hand side

As appears in Equation (3.11), the dynamics of the turbulence k is a function of both parameters θ_{ivc}, and N_{ivc}^{tumble}. These parameters are slow parameters that have to be accounted for in the correction computation of corrective terms. To this end, two trivial states $x_{\theta_{ivc}}$, and x_{tumble} are introduced

$$\begin{cases} \dfrac{dx_{\theta_{ivc}}}{d\theta} = 0 \\ x_{\theta_{ivc}}(\theta_{ivc}) = \theta_{ivc} \end{cases} \quad \text{and} \quad \begin{cases} \dfrac{dx_{tumble}}{d\theta} = 0 \\ x_{tumble}(\theta_{ivc}) = N_{ivc}^{tumble} \end{cases} \tag{3.16}$$

These new states can replace θ_{ivc}, and N_{ivc}^{tumble} in the right-hand sides of the differential equation (3.11).

Similarly, two new states $x_{M_{ivc}}$ and x_{M_f} with trivial dynamics replace M_{ivc} and M_f which do not appear anymore in the right hand side of the differential Equation (3.10).

3.1.7 The combustion model

Eventually, Equations (3.10), (3.11), (3.12), and (3.13) constitute a combustion model divided into two parts: a compression phase and a combustion phase separated by the ignition trigger. The whole state of the system is

$$\boldsymbol{x} = (x_f, k, P, T_u, \rho_u, Y_u, X, x_{\theta_{ivc}}, x_{tumble})^T$$

Its evolution is given by these differential equations, reproduced here for convenience under the form of a sequence of 2 differential systems.

i) initialization $\theta = \theta_{ivc}$

$$\begin{cases} x_f(\theta_{ivc}) = 0 \\ k(\theta_{ivc}) = C_1 {N_{ivc}^{tumble}}^2 {N_e}^2 \\ P(\theta_{ivc}) = P_{ivc} \\ T_u(\theta_{ivc}) = T_{ivc} \\ \rho_u(\theta_{ivc}) = \dfrac{M_{ivc} + M_f}{V_{ivc}} \\ Y_u(\theta_{ivc}) = \dfrac{M_f}{M_{ivc} + M_f} \\ X(\theta_{ivc}) = X_{ivc}, x_{\theta_{ivc}}(\theta_{ivc}) = \theta_{ivc}, x_{tumble}(\theta_{ivc}) = N_{ivc}^{tumble} \\ x_{M_{ivc}}(\theta_{ivc}) = M_{ivc}, x_{M_f}(\theta_{ivc}) = M_f \end{cases} \tag{3.17}$$

ii) compression phase from θ_{ivc} to θ_{sit}, $\theta_{ivc} \leq \theta \leq \theta_{sit}$

$$\begin{cases} \dfrac{dx_f}{d\theta} = 0 \\ \dfrac{dk}{d\theta} = C_3 {N_e}^2 \dfrac{dE^*_{kin}}{d\theta} - \dfrac{C_{diss}}{N_e} k(\theta) \\ \quad \text{where} \quad E^*_{kin}(\theta) = V(\theta)^2 \left(x_{tumble} \left(\dfrac{\theta - \theta_{TDC}}{x_{\theta_{ivc}} - \theta_{TDC}} \right) \delta_{\theta < \theta_{TDC}}(\theta) \right)^2 \\ \dfrac{dP}{d\theta} = -\gamma P \dfrac{dV(\theta)}{d\theta} \dfrac{1}{V(\theta)} \\ \dfrac{dT_u}{d\theta} = -(\gamma - 1) T \dfrac{dV(\theta)}{d\theta} \dfrac{1}{V(\theta)} \\ \dfrac{d\rho_u}{d\theta} = -\rho_u \dfrac{dV(\theta)}{d\theta} \dfrac{1}{V(\theta)} \\ \dfrac{dY_u}{d\theta} = 0, \dfrac{dX}{d\theta} = 0, \dfrac{dx_{\theta_{ivc}}}{d\theta} = 0, \dfrac{dx_{tumble}}{d\theta} = 0, \dfrac{dx_{M_{ivc}}}{d\theta} = 0, \dfrac{dx_{M_f}}{d\theta} = 0 \end{cases} \tag{3.18}$$

iii) combustion phase from θ_{sit}, $\theta_{sit} \leq \theta$

$$\begin{cases} \dfrac{dx_f}{d\theta} = \dfrac{1}{N_e}\dfrac{\rho_u Y_u}{x_{M_f}}\left(C_2 T_u^{\alpha} P^{\beta}(1-2.1X) + sigm(V_{fl})\sqrt{k}\right) S_{geo}(V_{fl},\theta) \\ \qquad \text{where} \quad V_{fl} = \max\left(V_{fl}^{min}, V(\theta) - (1-x_f)\dfrac{x_{M_{ivc}} + x_{M_f}}{\rho_u}\right) \\ \dfrac{dk}{d\theta} = C_3 {N_e}^2 \dfrac{\partial E_{kin}^*}{\partial \theta} - \dfrac{C_{diss}}{N_e} k(\theta) \\ \qquad \text{where} \quad E_{kin}^*(\theta) = V(\theta)^2 \left(x_{tumble}\left(\dfrac{\theta - \theta_{TDC}}{x_{\theta_{ivc}} - \theta_{TDC}}\right)\delta_{\theta<\theta_{TDC}}(\theta)\right)^2 \\ \dfrac{dP}{d\theta} = -\gamma\dfrac{P}{V}\dfrac{dV}{d\theta} + \dfrac{\gamma-1}{V} Q_{LHV} x_{M_f} \dfrac{dx_f}{d\theta} \\ \dfrac{dT_u}{d\theta} = -(\gamma-1)\dfrac{T_u}{V}\dfrac{dV}{d\theta} + \dfrac{(\gamma-1)^2}{\gamma}\dfrac{T_u}{PV} Q_{LHV} x_{M_f} \dfrac{dx_f}{d\theta} \\ \dfrac{d\rho_u}{d\theta} = -\dfrac{\rho_u}{V}\dfrac{dV}{d\theta} + \dfrac{\gamma-1}{\gamma}\dfrac{\rho_u}{PV} Q_{LHV} x_{M_f} \dfrac{dx_f}{d\theta} \\ \dfrac{dY_u}{d\theta} = 0, \dfrac{dX}{d\theta} = 0, \dfrac{dx_{\theta_{ivc}}}{d\theta} = 0, \dfrac{dx_{tumble}}{d\theta} = 0, \dfrac{dx_{M_{ivc}}}{d\theta} = 0, \dfrac{dx_{M_f}}{d\theta} = 0 \end{cases} \tag{3.19}$$

For sake of readability, $\frac{dx_f}{d\theta}$ has not been replaced by its value in the right hand side of the evolution of $\frac{dP}{d\theta}$, $\frac{dT_u}{d\theta}$, $\frac{d\rho_u}{d\theta}$. The slow variables influencing the combustion are the following

$$\mathbf{x_{slow}} = (P_{ivc}, T_{ivc}, V_{ivc}, X_{ivc}, M_{ivc}, M_f, N_{ivc}^{tumble}, \theta_{ivc})^T$$

All these parameters can be computed using measured or estimated signals. In details,

- P_{ivc} is equal to the measured intake manifold pressure at the *ivc*. This statement relies on the assumption that a pressure equilibrium is reached at the *ivc* between the cylinder and the intake manifold;
- T_{ivc} can be computed using the measured fresh air temperature and a burned gases temperature model;
- V_{ivc} is the cylinder volume at *ivc*. It is known very accurately;
- X_{ivc}, and M_{ivc} can be obtained using an appropriate cylinder filling model (see [4, 45]);
- N_{ivc}^{tumble} is the influence of the intake phase on the turbulence. It is obtained through an empirical relation $N_{ivc}^{tumble} = N_{emp}^{tumble}(m_{air}, N_e)$;
- M_f is the injected fuel. It can be computed from the air mass thanks to the stoichiometric assumption;

- θ_{ivc} is the *ivc* crankshaft angle. It is solely dependent on the VVT actuators positions which are measured with good accuracy.

3.2 Controller design

We now apply the combustion control method proposed in Chapter 2 on the presented model (3.17), (3.18), and (3.19). First, we study the regularity of the right-hand sides of the differential equations, and, then, we detail the control derivation.

3.2.1 A piecewise continuously differentiable model

The right-hand sides of the differential systems (3.18) and (3.19) are not continuously differentiable. In fact, they are only piecewise continuously differentiable and continuous ($C^0 \cap C^1_{pc}$) so that they can fit into the extension proposed in Section 2.5.1. We now check that the main assumption of Theorem 2.5.1, namely, the "crossing" assumption for each of both systems holds.

In these systems, two discontinuity hypersurfaces exists. The first one is $\theta - \theta_{TDC} = 0$. It appears in both systems. In fact, this relation holds only once but, depending on the ignition timing, it may be during compression or combustion. With the notations of Section 2.5.1, note $h(\boldsymbol{x}) = \theta - \theta_{TDC}$. One has to prove that the "crossing" equation holds. Since $\frac{\partial h}{\partial \boldsymbol{x}} = 0$ and $\frac{\partial h}{\partial \theta} = 1$, the conclusion is obvious.

The second discontinuity hypersurface only appears during combustion. It is given by

$$V_{min} - V(\theta) - (1 - x_f)\frac{x_{M_{ivc}} + x_{M_f}}{\rho_u} = 0$$

Again, note

$$h(\boldsymbol{x}, \theta) = V_{min} - V(\theta) - (1 - x_f)\frac{x_{M_{ivc}} + x_{M_f}}{\rho_u}$$

Simple computations show that the "crossing" equation is, in this case, equivalent to

$$-\frac{dV}{d\theta}(\theta_s) + \frac{x_{M_{ivc}}(\theta_s) + x_{M_f}(\theta_s)}{\rho_u(\theta_s)}\left(\frac{dx_f}{d\theta}(\theta_s) + \frac{1 - x_f(\theta_s)}{\rho_u(\theta_s)}\frac{d\rho_u}{d\theta}(\theta_s)\right) \neq 0, \quad (3.20)$$

where $\overline{\theta}_s$ is the crankshaft angle at which the solution to the differential system reaches the discontinuity hypersurface $h(\boldsymbol{x}, \theta) = 0$. The fact that the equation above never vanishes for the differential systems (3.18) and (3.19) can be verified numerically.

Finally, one should verify that both discontinuity hypersurfaces cannot be reached at the same time. Since the first discontinuity hypersurface is only $\theta - \theta_{TDC} = 0$, the crossing of this first relation only happens at time $\theta_s = \theta_{TDC}$.

Because, at this particular time, $\frac{dV}{d\theta}(\theta_{TDC}) = 0$, one get from the combustion phase differential system that the right-hand side of Equation (3.20) writes

$$\frac{x_{M_{ivc}}(\theta_s) + x_{M_f}(\theta_s)}{\rho_u(\theta_s)} \frac{dx_f}{d\theta}(\theta_s) \left(1 + (1 - x_f(\theta_s)) \frac{\gamma - 1}{\gamma} \frac{1}{P(\theta_s)T(\theta_s)} Q_{LHV} x_{M_f}(\theta_s)\right),$$

which is always positive ($0 < x_f < 1$ and $1 < \gamma$). Thus, both discontinuity hypersurfaces cannot be reached at the same time and the sensitivity Theorem for $C^0 \cap C^1_{pc}$ functions applies. One may now safely derive the correction from the model.

3.2.2 Derivation of the correction

First, let us focus on the particular characteristics of the studied engine and on its model. As noted in Section 1.3, static relations exist between the components of the vector $\boldsymbol{x_{slow}}$. These are

1. by assumption, the stoichiometric combustion is guaranteed $M_{ivc} = \frac{\phi_s}{1 - X_{ivc}} M_f$;
2. the ideal gas relation holds $P_{ivc}V_{ivc} = (M_{ivc} + M_f)RT_{ivc}$;
3. the volume relation holds $V_{ivc} = V(\theta_{ivc})$;
4. the tumble initialization depends on the aspirated air mass through an empirical look-up table $N^{tumble}_{ivc} = N^{tumble}_{emp}(m_{air}, N_e)$ (this is a modeling assumption).

Consequently, from the whole $\boldsymbol{x_{slow}}$ variables which are 8, only 4 are independent and are actually controlled by the actual slow variables (airpath and fuelpath) controller. The $\boldsymbol{x_{slow}}$ look-up table $MAP_{slow}(N_e, \overline{T}_q)$ is thus of dimension 4. In the following, we consider (without loss of generality) that the four independent variables are $P_{ivc}, \theta_{ivc}, T_{ivc}$ and X_{ivc}.

Finally, two questions remain to be answered: first, what is the reference value of the $\boldsymbol{x_{slow}}$ parameters with respect to which the correction shall be computed, and, secondly, what is the final form of the correction. Both questions were already answered in Section 2.5. The correction is

$$\delta\theta_{sit} = \boldsymbol{\alpha}(N_e, m^{est}_{air}) \cdot \boldsymbol{\delta x_{slow}}, \tag{3.21}$$

where $\boldsymbol{\delta x_{slow}} = \boldsymbol{x_{slow}} - \breve{\boldsymbol{x}}_{\boldsymbol{slow}}$, and $\boldsymbol{\alpha}$ are computed about the linearization point $(\breve{\boldsymbol{x}}_{\boldsymbol{slow}}, \overline{x}_{fast})$. One has to compute $\breve{\boldsymbol{x}}_{\boldsymbol{slow}}$.

In Section 2.5, $\breve{\boldsymbol{x}}_{\boldsymbol{slow}}$ is defined as the steady-state corresponding to the actual value of the entries of the fast parameters look-up table

$$\breve{\boldsymbol{x}}_{\boldsymbol{slow}}(N_e, x_{load}) = \overline{\boldsymbol{x}}_{\boldsymbol{slow}}(\boldsymbol{h}(N_e, m^{est}_{air})) \tag{3.22}$$

where $\boldsymbol{h}$ is the inverse of the air mass look-up table. The control scheme is depicted in Figure 2.6.

3.3 Results

3.3.1 Simulation setup

The proposed strategy, which takes the form of Equation (3.21), is validated on the simulation software AMESim [36]. The combustion model used in the simulator is presented in [40], and has been validated in [42] for engine control purposes. Basically, this simulation model is similar to the one presented in Section 3.1. Yet, wall heating losses are now taken into account and the flame geometrical shape is slightly different (see Section 3.1.4).

To simulate transients, the $\boldsymbol{x_{slow}}$ parameters were varied around a particular working point. As stated in the previous section, 4 static relations naturally exists between the slow variables. Since transients are simulated around a working point, the engine speed and the driver's torque request $\overline{T}_q$ are kept constant. The outputs of the slow look-up tables are thus constant. This gives $4 + 1 = 5$ static relations on the slow variables, which, once differentiated, gives 5 static relations on the slow variables offsets. The $\boldsymbol{\delta x_{slow}}$ parameters is thus generated with only $8-5 = 3$ independent parameters. We choose the following ones: the in-cylinder pressure at *ivc* P_{ivc}, the BGR at *ivc* X_{ivc}, and the *ivc* crankshaft angle θ_{ivc}. Transients are then simulated by creating artificial offsets on these three variables, the other components of the offsets vector are computed following the 5 discussed static relations.

3.3.2 Simulation results

Figure 3.5 reports simulation results. We simulate transient operations by creating arbitrary offsets on the $\mathbf{x_{slow}}$ parameters around a fixed working point. The evolution of the most significant part (x_f, P) of the state is depicted in Figures 3.5(a) and 3.5(b) for three particular combustions:

- The black curve represents the reference combustion. It has been obtained for a reference spark timing $\overline{\theta}_{sit}$, and, thus, defines the reference $\overline{\text{CA}_{50}}$ (about 369°CA on the considered point).

- The blue dashed curves corresponds to the combustion resulting from the introduction of the previously discussed offsets. In this case, no *sit* correction is used. One can see in Figure 3.5(a) that the CA_{50} significantly drifts away from its reference value.

- The red dotted curves corresponds to the same combustion in which we have activated the proposed *sit* correction (see Equation (3.21)). The resulting CA_{50} can be seen in Figure 3.5(a). The error between the actual and the reference CA_{50} has been drastically reduced.

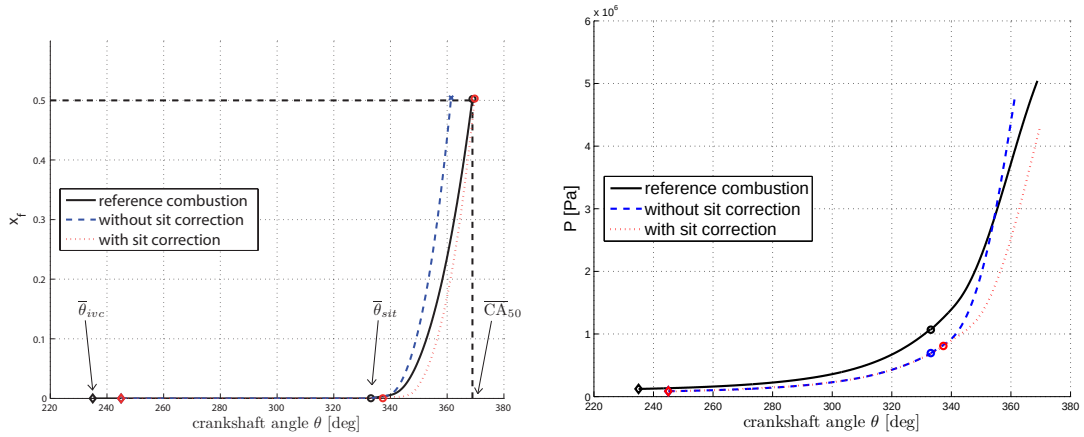

(a) x_f (b) $P(\theta)$

Figure 3.5: *Simulation results: MFB (state x_f in the model) and pressure P. Black curve: reference combustion, blue dashed curve: combustion with parameters offsets without sit correction, red dotted curve: combustion with the same parameters offsets and with sit correction. In (a) and (b), "◇" marks the θ_{ivc}, and "o" marks the spark initiation.*

An extensive exploration of the possible offsets has been conducted to validate the proposed correction. More precisely, every possible offset about the same reference values ($\overline{P}_{ivc} = 1.22\ 10^5$ Pa, $\overline{\theta}_{ivc} = 235$°CA, $\overline{X}_{ivc} = 0.18$) was tested with and without the proposed correction. For sake of readability, the variations are conducted with only 2 of the 3 variables at a time while the last one is kept constant. In Figures 3.6, 3.7, and 3.8, the absolute CA_{50} error is plotted against the variations of the different parameters, with and without the proposed correction. In these figures, only physically sound results are plotted. For instance, the tested variation may lead to a too low value of T_{ivc} (through the static relations discussed above) and is thus considered as an artifact that can not be observed in the reality. It is then blanked in the presented figures.

These figures clearly show that the proposed correction manages to considerably reduce the offsets between the optimal middle of the combustion CA_{50} and the actual one. With the proposed correction, the middle of the combustion is kept within a 2°CA neighborhood of the optimal one whatever the slow parameters errors are.

3.4 Conclusion

In this study on SI engines, we have proven that a phenomenological model can be used to compute open-loop spark timing correction to control the CA_{50}. Validation of this correction has been carried out in simulation on the AMESim

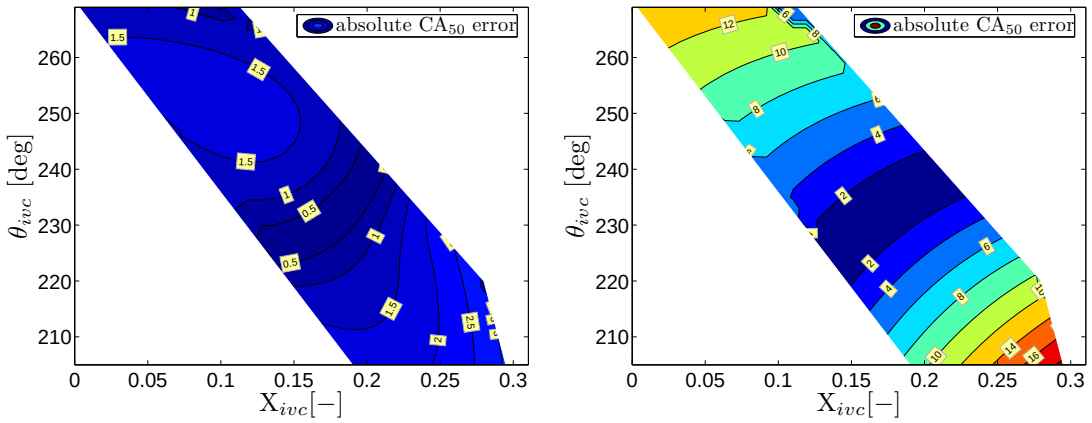

(a) with the correction (b) without the correction

Figure 3.6: *Simulation results: impact on the absolute CA_{50} error of variations of X_{ivc} and of θ_{ivc} about their reference values ($\overline{X}_{ivc} = 0.18$, $\overline{\theta}_{ivc} = 235° CA$) while keeping constant $\overline{P}_{ivc} = 1.22\ 10^5$ Pa. The same color scale is used with and without the correction. No data are plotted when the variations are not physically possible. With the proposed correction, the middle of the combustion is kept much closer from its optimal value.*

platform. Results show that the proposed method effectively permits to control the CA_{50} closer to its reference value. Again, the main advantage of the proposed method is that *it does not require any in-cylinder sensor.*

The next step is to validate this correction on experimental test-benches. This is the subject of on-going work. Based on the simulation results, one can expect improvements in experimental transient operations. On the other hand, interactions of the proposed correction with the knock phenomenon should be investigated since it is a limiting factor when dealing with spark ignition time control.

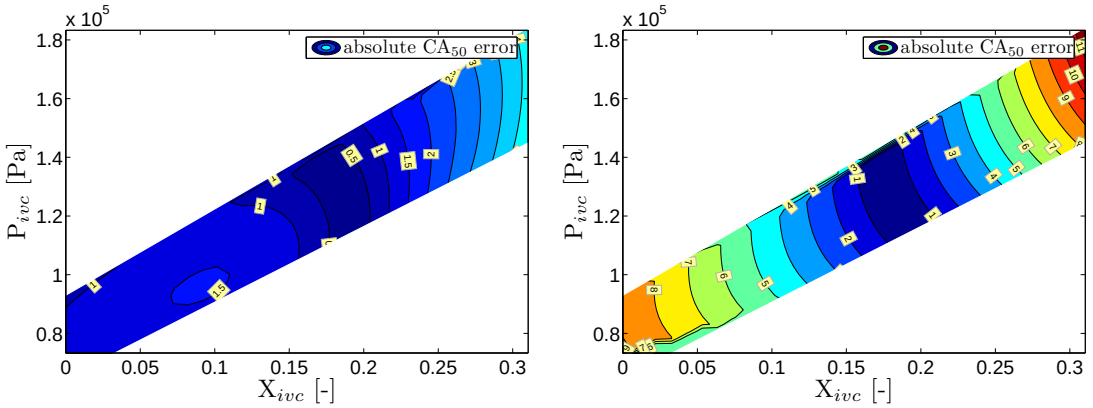

(a) with the correction (b) without the correction

Figure 3.7: *Simulation results: impact on the absolute CA_{50} error of variations of X_{ivc} and of P_{ivc} about their reference values ($\overline{X}_{ivc} = 0.18$, $\overline{P}_{ivc} = 1.22\ 10^5$ Pa) while keeping constant $\overline{\theta}_{ivc} = 235°CA$. The same color scale is used with and without the correction. No data are plotted when the variations are not physically possible. With the proposed correction, the middle of the combustion is kept much closer from its optimal value.*

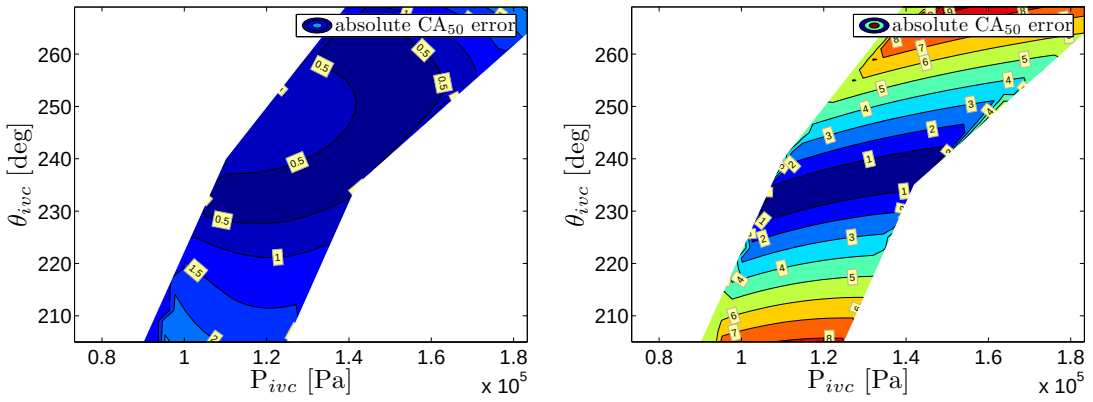

(a) with the correction (b) without the correction

Figure 3.8: *Simulation results: impact on the absolute CA_{50} error of variations of X_{ivc} and θ_{ivc} about their reference values ($\overline{P}_{ivc} = 1.22\ 10^5$ Pa, $\overline{\theta}_{ivc} = 235°CA$) while keeping constant $\overline{X}_{ivc} = 0.18$. The same color scale is used with and without the correction. No data are plotted when the variations are not physically possible. With the proposed correction, the middle of the combustion is kept much closer from its optimal value.*

Chapter 4

CI engine case studies

In this chapter, we apply the general method we proposed in Chapter 2 to the case of Compression Ignition engines. The most representative engine of the CI family is the Diesel engine. Its combustion, which is produced from a mixture of air, fuel and burned gases, may take various forms depending on the injection strategy and on the ratio of dilution under consideration (being represented by the BGR variable). We consider, without loss of generality, that the combustion phasing to control is the same in all cases: it is the middle of the combustion CA_{50}. In this chapter, two case studies are reported. They mainly differ in the employed injection mode.

The first study focuses on a mono-pulse injection Diesel engine which is made complex by the presence of a very sensitive combustion, namely the cool flame. Experimental results obtained on a test-bench and on a vehicle shows the relevance of the approach.

The second study addresses a multi-pulse injection Diesel engine. The injection pattern increases the number of available degrees of freedom at the expense of an increased complexity of the combustion process. While not directly fitting in the proposed one-trigger method of Chapter 2, simple assumptions permit to deduce a very similar strategy. In details, the whole injection pattern is delayed (or advanced) by a single control trigger. This approach does not exploit all the available degrees of freedom, but leads to quite encouraging test-bench results.

4.1 Diesel mono-pulse highly diluted case

In this first case study, a mono-pulse Diesel engine is considered. Its main characteristics is that the air charge is highly diluted by burned gas (the BGR can be as large as 40%) and that the injection is achieved in one single injection of mass M_f. Consequently, this case directly fit in the framework developed in Chapter 1. The intake and exhaust valve are fixed so that the *ivc* timing remains constant ($\theta_{ivc} = cst$). The goal of the combustion controller is to guarantee an accurate control of the middle of the combustion.

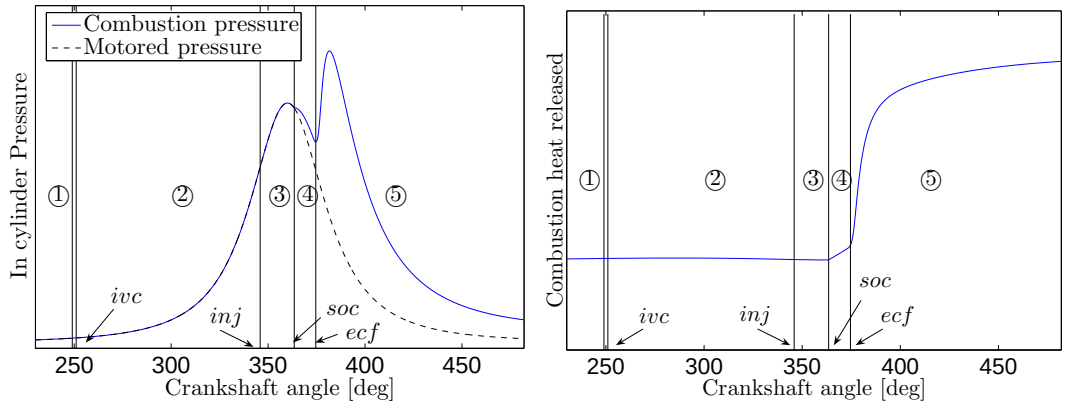

Figure 4.1: *Cycle for highly diluted Diesel: schematic in-cylinder pressure during one engine cycle and associated heat released: ①, cylinder filling; ②, compression; ③, auto-ignition; ④, cool flame; ⑤, combustion and expansion; ivc, intake valve closure; inj, injection; soc, start of combustion; and ecf, end of cool flame* ($360°\,CA$ *corresponds to the top dead center).*

During the cylinder compression phase, fuel is injected, and mixed with the compressed air and burned gas mixture. The fuel vaporizes and eventually auto-ignites after the so-called auto-ignition delay. Due to the high dilution, a cool flame [6, 11, 58] precedes the standard combustion. In fact, the cool flame is one main particularity of Diesel highly diluted engines[1]. Figures 4.1 depicts the typically observed in-cylinder pressure histories and the associated combustion heat released (MFB) during one cycle.

Sensitivity to airpath parameters By contrast with conventional Diesel combustion, highly diluted combustion is very sensitive to slight offsets of the initial cylinder conditions (such as pressure, temperature, and composition). Figures 4.2 and 4.3 stress the impact of variations in the intake manifold conditions (pressure and composition) on combustion phasings. In these experiments, the airpath parameters are changed one by one (either the intake manifold pressure or the BGR). These experiments clearly show that, while the auto-ignition delay slightly varies (especially when the BGR is varied), the most sensitive phenomenon happens between the start of combustion and the CA_{10}: it is the cool flame.

Choice of the control objective Diffusion combustion does not need consideration because it is only very slightly impacted by thermodynamic conditions. Thus, regulating the instant at which the cool-flame period ends (θ_{ecf}) seems to be sufficient to control the mid-point of combustion (CA_{50}) while decreasing the modeling complexity (no model is needed between the end of the cool flame and

[1]It may take other name such as pre-mixed combustion.

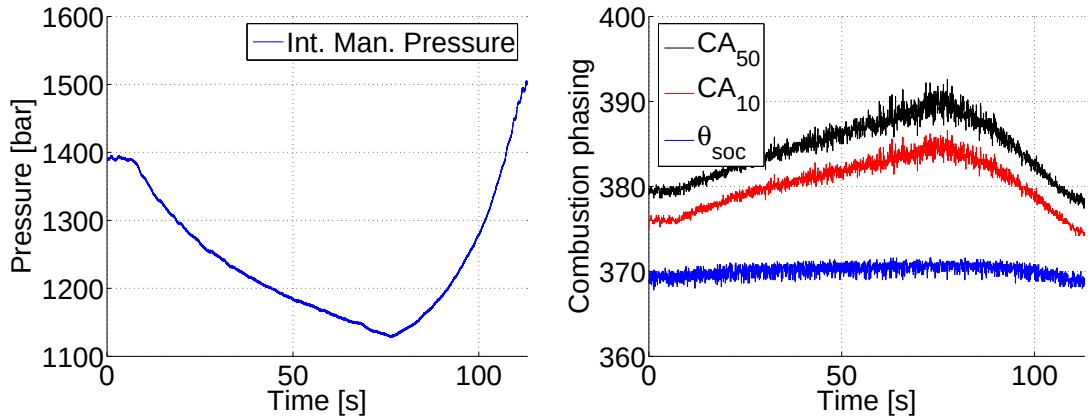

(a) Pressure (b) Combustion phasing

Figure 4.2: *Experimental results obtained for a HCCI Diesel engine at 2330 rpm. Influence of the intake manifold pressure on combustion phasings (keeping the other parameters constant).*

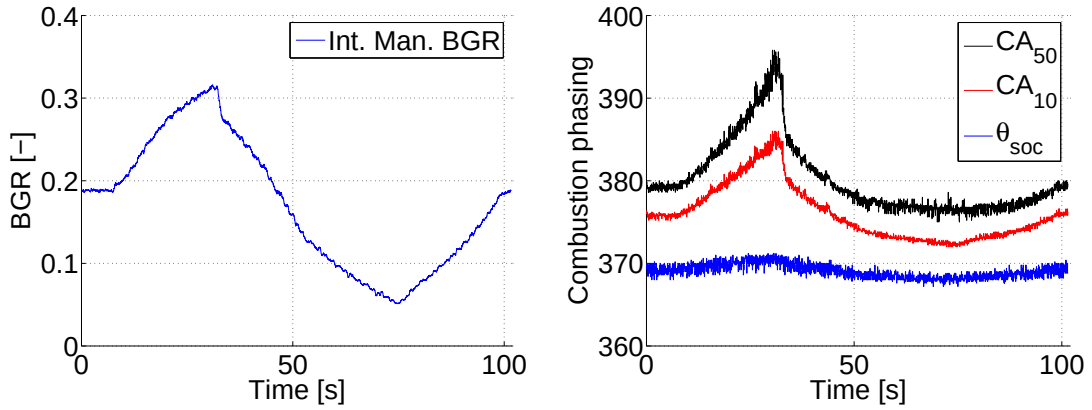

(a) BGR (b) Combustion phasings

Figure 4.3: *Experimental results obtained for a HCCI Diesel engine at 2330 rpm with a fixed injection pattern. Influence of the intake manifold burned gas ratio on combustion phasings (keeping the other parameters constant).*

the middle of combustion). Eventually, this assumption will be supported by the experimental results provided at the end of this section.

The engine cycle consists of three phases (compression, auto-ignition, and cool flame). It is depicted in Figure 4.4. These phases are separated by the start of injection θ_{inj}, the start of combustion θ_{soc}, and the end of the cool-flame period θ_{ecf}, respectively.

Since the valve distribution is fixed (i.e. θ_{ivc} is constant), the $\boldsymbol{x_{slow}}$ variables only include the thermodynamic conditions at *ivc*.

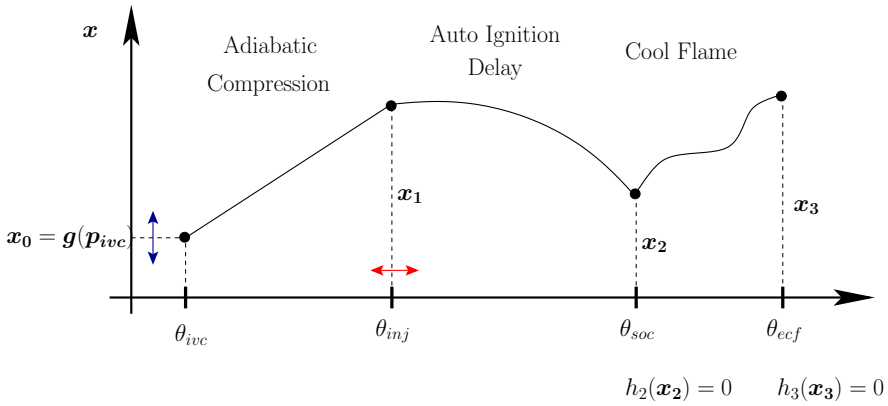

Figure 4.4: *Model of the mono-pulse Diesel cycle. θ_{inj} denotes the start of injection (control trigger), θ_{soc} the start of combustion, θ_{ecf} the end of the cool-flame period, θ_{ivc} the intake valve closure, and $\boldsymbol{p_{ivc}}$ all the necessary airpath-driven parameters. θ_{inj} updates are used to compensate for mismatches in the $\boldsymbol{p_{ivc}}$ parameters*

4.1.1 Combustion model

We now detail the two models used for the auto-ignition and cool flame phenomena. They will be used to relate the start of injection time θ_{inj} to the CA_{50}.

Auto-ignition model

The auto-ignition duration for a fuel/air/burned gas mixture is usually modeled with a Knock Integral Model (KIM) [23, 49, 63]. We will use such a model yielding an implicit relation between θ_{inj}, θ_{soc} and physical in-cylinder parameters such as $P(\theta)$, $T(\theta)$ and X (the air/fuel ratio ϕ can be also considered). It is usually found under the integral form

$$\int_{\theta_{inj}}^{\theta_{soc}} \mathcal{A}^{ai}(\boldsymbol{p}(\theta))\frac{d\theta}{N_e} \quad = \quad 1,$$

where $\mathcal{A}^{ai}$ is an Arrhenius function, and $\boldsymbol{p}(\theta) = (P(\theta), T(\theta), X)^T$. The control strategy proposed here can be used with any (piecewise continuously differentiable) function $\mathcal{A}^{ai}$. Barba et al. [6] adapted a phenomenological model for conventional Diesel applications

$$\begin{aligned} \boldsymbol{p}(\theta) &= (P(\theta), T(\theta), \phi) \\ \mathcal{A}^{ai}(\boldsymbol{p}(\theta)) &= c_1 \phi^{c_2} \left(\frac{P(\theta)}{P_{ref}}\right)^{c_3} \exp\left(-\frac{T_A}{T(\theta)}\right), \end{aligned} \tag{4.1}$$

where c_1, c_2, c_3, P_{ref}, and T_A are constant parameters. Swan et al. [63] used the following Arrhenius function

$$\begin{aligned} \boldsymbol{p}(\theta) &= (P(\theta), T(\theta), X, \phi) \\ \mathcal{A}^{ai}(\boldsymbol{p}(\theta)) &= \frac{\phi^x}{(C_1 + C_2 X)} \exp\left(-b\frac{P(\theta)^n}{T(\theta)}\right), \end{aligned} \tag{4.2}$$

where x, C_1, C_2, b and n are constant parameters. Lafossas et al. [41] extended the KIM to high BGR configurations. Then, this proposed model detailed below is suitable for highly diluted combustion such as HCCI. In details, one has

$$\begin{aligned} \boldsymbol{p}(\theta) &= (P(\theta), T(\theta), X)^T \\ \mathcal{A}^{ai}(\boldsymbol{p}(\theta)) &= \frac{A_1}{1 + C_1 X} P(\theta)^{n_1} \exp\left(-\frac{T_1}{T(\theta)}\right), \end{aligned} \tag{4.3}$$

where A_1, C_1, n_1, and T_1 are constant positive parameters (see Section 4.1.1 for their calibration). This model is used throughout this chapter and, in practice, for experiments.

Cool flame model

In a cool flame, combustion occurs at a very low reaction rate. Several chemical processes take place simultaneously, and, eventually, lead to the actual combustion. By analogy with the auto-ignition model, the cool flame duration can be represented with a KIM. The main in-cylinder parameters affecting the cool flame phenomenon are the pressure, the temperature, the composition (BGR), and the available fuel mass (which is in fact the injected fuel mass, since no injection is performed during the cool flame). The proposed model is

$$\int_{\theta_{soc}}^{\theta_{ecf}} \mathcal{A}^{cf}(\boldsymbol{p}(\theta), M_f) \frac{d\theta}{N_e} = 1,$$

where $\boldsymbol{p}(\theta) = (P(\theta), T(\theta), X)^T$, and $\mathcal{A}^{cf}$ is an Arrhenius function

$$\mathcal{A}^{cf}(\boldsymbol{p}(\theta), M_f) = \frac{A_2\ (M_f)^{q_2}}{1 + C_2 X} P(\theta)^{n_2} \exp\left(-\frac{T_2}{T(\theta)}\right), \tag{4.4}$$

where A_2, C_2, n_2, q_2, and T_2 are positive parameters (see Appendix 4.1.1 for their calibration).

Models calibration

In Equations (4.3) and (4.4) the parameter sets (A_1, C_1, n_1, T_1) and (A_2, C_2, n_2, q_2, T_2) can be obtained using a classic optimization process. To calibrate both sets, 100 working points were selected. They correspond to representative

variations of pressure, temperature, BGR, and injection timing for four different engine speeds (1000, 1500, 2000 and 2500 rpm).

Classic combustion analysis was carried out for each working point using cylinder pressure histories as presented in Appendix B (these sensors being available for the development engine test bed). This analysis allows to accurately determine of the actual start of combustion and the actual end of the cool flame. These results constitute the reference database used in the rest of this case-study.

Optimization-based calibration procedures were then carried out independently on the auto-ignition model and on the cool flame model. The global representativeness of the models is pictured in Figure 4.5, in which model predictions (the two models (4.3) and (4.4) being used sequentially) are compared to the reference database. There is a relatively good agreement between the experimental data and the model predictions.

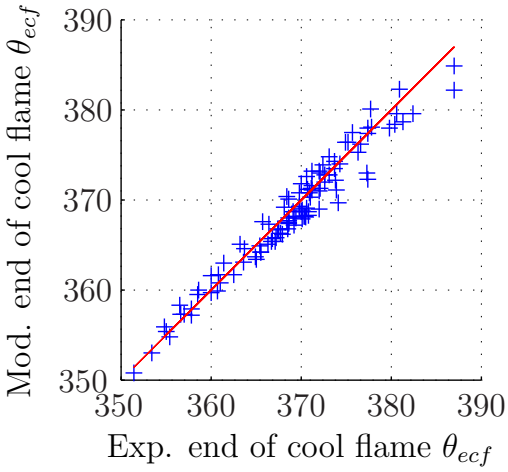

Figure 4.5: *Calibration of the auto-ignition and cool flame models: modeled vs. experimental ecf. 100 points were used to calibrate the model.*

4.1.2 Controller design

Statement of the cycle model

Both the auto-ignition model (4.3) and the cool-flame model (4.4) write under the form of implicit integrals over the crankshaft angle. These models can be simply expressed as differential equations using two artificial states τ_{ai} and τ_{cf}:

$$\begin{cases} \dfrac{d\tau_{ai}}{d\theta} = \dfrac{A_1}{1 + C_1 X} P(\theta)^{n_1} \exp\left(-\dfrac{T_1}{T(\theta)}\right) \dfrac{1}{N_e} \\ \tau_{ai}(\theta_{inj}) = 0 \end{cases} \tag{4.5}$$

and

$$\begin{cases} \dfrac{d\tau_{cf}}{d\theta} = \dfrac{A_2\ (M_f)^{q_2}}{1+C_2X} P(\theta)^{n_2} \exp\left(-\dfrac{T_2}{T(\theta)}\right) \dfrac{1}{N_e} \\ \tau_{cf}(\theta_{soc}) = 0 \end{cases} \tag{4.6}$$

Then, the transition from the auto-ignition phase to the cool-flame phase is defined as

$$\tau_{ai}(\theta) = 1,$$

and, the end of the cool-flame phase is defined as

$$\tau_{cf}(\theta) = 1.$$

The state gathering the variables needed to represent the three phases (compression, auto-ignition, and cool flame) is then

$$\boldsymbol{x} = (P, T, X, \tau_{ai}, \tau_{cf}), \tag{4.7}$$

the initial state of the first differential equation is

$$\boldsymbol{x_0} = (P_{ivc}, T_{ivc}, X_{ivc}, 0, 0), \tag{4.8}$$

and finally, the evolution of the state during the three considered phases is [2]

i) Compression:

$$\boldsymbol{f_0}(\boldsymbol{x}, \theta) = \begin{pmatrix} -\gamma P \dfrac{dV(\theta)}{d\theta} \dfrac{1}{V(\theta)} \\ -(\gamma-1)T \dfrac{dV(\theta)}{d\theta} \dfrac{1}{V(\theta)} \\ 0 \\ 0 \\ 0 \end{pmatrix} \tag{4.9}$$

ii) Auto ignition:

$$\boldsymbol{f_1}(\boldsymbol{x}, \theta) = \begin{pmatrix} -\gamma P \dfrac{dV(\theta)}{d\theta} \dfrac{1}{V(\theta)} \\ -(\gamma-1)T \dfrac{dV(\theta)}{d\theta} \dfrac{1}{V(\theta)} \\ 0 \\ \dfrac{A_1}{1+C_1X} P(\theta)^{n_1} \exp\left(-\dfrac{T_1}{T(\theta)}\right) \dfrac{1}{N_e} \\ 0 \end{pmatrix} \tag{4.10}$$

[2] We recall that f_i is the right-hand side of the ith differential system of the sequence.

iii) Cool flame:

$$\boldsymbol{f_2}(\boldsymbol{x},\theta) = \begin{pmatrix} -\gamma P \dfrac{dV(\theta)}{d\theta}\dfrac{1}{V(\theta)} \\ -(\gamma-1)T\dfrac{dV(\theta)}{d\theta}\dfrac{1}{V(\theta)} \\ 0 \\ 0 \\ \dfrac{A_2\ (M_f)^{q_2}}{1+C_2X}P(\theta)^{n_2}\exp\left(-\dfrac{T_2}{T(\theta)}\right)\dfrac{1}{N_e} \end{pmatrix} \tag{4.11}$$

Correction computation

Equations (4.8), (4.9), (4.10), and (4.11) constitute the cycle model as described in Chapter 2. The strategy proposed in Section 2.4 can be directly applied to this case. It gives the gain $\boldsymbol{\alpha}$ of the correction as a function of the entries of the fuelpath look-up table which, as explained in §2.6.2, can me mapped as a function of the engine speed and the drivers torque request. This gives

$$\delta\theta_{inj} = \boldsymbol{\alpha}(N_e, \overline{T}_q)\cdot(\delta P_{ivc}, \delta T_{ivc}, \delta X_{ivc})^T \tag{4.12}$$

Furthermore, thanks to the particular form of the differential systems, one may simplify the expressions and obtain an explicit analytic expression. The interested reader can refer to [31], or to the Appendix E where analogous manipulations are reported.

Relating *ivc* values to available measurements

The values $(P_{ivc}, T_{ivc}, X_{ivc})$ are the airpath driven variables of interest in this application because they appear in the preceding model initial conditions (Equation (4.8)). However, in common engine setups, there exists no sensor directly measuring any of these values since they are in-cylinder thermodynamic conditions. Interestingly, they can be directly related to the intake manifold conditions $(P_{int}, T_{int}, X_{int})$, which are classically measured or observed, from simple calculations relying on classic assumptions. The cylinder pressure at *ivc* is assumed to equal the intake manifold pressure right before the *ivc*. This assumption is supported by the fact that the pressure equilibrium is reached at the *ivc* between the intake manifold and the cylinder. The cylinder temperature at *ivc* is reconstructed from the intake manifold temperature (measured) and the volumetric efficiency (usually mapped) via the ideal gas law (in the following equation M_{ivc} is the mass of gas trapped in the cylinder)

$$\left\{\begin{array}{lcl} P_{ivc} &=& P_{int} \\ \eta_{vol} &=& M_{ivc}\frac{RT_{int}}{P_{int}V_{cyl}} \\ M_{ivc} &=& \frac{P_{ivc}V_{ivc}}{RT_{ivc}} \end{array}\right. \quad \text{and, then} \quad \left\{\begin{array}{lcl} P_{ivc} &=& P_{int} \\ T_{ivc} &=& \frac{V_{ivc}}{V_{cyl}}\frac{T_{int}}{\eta_{vol}} \end{array}\right.$$

Finally, the BGR at *ivc*, X_{ivc}, is assumed to equal the BGR in the intake manifold X_{int}, neglecting then in cylinder residual burned gases in the estimation of X_{ivc}[3].

Finally, the intake manifold conditions $(P_{int}, T_{int}, X_{int})$ are inferred either from measurements (using temperature and pressure sensors in the intake manifold) or from an observer (the reader can refer to [9], e.g., where such an observer for X_{int} is described). Thanks to these considerations, the *ivc* parameters $(P_{ivc}, T_{ivc}, X_{ivc})$ can be considered as known functions of the intake manifold conditions.

4.1.3 Results on a test-bench

Experimental set-up

All experimental results presented here were obtained on a four-cylinder direct injection Diesel engine running in HCCI combustion mode. It is pictured in Figure 4.6. Its specifications are listed in Table 4.1. The engine is an upgrade of a turbocharged multi-cylinder commercial engine. A low-pressure EGR circuit is used to extract hot burned gases downstream of the turbine to introduce them upstream of the compressor. A valve allows the EGR to be controlled. Finally, both the air and the EGR circuits include a cooler to keep the intake manifold temperature at approximately 330 K.

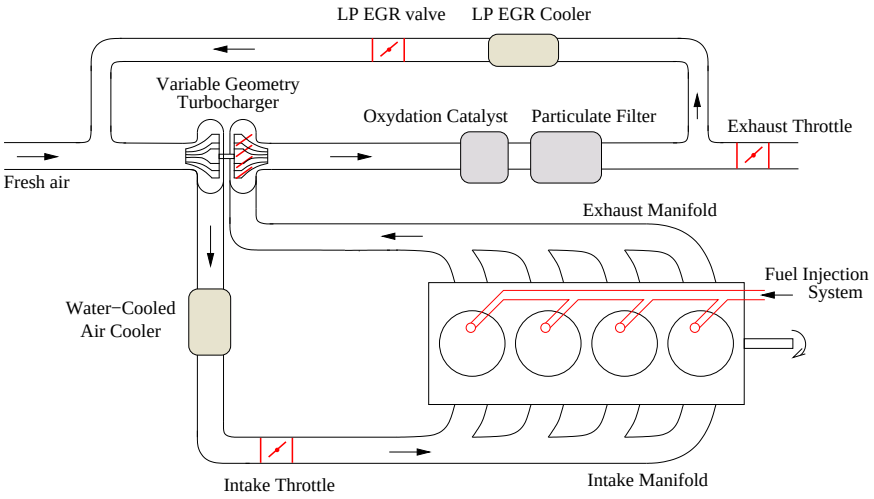

Figure 4.6: *Four-cylinder HCCI Diesel engine with direct injection, low-pressure EGR recirculation and a turbocharger. High BGR values are used to dilute the mixture before combustion.*

Since the intake manifold temperature is almost constant (within an error of 10 K) in the engine set-up, the experimental results only reflect the adaptation of the fuelpath to pressure and BGR regulation errors.

[3]Slight errors are thus made on the estimation of the real in cylinder conditions.

Bore × stroke	87.0 × 92.0 mm
Number of cylinders	4
Compression ratio	14:1
Displacement	2.2 l
Injection device	Solenoid
Maximum injection pressure	1600 bar
Piston bowl design	NADI^{TM} [68]
Intake valve closure	$\theta_{ivc} = 232°$
	(360°CA is top dead center)

Table 4.1: *Diesel engine set-up*

Experimental results

Figures 4.7, 4.8 and 4.9 show the experimental results obtained on the presented test-bench for three torque variations at constant engine speed. For comparison, the plots show the same trajectory with (blue lines) and without (red lines) the proposed correction. For all three scenarios, the torque trajectory is shown in part (a). As mentioned in Section 1.2, the airpath control regulates the intake manifold pressure and BGR around their reference values to meet the torque demand (parts (b) and (c)). Non-instantaneous tracking of the airpath reference values induces the new fuelpath controller to correct the reference value for the injection crankshaft angle (part (d)). The injection crankshaft angle sent to the injectors is then different from its reference value. The influence of the proposed combustion control on engine noise is shown in part (e) of the figures, and the evolution of the middle of the combustion process in part (f).

Increasing torque trajectory (tip-ins) Figure 4.7 shows an increasing torque trajectory at a constant engine speed of 1500 rpm. During these transients, without any particular combustion control, combustion is drastically delayed (see the second and third transients in Figure 4.7(f)). In response, the proposed controller modifies the start of injection to bring the combustion forward. In fact, the correction slows down the start of injection to compensate for the airpath dynamics. The result appears clearly in Figure 4.7(f). The middle of the combustion closely follows the corresponding reference steps, and the large overshoots have disappeared. Improvements in engine noise are also evident in Figure 4.7(e), in fact, the noise transients are smoothed out. This results in significant enhancements of the acoustic comfort[4].

[4]The driver is much more disturbed by variations than by the noise level.

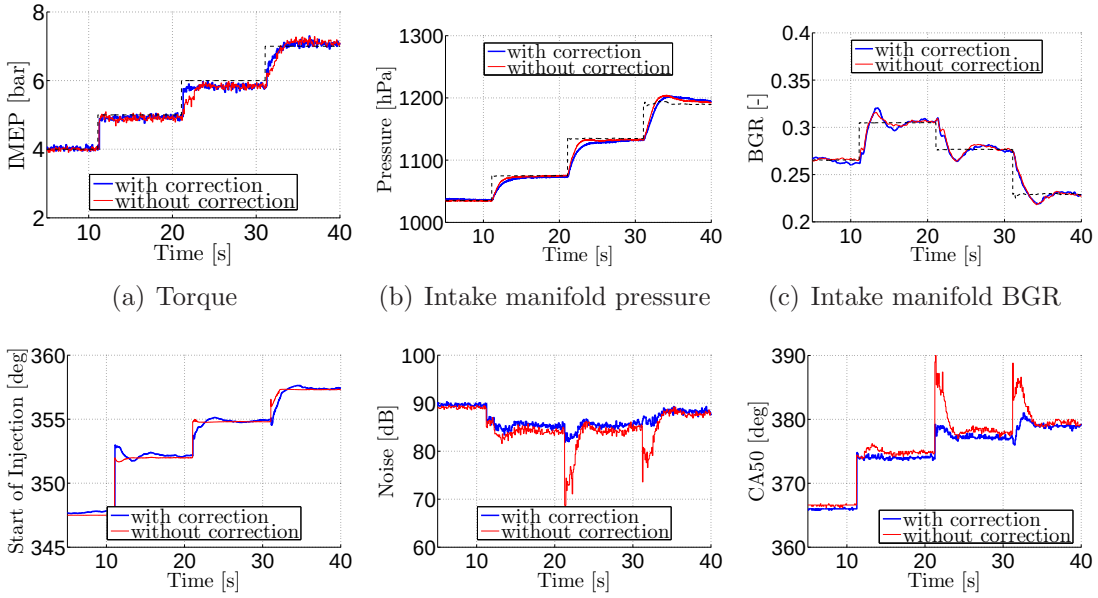

(a) Torque (b) Intake manifold pressure (c) Intake manifold BGR

(d) Injection crankshaft angle (e) Noise (f) CA_{50}

Figure 4.7: *Test-bench results for a four-cylinder HCCI engine with direct injection for increasing torque demand at a constant speed of 1500 rpm with and without the proposed control strategy.*

Decreasing torque trajectory (tip-outs) Figure 4.8 shows a decreasing torque trajectory at a constant engine speed of 1500 rpm. During these transients, without any particular combustion control, combustion is brought forward (as in the transients in Figure 4.7(f)) due to a lack of BGR and of pressure. In response, the proposed controller delays the injection to delay the whole combustion process. Undershoots of the middle of the combustion have disappeared (Figure 4.7(f)). Noise overshoots during transients, which are very unpleasant for car passengers, have also been reduced (gain of almost 2 dB).

Results for various engine speeds Similar results were obtained at different speeds. Figure 4.9 shows the torque demand trajectory at a constant engine speed of 2000 rpm. Again, improvements due to the proposed controller are evident in the middle of the combustion variations during transients.

Impact of the proposed controller on the airpath dynamics In §2.6.2, the influence of the proposed controller on existing control strategies was discussed. It was claimed that this influence is negligible. Indeed, the experimental results presented in this case study support that assumption. More precisely, in Figures 4.7, 4.8 and 4.9, the trajectories of airpath driven parameters (BGR and pressure) with the correction do not show significant improvement or deterioration when compared against the one without the correction. There always exists

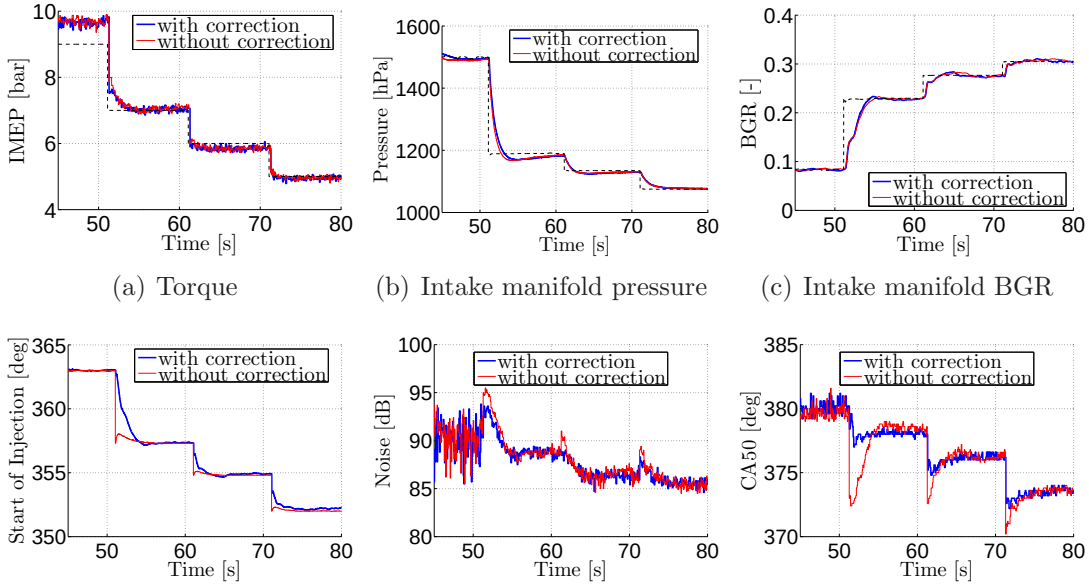

(a) Torque (b) Intake manifold pressure (c) Intake manifold BGR

(d) Injection crankshaft angle (e) Noise (f) CA_{50}

Figure 4.8: *Test-bench results for a four-cylinder HCCI engine with direct injection for decreasing torque demand at a constant speed of 1500 rpm with and without the proposed control strategy.*

differences between the two types of trajectories, but they are smaller than the natural experimental repeatability errors.

Conclusions from the test-bench results

The results of this first case study clearly stress the relevance of the strategy which was proposed in Chapter 2. In spite of airpath regulation errors, such as slow transient dynamics or hardware malfunctions, the combustion midpoint occurs at the reference timing.

The timings for auto-ignition and the cool flame are the most sensitive to airpath regulation errors. As observed from the test-bench results, controlling the end of the cool flame provides good control of the whole combustion process.

The proposed combustion controller permits thus to increase the robustness of the combustion towards airpath regulation lags. This software improvement provides a mean to control the combustion, even during transients, without any hardware upgrade.

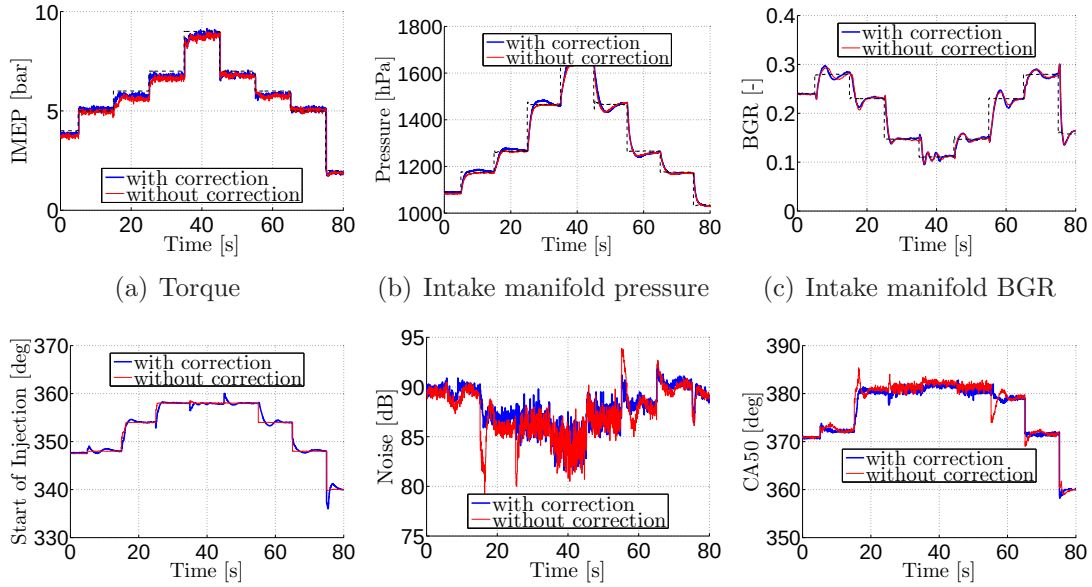

(a) Torque (b) Intake manifold pressure (c) Intake manifold BGR

(d) Injection crankshaft angle (e) Noise (f) CA_{50}

Figure 4.9: *Test-bench results for a four-cylinder HCCI engine with direct injection for increasing and then decreasing torque demand at a constant speed of 2000 rpm with and without the proposed control strategy.*

4.1.4 Results onboard a vehicle

Experimental set-up

The experimental results exposed in Section 4.1.3 demonstrate that the control of the combustion phasing is a key to manage low-temperature combustion. In §4.1.1 and §4.1.2, a technical solution was described, which does not require any hardware upgrade, and solely uses injection timing to control the end of the cool flame phenomenon. Experimental results presented in Section 4.1.3 show that controlling this combustion timing is a relevant approach to control the whole combustion process. Finally, the last step of this study investigates the impact of the proposed strategy on pollutant emissions and engine noise.

To obtain estimates of the emissions and noise produced under real representative driving conditions, experiments were conducted on-board a vehicle equipped with high-frequency sensors to capture data during sharp transients. We now report the obtained results. To highlight the benefits of the proposed strategy, a challenging part of the new European driving cycle (NEDC) was chosen. It consists of one urban driving cycle (ECE) followed by an extra-urban driving cycle (EUDC). The vehicle used is a demonstration car developed at IFP on the basis of a Renault VelSatis (details can be found in [50]) equipped with a HCCI engine that differs from the engine described in §4.1.3 in only two aspects:

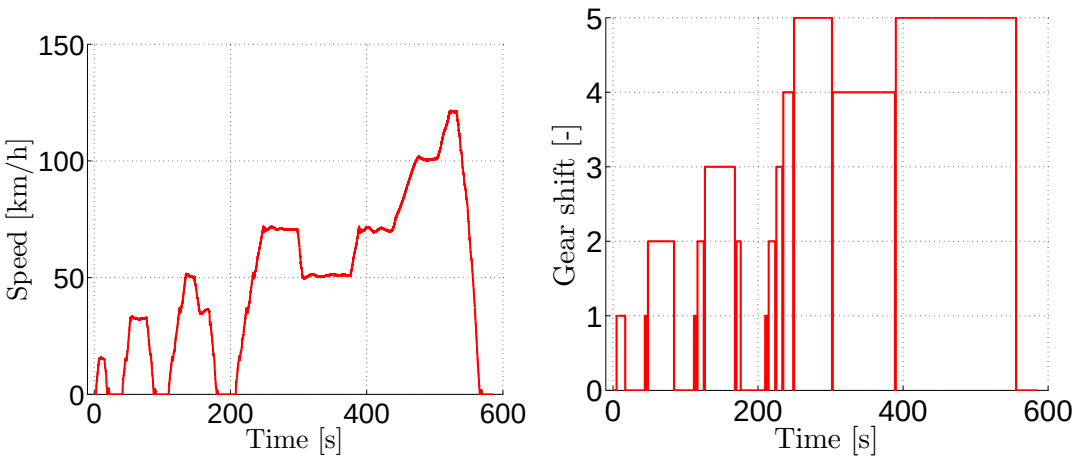

(a) Vehicle speed

(b) Gear shift

Figure 4.10: *Vehicle speed and gear shift results for a four-cylinder HCCI vehicle with direct injection during a normalized ECE (0–200 s) cycle and an EUDC (200–600 s) cycle.*

- The EGR is a high-pressure circuit. Interestingly, this technological change is treated in a straightforward manner in the control scheme (which is independent of the nature of the EGR source). No particular tuning is required.

- To reduce engine noise, a pilot injection is used at some operating points. It consists of at most 4% of the total injected mass and is injected at a crankshaft angle of approximately 20°CA before the main injection.

This pilot injection was not taken into account in the modeling in Section 4.1.1. However, for simplicity, the following assumptions are made:

- Since the mass of the pilot injection is almost negligible compared to that of the main injection, the correction developed in §4.1.2 is applied to the main injection without any particular modification.

- Since the pilot injection occurs at a specific crankshaft angle before the main injection, the pilot injection is equally delayed or advanced as the main injection.

In summary, for operating points equipped with pilot injection, the correction shifts the whole injection pattern, whereas for operating points without pilot injection the correction is classically applied to the main injection timing only.

Results are presented in Figures 4.10, 4.11, and 4.12. Figure 4.10 gives an overview of the vehicle speed and gear shift during the driving cycle, while Figure 4.12 provides more detailed views of the previous results during a representative tip-in.

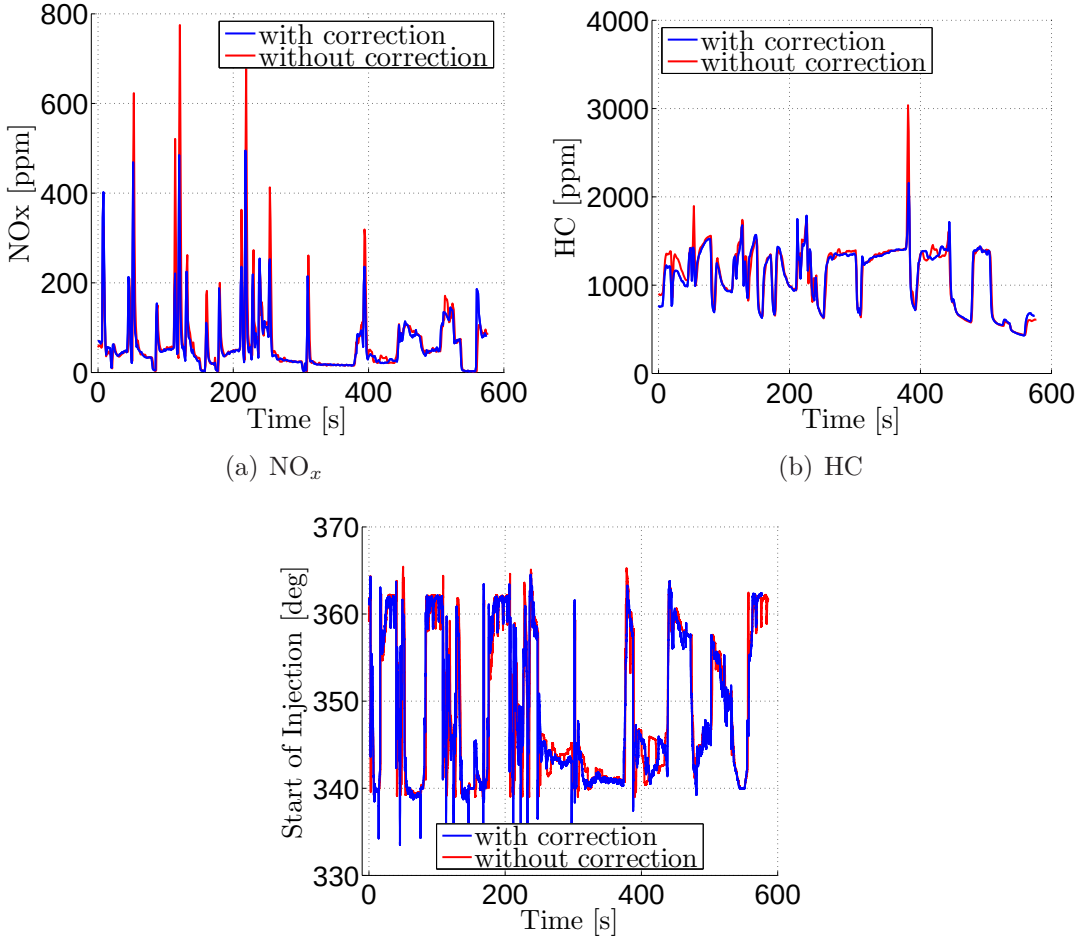

(a) NO_x

(b) HC

(c) Injection crankshaft angle

Figure 4.11: *Vehicle results for a four-cylinder HCCI Diesel engine with direct injection. Injection crankshaft angle, NO_x and HC emissions during a normalized ECE (0–200 s) cycle and an EUDC (200–600 s) cycle.*

Vehicle results for the whole cycle

Figure 4.11(a) and 4.11(b) show nitrogen oxide (NO_x) and unburned hydrocarbon (HC) emissions obtained during this cycle with and without the proposed correction (the start of injection can be seen in both cases in Figure 4.11(c)). On overall, NO_x peaks are drastically reduced (by a factor of two). The HC peaks are also reduced, albeit to a lesser extent. HC transients are hardly visible in both cases, except at $t = 375$ s, which is discussed in the next section.

Vehicle results during a tip-in

The results of a tip-in are shown in Figure 4.12. On two occasions, the produced torque reveals problematic. At $t = 375$ s a misfire occurs. Later, a smaller

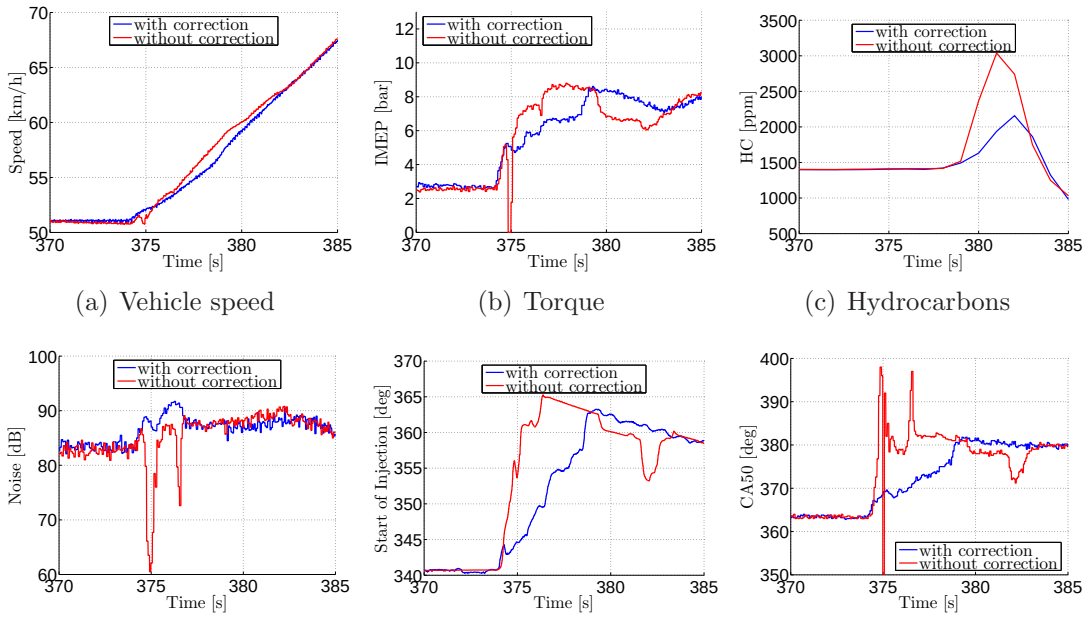

(a) Vehicle speed (b) Torque (c) Hydrocarbons

(d) Noise (e) Start of injection (f) CA_{50}

Figure 4.12: *Vehicle results for a four-cylinder HCCI Diesel engine with direct injection. Effect of correction on a tip-in at 50 km/h. Misfires occuring about 375 s and 377 s disappear when our control strategy is activated.*

decrease can be observed at $t = 377$ s. These are evident in Figure 4.12(b), and correspond to the combustion phasing shifts depicted in Figure 4.12(f). In both cases, the combustion is so much delayed that the torque produced drastically decreases while huge noise variations can be observed (Figure 4.12(d)). This negatively affects both driveability and acoustic comfort. The first misfire is also responsible for the speed variation at the beginning of the tip-in in Figure 4.12(a), and, most importantly, for the overwhelming HC production detected at $t = 380$ s in Figure 4.12(c) (after a lag due to the flow through the exhaust line and the analysis process). Using *soi* corrections computed by our proposed method, as observed in Figure 4.12(e), all these issues are resolved: transients in the combustion phasing are controlled, the misfires disappear, HC production is substantially reduced, and the noise level remains close to its steady-state value.

4.1.5 Conclusion on the mono-pulse combustion control

An improvement for fuelpath control of a HCCI Diesel engine has been presented. Instead of directly setting the injection crankshaft angle to its reference value, the proposed controller synchronizes the fuelpath to the airpath. In particular, this makes the combustion robust to airpath regulation errors (during transients or malfunctions). This controller is mainly based on the linearization

of an auto-ignition delay model (KIM) and a cool flame model. Provided an estimate of in-cylinder conditions at *ivc* is known (here, the conditions are inferred from the intake manifold signals), this method is very general.

- It is independent of the airpath structure. It can be applied to engines with external or internal gas recirculation, and to naturally aspirated engines, throttled engines and/or those with turbochargers.

- The method does not need any hardware upgrade. In particular, *there is no need for any in-cylinder sensor*.

The experimental results highlight the relevance of this new approach. Auto-ignition and the cool flame are critical phenomena for the whole combustion process. Controlling the end of the cool flame leads to an improvement in combustion stability. During transients, the combustion phasing is closely controlled, which in turn improves the torque response and smoothes out noise transients. Finally, the vehicular results demonstrate that combustion phasing control is beneficial in terms of pollutant emissions. It reduces NO_x peaks during transients by a factor of almost two and prevents HC peaks by stabilizing the combustion phasings.

The results obtained for a Diesel engine with a mono-pulse injection strategy (and extended to a pilot-main injection strategy by simply ignoring the pilot injection) are very encouraging. This leads to the next section in which we explicitly account for the influence of the pilot injection in more details in the combustion controller.

4.2 Diesel multi-pulse highly diluted case

In this section, we focus on a natural extension of mono-pulse Diesel combustion control, namely the multi-pulse Diesel combustion control.

The application considered here is a slightly modified version of the one studied in earlier Section 4.1. In fact, the only hardware modification is situated in the combustion chamber. Instead of the NADI^{TM} [68] mono-pulse dedicated combustion chamber, a conventional Diesel one has been used. The air charge is still diluted with burned gas at a relatively high ratio (up to 30%). The conventional chamber design permits to extend the injection pattern to a multi pulse one which is now detailed.

Multi-pulse injection The injection of the fuel mass is split into several small injections, each of these being injected separately into the cylinder. In multi-pulse injection, many different patterns can be considered depending on the number of injection (2, 3 or more) and the fuel mass distribution. However, two common injection patterns are as follows:

- *split injection*. The overall fuel mass is divided into two equal parts which are injected separately.

- *pilot/main/post*. The injection pattern consists of three injections starting with a first small injection (pilot injection of mass M_f^{pilot}). The second injection is the main one and handles most of the fuel mass (mass M_f^{main}). Eventually a last injection (post injection of mass M_f^{post}) ends the injection process. The total injected mass is $M_f = M_f^{pilot} + M_f^{main} + M_f^{post}$.

This strategy provides numerous degrees of freedom. They can be used to improve the steady-state behavior of the engine. The main advantage of this injection strategy is that it naturally improves the robustness of the combustion process. Advantages may also reside in the domains of pollutant emissions and noise. In particular, a small injection at the beginning of the cycle can reduce the noise because it smoothes out the ROHR during the main injection. It can also reduce smoke since it homogenizes the air and burned gases charge.

Conversely, during transients, this strategy increases the complexity of the combustion phasing. As in the mono-pulse case, conventional combustion control strategies focus on controlling the injection pattern as if the system was at steady-state. No particular effort is made to account for the dynamics of the engine various subsystems. This is clearly not optimal.

Transient multi-pulse injection Because multi-injection provides more degrees of freedom than necessary, it does not directly fit into the frame of Chapter 2 where a single trigger is considered. However, some simple assumptions can be used to formulate a problem very similar to the mono-pulse. The main difference is the number of available variables - one in the mono-pulse case, and two (mass and timing) for each injection in the multi-pulse case - to control the combustion phasing. One trigger can be chosen to control one particular combustion phasing. Applying the proposed strategy will provide a control of the chosen combustion phasing.

This pairing of one control variable with one control objective is clearly sub-optimal (considering all the pairing possibilities). It may be seen as a simple extension of the proposed strategy to a multi-trigger case. A more complete extension will be discussed in the conclusion of the thesis.

Choice of the trigger In the considered case, the injection pattern consists of a pilot/main/post sequence. However, since the post injection is quite late in the cycle, it does not impact on the combustion phasing. In fact, the late injection is mainly used to increase the temperature of the exhaust line in view of pollutant after treatment device activation (see [44, and reference therein]). It is thus of little practical interest for combustion phasing control. The injection pattern and the associated ROHR is depicted in Figure 4.13.

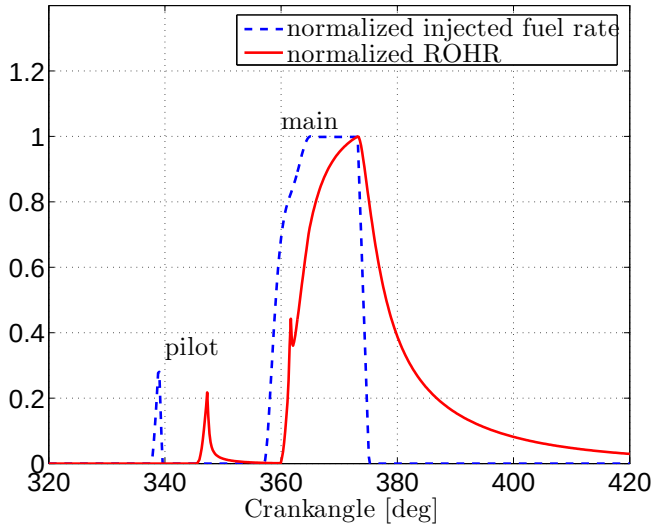

Figure 4.13: *Considered injection pattern schematic view: 2 injections (pilot/main) in dashed blue and the corresponding ROHR (Rate Of Heat Release) in solid red.*

In the case pictured in Figure 4.13 (2 injections), 4 control variables are available (2 masses and 2 timings). However, since the overall fuel mass is constrained by the torque control strategy (as in the mono-pulse case), only 3 degrees of freedom are in fact available. Some additional observations on the calibration procedure and on the influence of the pilot injection helped us to choose between the three triggers. These observations are now detailed.

A quick analysis of common fuelpath calibration results shows that the timing of the pilot injection has only a sense relatively to the timing of the main injection. In fact, calibration engineers introduce the pilot injection approximately 20°CA before the main injection. The whole injection pattern is then calibrated together.

The influences of the timing and mass of the pilot injection on the combustion phasing have been investigated about some operating conditions. Figure 4.14 shows experimental results of variations of the injection timing on the combustion phasing (through the MFB as considered in Appendix B). While the temporal position of the pilot injection is varied from 330°CA to 341.5°CA, the MFB does not show any significant variations. Figure 4.15 reports experimental results of variations of the pilot injection mass on the combustion phasing. This variable clearly has an impact on the MFB, and, thus, on the combustion phasing. In particular, it impacts on the beginning of the combustion.

At the light of these two observations on the calibration procedure and on the influence of the pilot injection on the combustion phasing, we choose to *control the start of combustion of the main combustion* (denoted by θ_{soc}) *using the start of the main injection* (denoted again by θ_{inj}). Then, we keep both the pilot injection mass and the time interval between the pilot and the main injections constant.

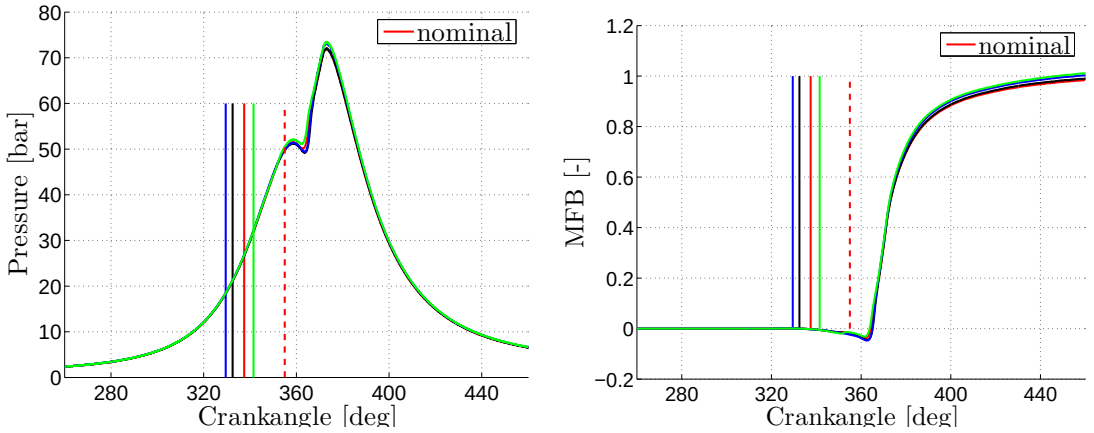

(a) In-cylinder Pressure (b) MFB

Figure 4.14: *Experimental results obtained for a four-cylinder Diesel engine: Variation of the timing of the pilot injection at fixed operating conditions and its influence on the in-cylinder pressure and MFB. In solid line, the different tested pilot timings (red is the reference one) and in dashed line the main injection. This timing has little effect on the combustion.*

In fact, the overall injection pattern is brought forward or delayed without any further change. Interestingly, the mass of the pilot injection is only considered as a disturbance of the auto-ignition process onto the main injection. Having defined a single trigger, this combustion control problem now can be addressed by the general method of Chapter 2.

4.2.1 Combustion model

We now detail the models used for the auto-ignition delay of the main injection, along with calibration results.

Auto ignition model In Section 4.1.1, the classical form for auto-ignition delay was introduced. It is needed to slightly modify it to take into account the influence of the pilot injection. As recalled in the introduction, only the mass of the pilot injection is considered. Consequently, we propose the following model

$$\int_{\theta_{inj}}^{\theta_{soc}} \mathcal{A}^{ai}(\boldsymbol{p}(\theta), M_f^{pilot}) \frac{d\theta}{N_e} = 1, \tag{4.13}$$

with

$$\begin{aligned} \boldsymbol{p}(\theta) &= (P(\theta), T(\theta), X)^T \\ \mathcal{A}^{ai}(\boldsymbol{p}(\theta), M_f^{pilot}) &= A \frac{1 + kM_f^{pilot}}{1 + CX} P(\theta)^n \exp\left(-\frac{T_A}{T(\theta)}\right), \end{aligned} \tag{4.14}$$

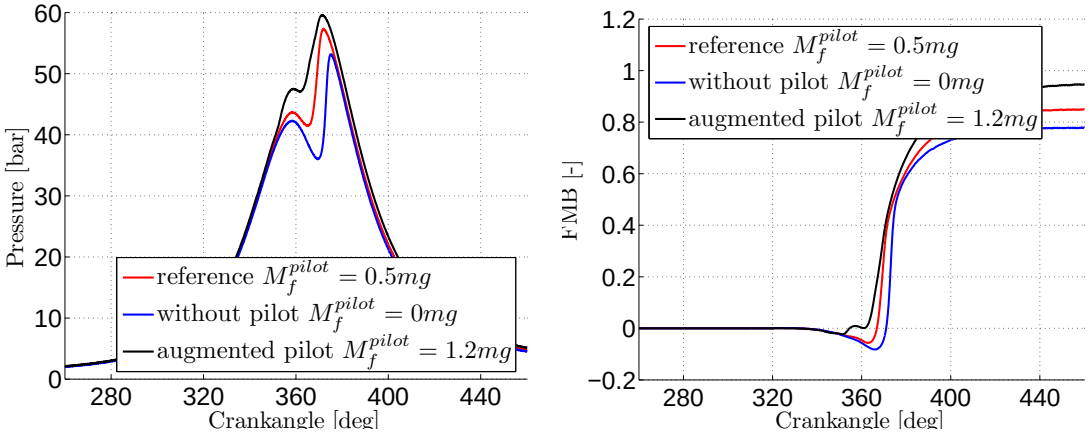

(a) In-cylinder Pressure (b) MFB

Figure 4.15: *Experimental results obtained for a four-cylinder Diesel engine: Variation of the mass of the pilot injection at fixed operating conditions and its influence on the in-cylinder pressure and MFB. In solid line, the pilot and main injection phasing. This mass has a significant impact on the combustion.*

This choice is debatable. In fact, it is a clear illustration of the tradeoff between a precise model and a model simple to calibrate and to use (as discussed already in Appendix B). The calibration of the chosen model follows.

Calibration The model has been calibrated using 44 working points representing individual variations of the model entries around 4 engine working points. The agreement between experimental data and model predictions is illustrated in Figure 4.16.

4.2.2 Controller design

Statement of the model

The auto-ignition model writes under the form of an implicit integral. Following §4.1.2, this model is transformed into a differential equation using an artificial states τ_{ai}

$$\begin{cases} \dfrac{d\tau_{ai}}{d\theta} = A\dfrac{1+kM_f^{pilot}}{1+CX}P(\theta)^n \exp\left(-\dfrac{T_A}{T(\theta)}\right)\dfrac{1}{N_e} \\ \tau_{ai}(\theta_{inj}) = 0 \end{cases} \tag{4.15}$$

The end of the auto-ignition phase is defined as $\tau_{ai}(\theta) = 1$.

The state gathering both phases (compression, auto-ignition) is then

$$\boldsymbol{x} = (P, T, X, \tau_{ai}), \tag{4.16}$$

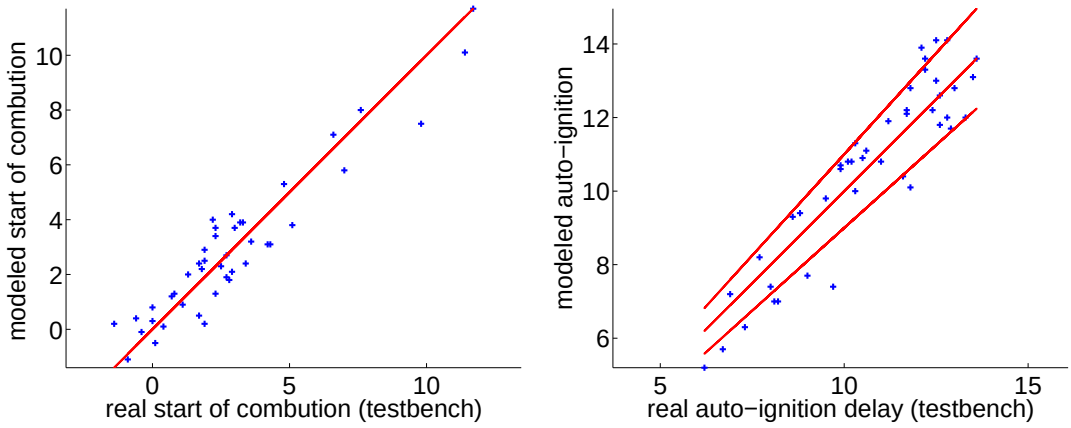

Figure 4.16: *Result of the calibration process of the auto-ignition model. The results are presented in terms of start of injection and duration of the auto-ignition (AI) phase. On the left, the red line states the perfect fit. On the right, the three lines stand for the perfect fit (line in the middle) and for the ±10% fit.*

the initial state of the first differential equation is

$$\boldsymbol{x_0} = (P_{ivc}, T_{ivc}, X_{ivc}, 0), \tag{4.17}$$

and finally, the evolution of the state during both phases is

i) compression:

$$\boldsymbol{f_0}(\boldsymbol{x}, \theta) = \begin{pmatrix} -\gamma P \dfrac{dV(\theta)}{d\theta} \dfrac{1}{V(\theta)} \\ -(\gamma - 1) T \dfrac{dV(\theta)}{d\theta} \dfrac{1}{V(\theta)} \\ 0 \\ 0 \end{pmatrix} \tag{4.18}$$

ii) auto-ignition:

$$\boldsymbol{f_1}(\boldsymbol{x}, \theta) = \begin{pmatrix} -\gamma P \dfrac{dV(\theta)}{d\theta} \dfrac{1}{V(\theta)} \\ -(\gamma - 1) T \dfrac{dV(\theta)}{d\theta} \dfrac{1}{V(\theta)} \\ 0 \\ A \dfrac{1 + k M_f^{pilot}}{1 + CX} P(\theta)^{n_1} \exp\left(-\dfrac{T_1}{T(\theta)}\right) \dfrac{1}{N_e} \end{pmatrix} \tag{4.19}$$

Computation of the correction

Equations (4.17), (4.18), and (4.19) constitute the cycle model as is described in Chapter 2. The strategy proposed in Section 2.4 can be directly applied, and gives the gain "$\boldsymbol{\alpha}$" of the correction as a function of the entries of the airpath look-up table

$$\delta\theta_{inj} = \boldsymbol{\alpha}(N_e, \overline{T}_q) \cdot (\delta P_{ivc}, \delta T_{ivc}, \delta X_{ivc})^T \tag{4.20}$$

As explained in §2.6.2, the gain "$\boldsymbol{\alpha}$" can me mapped as a function of the engine speed and the drivers torque request. Furthermore, thanks to the particular form of the right-hand sides (4.18), and (4.19), simplifications in the controller synthesis Algorithm 2.6.1 lead to a simple explicit analytic expression for the gain "$\boldsymbol{\alpha}$" (see Appendix E).

Relating *ivc* values to available measurements

Since the experimental setup is the same as in the mono-pulse case study (see Section 4.1), the *ivc* values of the airpath driven parameters are computed in the same way. The reader can refer to §4.1.2.

4.2.3 Test-bench results

Experimental set-up

All experimental results presented here were obtained on a four-cylinder direct injection Diesel engine pictured in Figure 4.17. Its specifications are listed in Table 4.2. The engine is an upgrade of a turbocharged multi-cylinder commercial engine. A low-pressure EGR circuit is used that extracts hot burned gases downstream of the turbine and introduces them upstream of the compressor. A valve allows the EGR to be controlled. Finally, both the air and the EGR circuits include a cooler to keep the intake manifold temperature at approximately 330 K.

Since the intake manifold temperature is almost constant (within an error of 10 K) in the engine set-up, the experimental results reflect only the adaptation of the fuelpath to pressure and BGR regulation errors.

Experimental results

Torque trajectories Figures 4.18, 4.19, 4.20, 4.21, 4.22, and 4.23 report experimental results obtained on the presented test-bench for torque variations at constant engine speed. For comparison, the plots contain the same trajectory with (blue lines) and without (red lines) the proposed correction. For all three scenarios, the torque trajectory is shown in part (a). As mentioned in Chapter 1, the airpath control system regulates the intake manifold pressure and BGR around their reference values to meet the torque demand (parts (b) and (c)). The

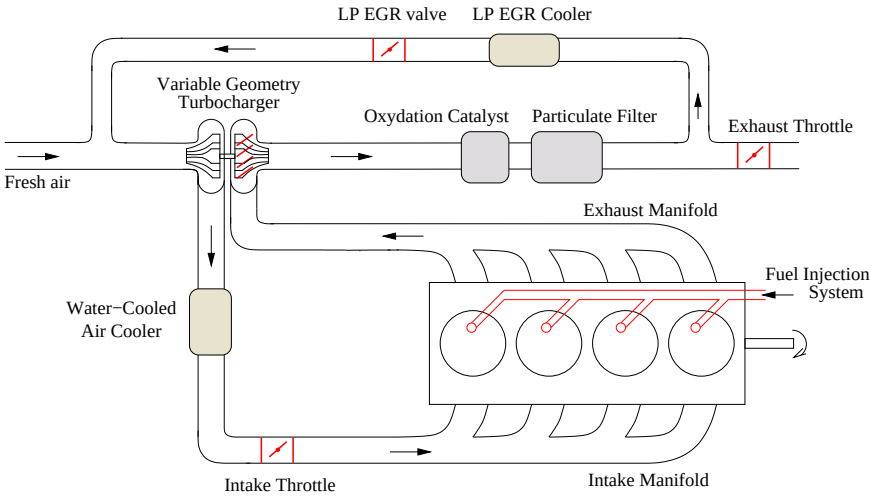

Figure 4.17: *Four-cylinder HCCI Diesel engine with direct injection, low-pressure EGR recirculation and a turbocharger. High BGR values are used to dilute the mixture before combustion.*

mass of the pilot injection is shown in part (d). Non-instantaneous tracking of the airpath reference values induces the new fuelpath controller to correct the reference value for the injection crankshaft angle (part (e)). The injection crankshaft angle sent to the injectors is then different from its reference value. The influence of the proposed combustion control method on combustion phasing (the start of combustion of the main injection CA_0 and the middle of the combustion CA_{50} are shown) is reported in part (f).

The first sequence of experimental tests is a torque trajectory composed of increasing and the decreasing torque requests. These experiments are conducted at constant engine speed of 1500 rpm (Figure 4.18), 2000 rpm (Figure 4.19), and 2500 rpm (Figure 4.20). As recalled in the introduction of this case study, the combustion is naturally partially stabilized by the pilot injection. This appears in the combustion phasing transients which present smaller over- and undershoots during transient than in the mono-pulse case (the reader can compare the results of §4.1.3). Consequently, the proposed correction is smaller during transients. However, transients happening around 40 s and 50 s show great improvements in terms of the evolution of the control variable (CA_{00})[5]. This can also be seen in the second sequence of experimental results. These are larger torque requests which can be seen as tip-ins and tip-outs. These experiments are conducted at a constant engine speed of 1500 rpm (Figure 4.21), 2000 rpm (Figure 4.22), and 2500 rpm (Figure 4.23), respectively. The over- and undershoots appearing during transients are completely cut-off thanks to the proposed start of injection controller.

[5]Discussion about the evolution of the middle of the combustion is postponed until the conclusion of this section.

Bore × stroke	87.0 × 92.0 mm
Number of cylinders	4
Compression ratio	14:1
Displacement	2.2 l
Injection device	Solenoid
Maximum injection pressure	1600 bar
Piston bowl design	conventional
Intake valve closure	$\theta_{ivc} = 232°$
	(360°CA is top dead center)

Table 4.2: *Diesel engine set-up*

Artificial BGR transient To validate the proposed strategy further, we propose another experiment. Figure 4.24 depicts a simulation of BGR[6] transients by artificially shifting the actual BGR from its reference value while keeping the other parameters constant (in particular, the pressure and temperature are set to their reference value). This permits to have larger offsets than in the previous experiments since the BGR actual value is not constrained by the actual airpath dynamics. The results have been conducted at a constant speed of 1500 rpm, and are presented in Figure 4.24. The various data are plotted against the actual BGR value. In Figure 4.24(a), the combustion phasing evolution with and without the proposed correction are depicted. It clearly appears that the correction permits to regulate the start of combustion to its setpoint even in the presence of huge BGR offsets.

In Figure 4.24(b), the variations of the torque produced by the engine are depicted. It clearly appears that the produced torque remains closer to its setpoint when the proposed strategy is activated. In fact, larger BGR variations could be addressed (with higher BGR, simulating sharper transients) with the correction. By contrast, no data beyond 33% for the BGR is reported without the correction since the engine stalls over this limit (the produced torque vanishes). Thanks to the correction, experiment up to 40% could be carried out without any problem. One way of evaluating the produced torque is the torque variability. Roughly speaking, the more the produced torque oscillates (even at steady-state), the more the mechanical constraints in the powertrain increase. Its variability is simply computed as the standard deviation of the normalized torque (the result is then expressed in percentage, and a stability of 1% is usually accepted in the calibration process). Figure 4.24(c) represents the torque variability as a function of the actual BGR. Without the proposed controller (in red), the torque variability increases strongly as soon as the BGR reaches 25%

[6]BGR is the airpath parameter influencing at most the combustion

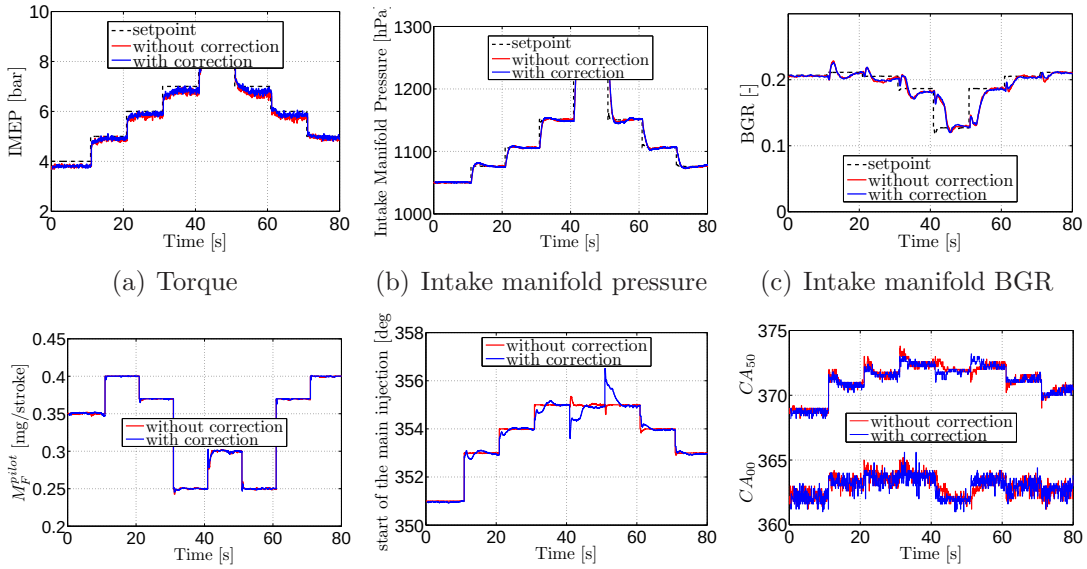

(a) Torque (b) Intake manifold pressure (c) Intake manifold BGR

(d) Mass of the pilot injection (e) Injection crankshaft angle (f) combustion phasing

Figure 4.18: *Test-bench results for a four-cylinder Diesel engine with direct injection for step torque demand at a constant speed of 1500 rpm with and without the proposed control strategy. Over- and undershoots are significantly diminished.*

(that is a BGR error of 5%). In fact, since the BGR increases, and that this is not taken into account by the injection process, combustion phasings are delayed. The combustion stability is jeopardized as well, and makes the produced torque oscillate more. When activating the proposed controller, BGR up to 35% may be reached (practically, this is the higher BGR value that can be reached with this engine) with hardly any impact on the stability.

Finally, Figure 4.24(d) shows that the engine noise remains closer to its steady-state value thanks to the proposed correction. Even if the noise level is higher, evolution during transients is smoother, which is beneficial in terms of acoustic comfort.

4.2.4 Conclusion on the multi-pulse extension

At the light of the presented experimental results, the proposed strategy, along with the modeling assumptions, reveal to be an efficient combustion phasing controller in the Diesel multi-pulse framework.

On the other hand, one may take a look at the evolution of the middle of the combustion (CA_{50}) in the different experiments. While the start of the combustion is well regulated to its tracked setpoint, the middle of the combustion still show non-optimal transients. This is not unexpected since the chosen combustion phasing is the start of the combustion. However, this behavior emphasizes the

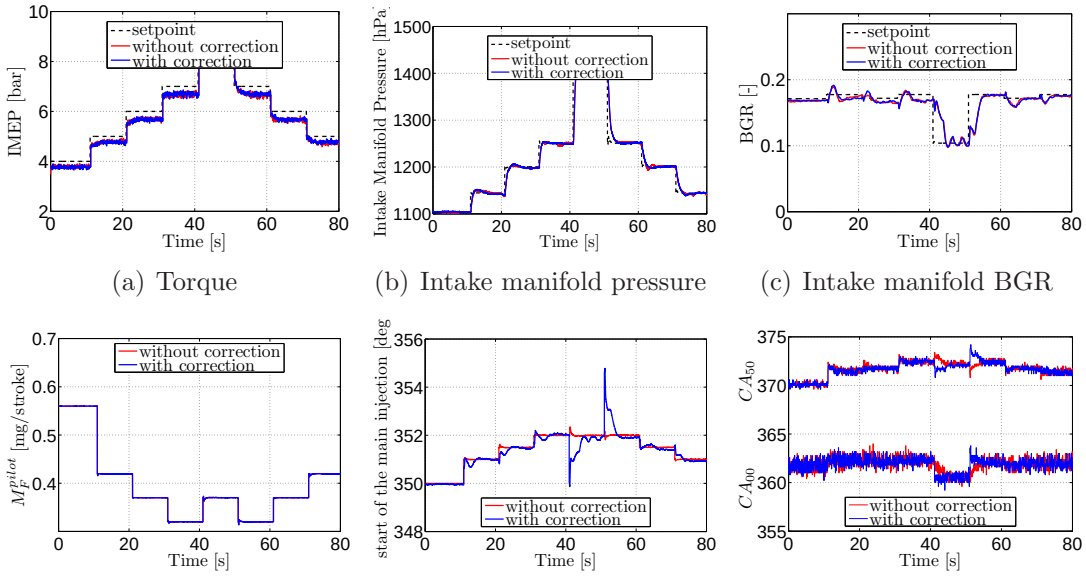

(a) Torque (b) Intake manifold pressure (c) Intake manifold BGR

(d) Mass of the pilot injection (e) Injection crankshaft angle (f) combustion phasing

Figure 4.19: *Test-bench results for a four-cylinder Diesel engine with direct injection for step torque demand at a constant speed of 2000 rpm with and without the proposed control strategy. Over- and undershoots are significantly diminished.*

fact that the phenomena happening between the start of the main combustion and the middle of the combustion are sensitive to the airpath regulation errors. An ideal combustion phasing controller, in view of middle of combustion control, would have then to include more than just an auto-ignition model. As stated in the introduction, this section is just a rough extension of the proposed one-trigger strategy to multi-injection Diesel engine. Further extensions are possible.

The fact that the start of the combustion (the control objective) is well regulated permits to validate the approach, and let us conclude that an approach explicitly accounting for the complex combustion kinetics after the auto-ignition and for the available triggers would represent a good solution to control the middle of the combustion.

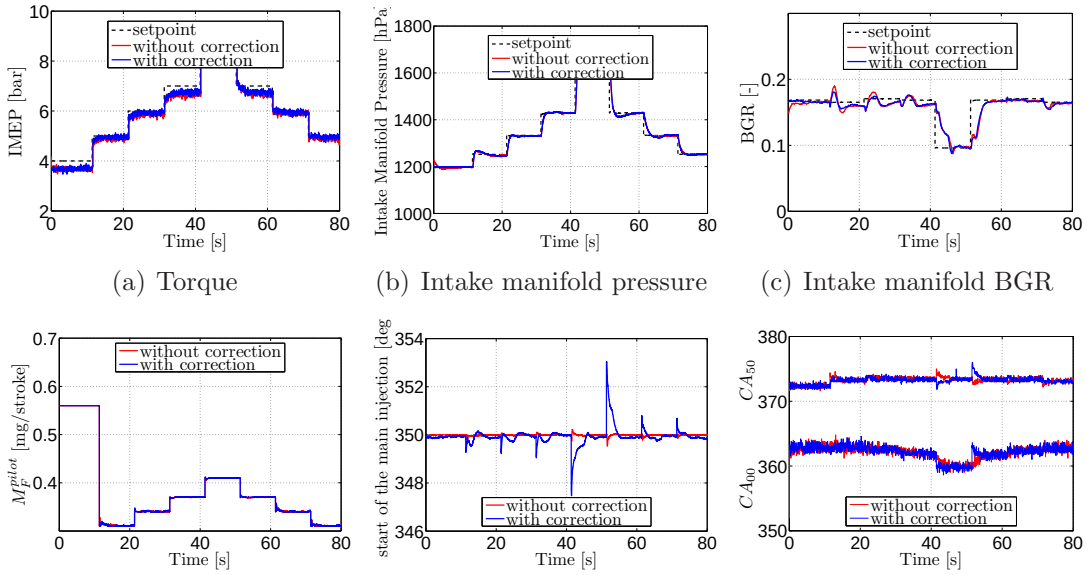

(a) Torque (b) Intake manifold pressure (c) Intake manifold BGR

(d) mass of the pilot injection (e) Injection crankshaft angle (f) combustion phasing

Figure 4.20: *Test-bench results for a four-cylinder Diesel engine with direct injection for step torque demand at a constant speed of 2500 rpm with and without the proposed control strategy. Over- and undershoots are significantly diminished.*

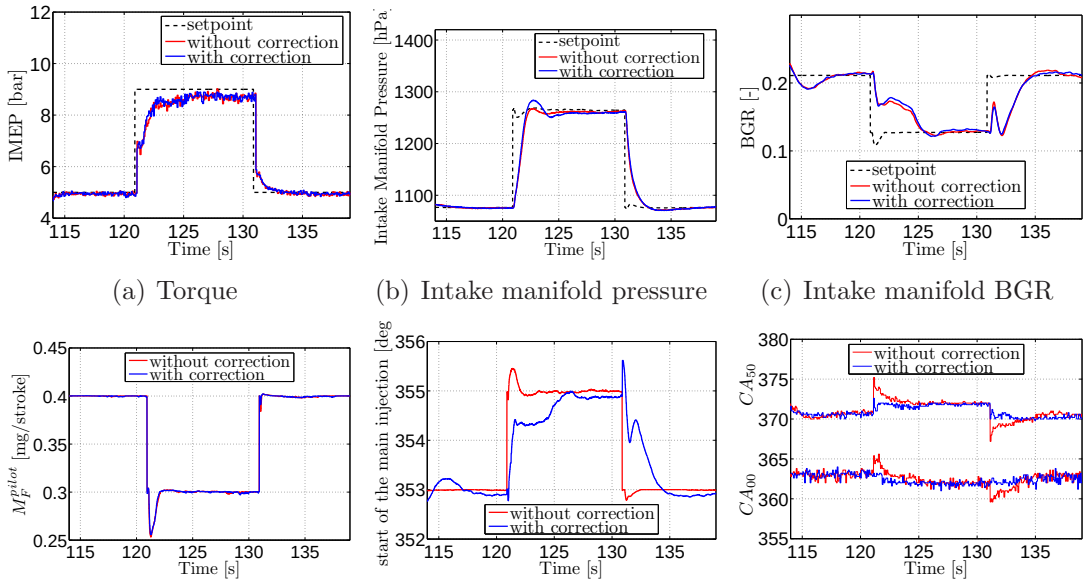

(a) Torque (b) Intake manifold pressure (c) Intake manifold BGR

(d) mass of the pilot injection (e) Injection crankshaft angle (f) combustion phasing

Figure 4.21: *Test-bench results for a four-cylinder Diesel engine with direct injection for a tip-in tip-out torque demand at a constant speed of 1500 rpm with and without the proposed control strategy. Over- and undershoots are significantly diminished.*

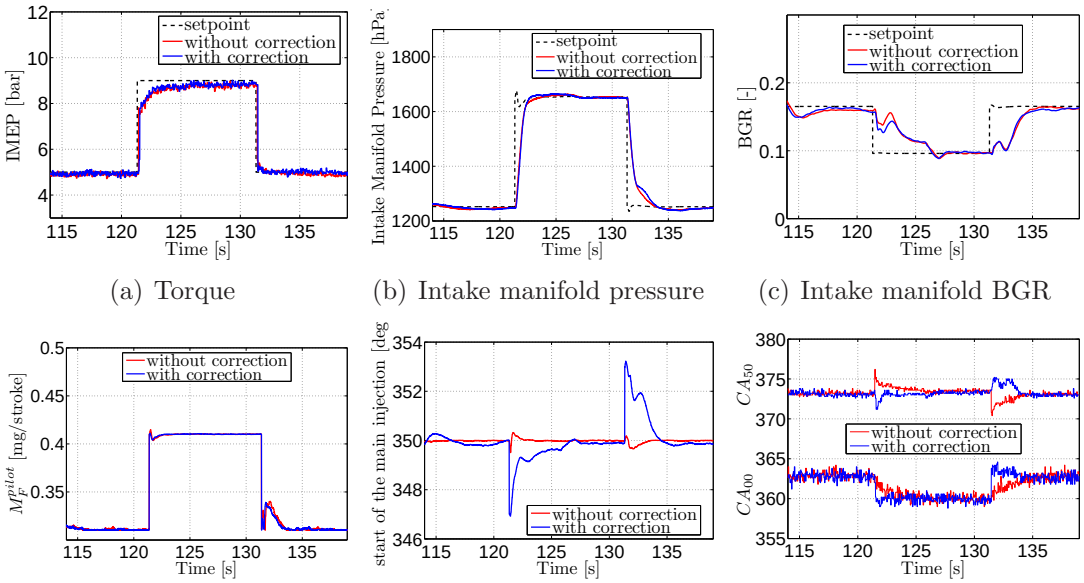

(a) Torque (b) Intake manifold pressure (c) Intake manifold BGR

(d) mass of the pilot injection (e) Injection crankshaft angle (f) combustion phasing

Figure 4.22: *Test-bench results for a four-cylinder Diesel engine with direct injection for a tip-in tip-out torque demand at a constant speed of 2000 rpm with and without the proposed control strategy. Over- and undershoots are significantly diminished.*

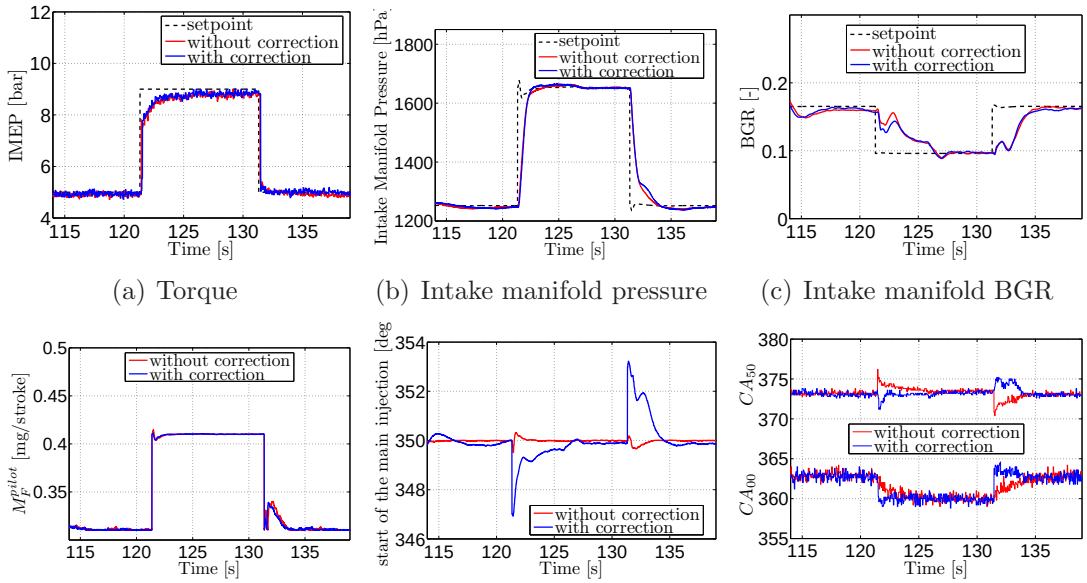

(a) Torque (b) Intake manifold pressure (c) Intake manifold BGR

(d) mass of the pilot injection (e) Injection crankshaft angle (f) combustion phasing

Figure 4.23: *Test-bench results for a four-cylinder Diesel engine with direct injection for a tip-in tip-out torque demand at a constant speed of 2500 rpm with and without the proposed control strategy. Over- and undershoots are significantly diminished.*

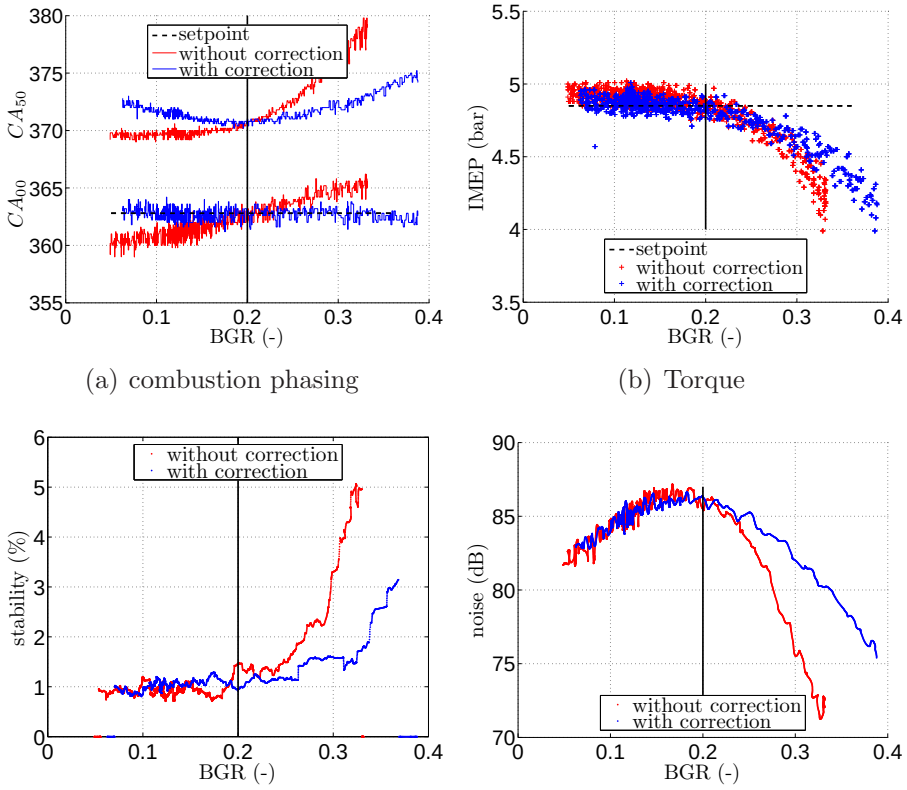

(a) combustion phasing

(b) Torque

(c) mass of the pilot injection

(d) Injection crankshaft angle

Figure 4.24: *Test-bench results for a four-cylinder Diesel engine with direct injection for artificial BGR deviations at a constant speed of 1500 rpm with (blue) and without(red) the proposed control strategy. The black vertical line represents the BGR setpoint value (20%). Corrections of the start of injection is thus made with respect to this value.*

Chapter 5

Conclusion and extensions

Modern engines are composed of subsystems with unbalanced settling times. This problem has been largely overlooked until now, but during transients these imbalances negatively impact on the combustion. In this work, a combustion control mechanism is presented that uses the fast control variable to compensate for deviations of the slow variables from their optimal values.

The fast variable in question is either the injection time (in the case of a CI engine) or the spark ignition time (in the case of a SI engine). This trigger is adapted in real time to make the combustion phasings follow their optimal steady-state values. The required adjustment is determined by analyzing a theoretical combustion model. Through a sensitivity analysis of the model, one can calculate corrections to the steady-state look-up tables typically used to control these triggers.

The presented strategy is very general:

- It can be applied to any kind of engine (SI/CI) and complements the classical control approach.
- It is independent of the engine structure. Indeed, we showed that it can be applied to any kind of engine. Moreover, the controller synthesis strategy is independent from the engine calibration. The controller synthesis depends only on the structure of the combustion model and not on the initial conditions.
- It is suitable for the most general form of combustion model (a sequence of differential systems).
- The controller does not require any hardware upgrade to be applied. In particular, *no in-cylinder sensors are required*.

The proposed strategy action is visible during transients. Also, it easily handles malfunctions such as device ageing (EGR valve clogging) and unexpected regulation errors, which usually yield some malicious combustion phasing shift.

Even if no really optimal behavior of the engine can be recovered due to severe hardware or software malfunctions, this may be sufficient for the vehicle to reach the closest garage.

The simulation and experimental results presented in this thesis have stressed the relevance of this new approach.

In SI engines, the whole combustion model has been used to derive a middle of combustion controller. Simulation results have shown improvements in term of optimum middle of combustion tracking in the presence of large airpath errors.

In CI engines, two applications have been studied. In the case of mono-pulse injection, the auto-ignition and the cool flame revealed as the critical phenomena for the whole combustion process. Controlling the end of the cool flame has improved the combustion stability. During transients, the combustion phasing is closely controlled, which, in turn, *improves the torque response* and *smoothes out noise transients*. Vehicle results have demonstrated that combustion phasing control is beneficial in terms of pollutant emissions. It *reduces NO_x peaks* during transients by a factor of almost two and *prevents HC peaks*. In a multi-pulse injection engine, the strategy developed earlier was extended to a pilot-main injection strategy. Empirical simplifications led to consider an equivalent mono-trigger problem directly fitting into the proposed control frame. Transient results obtained on a test bench showed that the approach succeeds in managing undesirable transient behavior.

The last case study leads to consider one possible extension of the proposed combustion controller. In the case of multiply triggered systems such as the multi-pulse CI engine, the control objectives can also be multiple. More precisely, one could not only control one particular combustion phasing, but as many combustion phasings as the numbers of triggers. To perform this, the sensitivity analysis discussed in Chapter 2 has to be extended; this is actually the subject of ongoing researches.

To conclude this thesis, we would like to mention several future directions in the field of engine control, which, interestingly, could benefit from the proposed combustion control method. A first example is the flex-fuel technology which is currently being developed to diversify the hydrocarbon supplies of automotive engines. Frequently, the nature of the injected fuel varies which impacts on the combustion properties of the fuel. Among these, one can mention the well known RON (Research Octane Number) index which stands for auto-ignition properties. These fuel changes can be seen as transients that could easily be handled by our method and prevent extensive calibrations.

A second example is the ubiquitous trend toward hybridization which couples two or more sources of energy (electrical and thermal) with different natural settling times. High-level energy management systems generate frequent torque

transients. The proposed method could be of interest to master the combustion during these transients in an efficient manner.

At last, we should mention that the proposed method can also be considered as a low-level controller. It could easily be modified to create a high-level controller (usually referred to as pollutant and noise supervisor) based on pollutant and noise models targeting a different trade-off than the one mapped in the static look-up tables.

Appendix A

Improved model inversion

To overcome the mismatches between actual combustion phasing and the reference one due to modeling errors, an improvement of the method presented in §2.1.2 is proposed in this appendix. Instead of directly using the actual combustion phasing look-up table, it is proposed to modify it by adding a bias $\overline{\Delta}$ taking into account these errors. Equation (2.2) becomes

$$x_{fast} = \mathcal{M}^{-1}(\boldsymbol{x_{slow}}, \overline{\mathrm{CA}}_{\mathrm{X}} + \overline{\Delta}) \tag{A.1}$$

This artificial bias is computed to guarantee that, during steady-state operations, the combustion phasing does not differ from the optimal one. In details,

$$\begin{aligned} 0 = \mathrm{CA}_{\mathrm{X}} - \overline{\mathrm{CA}}_{\mathrm{X}} &= \mathcal{M}(\boldsymbol{x_{slow}}, x_{fast}) + \epsilon_{\mathcal{M}}(\boldsymbol{x_{slow}}, x_{fast}) - \overline{\mathrm{CA}}_{\mathrm{X}} \\ &= \mathcal{M}(\boldsymbol{x_{slow}}, \mathcal{M}^{-1}(\boldsymbol{x_{slow}}, \overline{\mathrm{CA}}_{\mathrm{X}} + \overline{\Delta})) \\ &\quad + \epsilon_{\mathcal{M}}(\boldsymbol{x_{slow}}, \mathcal{M}^{-1}(\boldsymbol{x_{slow}}, \overline{\mathrm{CA}}_{\mathrm{X}} + \overline{\Delta})) - \overline{\mathrm{CA}}_{\mathrm{X}} \\ &= \overline{\Delta} + \epsilon_{\mathcal{M}}(\boldsymbol{x_{slow}}, \mathcal{M}^{-1}(\boldsymbol{x_{slow}}, \overline{\mathrm{CA}}_{\mathrm{X}} + \overline{\Delta})) \end{aligned} \tag{A.2}$$

In steady-state, the last equation of (A.2) is fully known (the model error $\epsilon_{\mathcal{M}}$ is computable as the difference between the actual and modeled combustion phasing). Equation (A.2) can thus be solved (off-line) to find the bias $\overline{\Delta}$. Finally, repeating this calculus, the bias is mapped through a look-up table.

This operation guarantees that, in steady-state, the combustion phasing control error vanishes. This solution can in fact be interpreted as a mapping of the error model $\epsilon_{\mathcal{M}}$ through the look-up table $\overline{\Delta}$. During transients, the interpolation of the look-up table $\overline{\Delta}$ provides, through Equation (A.1), a control x_{fast} corrected by the look-up table $\overline{\Delta}$.

The main drawback of this method is its computational burden. It is still required to invert the model online (A.1). Moreover, we claim that the solution we propose in this thesis almost provides the same controller with hardly any on-line computation time. This is now illustrated with experimental results.

Both strategies (model inversion and improved model inversion) have been compared with the proposed correction strategy in the Diesel multi pulse case

study (see Section 4.2, in particular, in that case study, $\overline{\mathrm{CA}}_{\mathrm{X}} = \overline{\mathrm{CA}}_{00}$). Figure A.1 depicts the necessary look-up table of the start of reference start of combustion and of the bias $\overline{\Delta}$. The bias is constructed to satisfy Equation (A.2).

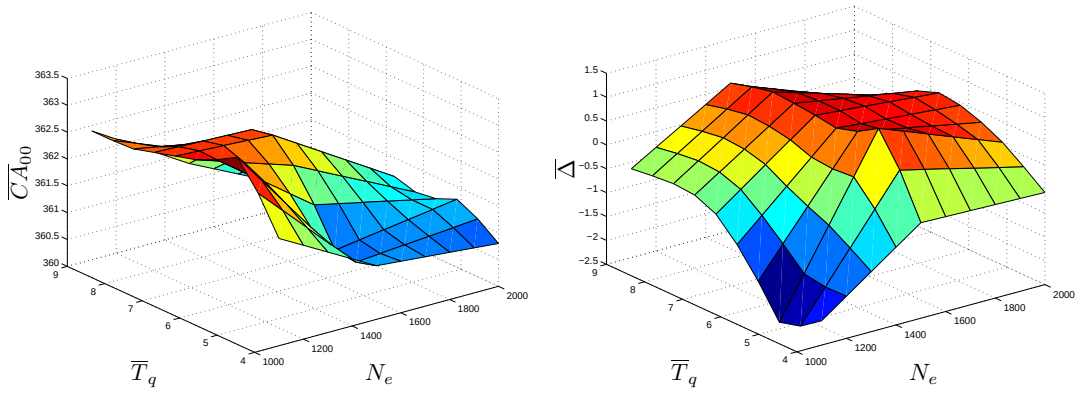

(a) CA_{00} look-up table (b) $\overline{\Delta}$

Figure A.1: *Look-up table of the controlled combustion phasing (CA_{00}) and of its bias ($\overline{\Delta}$). The entries of the look-up tables are the engine speed (expressed in rpm) and the drivers torque demand (expressed in IMEP[bar]).*

Since the model is expressed under the very particular form of an implicit equation (see Equation (4.13)) it is easy to invert. One simply has to integrate backward the current integral from the chosen combustion phasing $\overline{\mathrm{CA}}_{00}$ to find the controlled input θ_{inj}.

The experimental results are presented in Figures A.2. This figure gathers the evolutions of the considered variables for three different strategies: i) the proposed correction, ii) the model inversion strategy, and iii) the model inversion strategy with the combustion phasing bias. The torque trajectory depicted in A.2(a) is carried out at a constant engine speed of 1500 rpm. The slow parameters evolutions are reported in Figures A.2(b) and A.2(c) (intake manifold pressure and intake manifold BGR). They track their setpoints plotted in dashed lines. No impact of the different strategies on the slow variables regulations can be seen in these figures. Thus, difference only appear in the fast variable control: the start of combustion. The evolution of the start of injection is depicted in Figure A.2(d) and the resulting start of combustion in Figure A.2(e). At steady state, since the proposed correction vanishes, it provides the optimal start of injection and then the optimal start of combustion. Then, as claimed in §2.1.2, the model inversion strategy propagates the modeling error in the controlled variable and on the combustion phasing evolution (see the gap between the green and blue lines), while the model inversion and bias strategy manages to provide the optimal start of injection. Moreover, even during transients, the correction strategy and the inversion model with bias provide the same control value (the red and blue lines are almost identical).

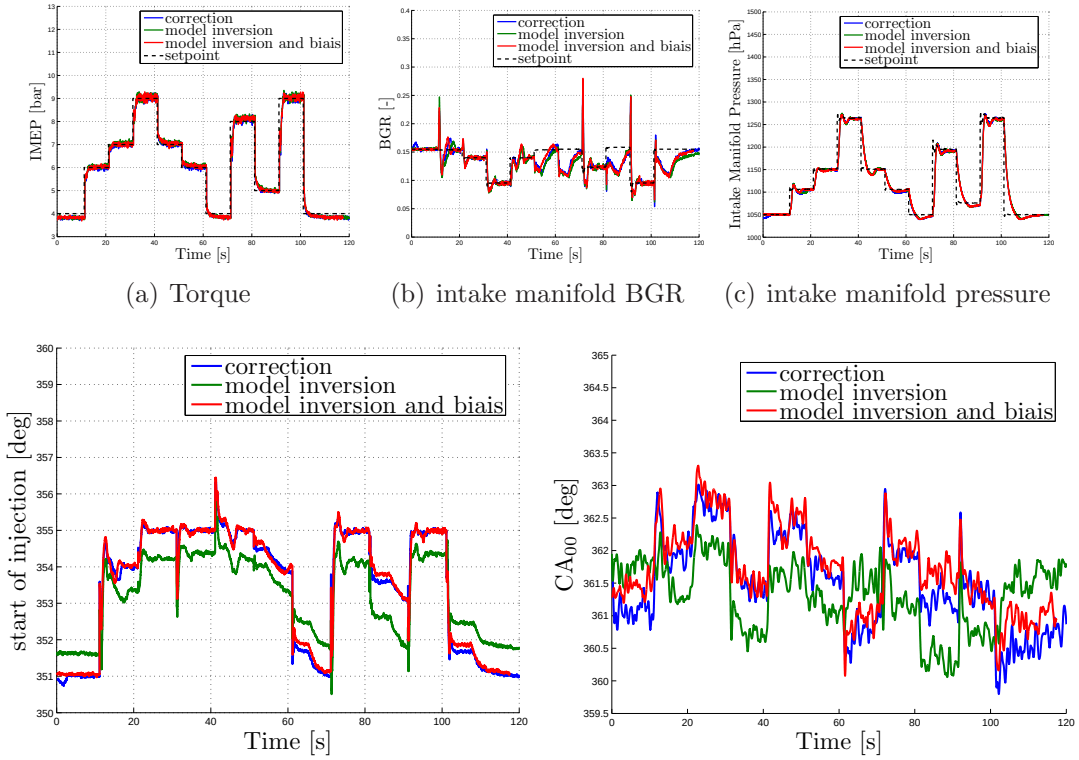

(a) Torque (b) intake manifold BGR (c) intake manifold pressure

(d) Injection crankshaft angle (e) start of combustion

Figure A.2: *Test-bench results for a four-cylinder Diesel engine with direct injection. Test of different strategies: with the proposed correction (correction), through a model inversion (model inversion) and through a model inversion with a combustion phasing bias (model inversion and bias).*

Appendix B

Combustion phasing extraction and models calibration

In view of model calibration (see §2.3.2) and of controller validation (see §2.6.3), the actual combustion phasings have to be reconstructed on experimental test-benches. This appendix gathers the few tools used in the discussed case-studies to extract the combustion phasings from the available sensors and some remarks about model calibration.

B.1 Combustion analysis

The development phase of the proposed combustion controller includes a combustion model calibration. To this end, the combustion phasings have to be measured on the test-bench and compared to the one computed by the model. Moreover, the experimental validation of the proposed controller is mainly based on combustion phasings monitoring during transient operation.

Thus, the combustion analysis which provides the combustion phasing has to match requirements of both processes. In particular, it has to be robust enough to natural cycle to cycle variations, and simple enough to be implementable in real-time. We now expose how the combustion can be monitored using in-cylinder pressure sensors.

B.1.1 Combustion evolution reconstruction

The combustion phenomena in the chamber are the results of very complex chemical and physical reactions. Yet, no sensor exists to directly monitor the evolutions of these processes. Indirect means must be considered instead. On classic engine development test-benches[1], in-cylinder pressure sensors are used

[1]Again, these in-cylinder sensors are *only* used for the validation of the proposed controller at a test-bench.

to measure the evolution of thermodynamical conditions. These conditions are representative of the combustion process and permit to reconstruct its evolution through the Rate Of Heat Release (ROHR) and the Mass Fraction Burned (MFB). More precisely, if the gases in the cylinder are assumed to follow the ideal gas law (neglecting the change in the value of γ), the following relation holds (see the classic reference [23])

$$\frac{dQ_n}{d\theta} = \frac{\gamma}{\gamma - 1} P(\theta) \frac{dV}{d\theta}(\theta) + \frac{1}{\gamma - 1} V(\theta) \frac{dP}{d\theta}(\theta), \tag{B.1}$$

where Q_n is the apparent net heat-release rate, and V is the predetermined volume of the cylinder (which is a known function of the crankshaft angle). This heat-release rate is the sum of two main terms, the combustion ROHR Q, and the wall heating losses Q_w

$$\frac{dQ_n}{d\theta} = \frac{dQ}{d\theta} - \frac{dQ_w}{d\theta} \tag{B.2}$$

Thus, using common wall heat losses correlations [5, 35, 72] and the measured in-cylinder pressure P in Equations (B.1) and (B.2), one can easily determine the evolution of the ROHR. Figure B.1 shows the results of the proposed ROHR reconstruction on a CI engine test-bench. The combustion ROHR is depicted in the sub-figure (b) and is obtained after a combustion analysis of the in-cylinder pressure depicted in sub-figure (a). The combustion is clearly visible as it corresponds to the sharp positive peak in the ROHR. The small drop just before the combustion is due to the fact that the fuel is in liquid phase, and that it is cooler than the rest of the in-cylinder gases. Thus, the heating of the fuel and its evaporation makes the apparent combustion ROHR negative.

Finally, to complete the combustion analysis, the ROHR can be integrated to compute the combustion heat release

$$Q(\theta) = \int_{\theta_{ivc}}^{\theta} \frac{dQ}{d\theta} d\theta \tag{B.3}$$

Classically, this equation is normalized into a MFB through the fuel low heating Q_{LHV} value [23] which gives the available chemical energy in the fuel per mass unit and the total fuel mass M_f

$$MFB \triangleq \frac{Q}{Q_{LHV} M_f} = \frac{1}{Q_{LHV} M_f} \int_{\theta_{ivc}}^{\theta} \frac{dQ}{d\theta} d\theta \tag{B.4}$$

Figure B.1(c) shows the MFB for the analyzed in-cylinder pressure. It ranges from 0 to 1, except when, during the already mentioned fuel vaporization and heating, it becomes slightly negative.

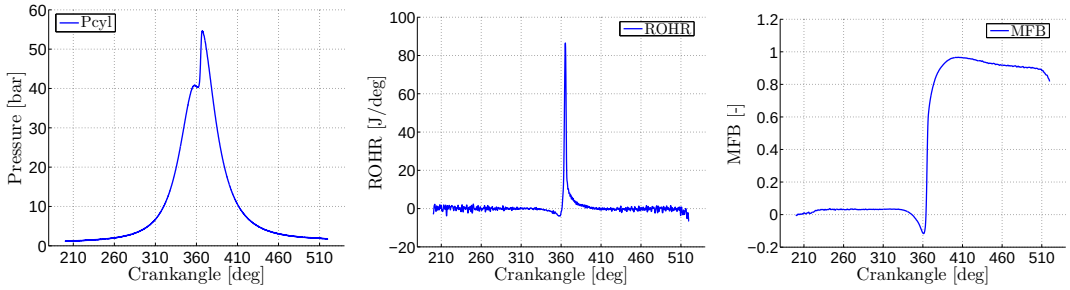

(a) In-cylinder pressure (b) ROHR (c) MFB

Figure B.1: *Combustion analysis on a Direct Injection (DI) Diesel engine.* $360°CA$ *is TDC.*

B.1.2 Combustion phasing extraction

Once the combustion (ROHR and MFB) is reconstructed as described above, the combustion phasing have to be computed. By definition of the $\mathrm{CA_X}$, one has

$$\mathrm{MFB}(\mathrm{CA_X}) = \frac{\mathrm{X}}{100} \tag{B.5}$$

The detection is then easy to perform from the MFB historie.

However, in the case of CI engines, this is not enough to reconstruct the beginning of the combustion. Indeed, due to the high sensitivity of the beginning of the combustion to the fuel heating and evaporation, and noise in the MFB signal, the detection of the $\mathrm{CA_0}$ with the preceding equation can be troublesome. Instead, it is proposed to use the minimum of the MFB as start of combustion. On notes

$$\mathrm{CA_0} \triangleq \arg\min(\mathrm{MFB}) \tag{B.6}$$

This reveals a very robust approach. For instance, the start of the combustion depicted in Figure B.1 is approximatively $\mathrm{CA_0} = 360°\mathrm{CA}$. Physically, this $\mathrm{CA_0}$ corresponds to the instant when the combustion process begins to overwhelm the heating and evaporation of the fuel.

B.2 Calibration

Certainly, the calibration procedure of the model has to be carefully conducted in order to lead to an accurate controller. The first step is to define a calibration database. Then, the calibration of the chosen model can be carried out by an optimization process with appropriate criteria.

B.2.1 Calibration database

The modeling process has been a part of engine controller design for years. To this end, 0-D models have been developed. Their calibration is classically conducted using as database working points distributed over the whole operating range. This has revealed sufficient to provide accurate calibration of the engine airpath models. However, the combustion models cannot be calibrated with such a database. More precisely, while global quantities such as IMEP can accurately be reconstructed, the combustion phasing cannot.

This is mainly due to the chosen calibration database. To calibrate a model, it is necessary to individually stimulate its entries[2]. Using steady states from over the whole operating range as entries does not provide individual variations of the entries of the combustion model (which are the in-cylinder thermodynamical and physical conditions). In fact, these initial conditions are usually mapped as functions of the engine speed and the driver's torque demand. The calibration database is then only 2-dimensional since at most only 2 parameters are varied.

It is essential to use a database dedicated to the calibration of the engine. Individual excitation of the models entries can be carried out around any working point (changing the BGR while keeping the pressure, and the temperature constant, and so on). As the model is a phenomenological model involving few parameters (as opposed to black-box or grey-box models, such as neural networks), a few working points may be used. The calibration database is then multi-dimensional (as many dimension as the number of entries) around any of the 4 or 5 chosen working points. The combustion phasings on each point of the calibration database is extracted following the process of Section B.1.

B.2.2 Optimization process

Once the database is generated, the calibration of the model can be carried out using classic optimization methods (least-square, and non-linear least-square, mostly). However, the criteria have to be chosen carefully. Classic criteria such as the IMEP are not relevant to evaluate the optimization process because they are too global.

The combustion model is used to control the combustion phasing by compensating the combustion phenomenon duration offsets. The evaluation of the model calibration should focus on the duration of these processes. Moreover, when the different processes composing the combustion which are separated (such as the auto-ignition and the combustion itself can be separated by the start of combustion in CI engines), it is relevant to separate them in the calibration.

[2]as is also related to the "persistency of excitation" assumption in real-time identification process.

Appendix C

Controller synthesis computation

C.1 Matrix coefficients

Equations (2.20), (2.21), and (2.22) yield the matrices

$$\boldsymbol{\Xi} = \left(\begin{array}{c|ccccccc} 1 & 0 & 0 & & & & \\ \hline c_1^1 & b_1^1 + c_1^2 & b_1^2 & 0 & & & \\ c_2^1 & b_2^1 + c_2^2 & b_2^2 + c_2^3 & b_2^3 & \ddots & & \\ \vdots & \vdots & \vdots & \vdots & \ddots & \ddots & \\ c_{n-1}^1 & b_{n-1}^1 + c_{n-1}^2 & b_{n-1}^2 + c_{n-1}^3 & b_{n-1}^3 + c_{n-1}^4 & \dots & b_{n-1}^n & 0 \\ c_n^1 & b_n^1 + c_n^2 & b_n^2 + c_n^3 & b_n^3 + c_n^4 & \dots & b_n^n + c_n^{n+1} & b_n^{n+1} \\ \hline 0 & 0 & 0 & 0 & \dots & 0 & 1 \end{array}\right)$$

and

$$\boldsymbol{E} = \begin{pmatrix} 0 & 1 \\ e_1 & 0 \\ e_2 & 0 \\ e_3 & 0 \\ \dots & \dots \\ \dots & \dots \\ e_n & 0 \\ 0 & 0 \end{pmatrix}$$

where

$$b_i^j = \int_0^1 \boldsymbol{\gamma_{i-1}}(u)^T \boldsymbol{b_{j-1}}(u) du$$

$$c_i^j = \int_0^1 \boldsymbol{\gamma_{i-1}}(u)^T \boldsymbol{c_{j-1}}(u) du$$

$$e_i = -\boldsymbol{\gamma_0}(0)^T \frac{\partial \boldsymbol{g}}{\partial \boldsymbol{p_{ivc}}}(\overline{\boldsymbol{p}}_{\boldsymbol{ivc}})$$

These coefficients are expressed in terms of the time variable u. A first simplification is to use the inverse change of time given in §2.4.1.

C.1.1 Inverse change of time

Let $\boldsymbol{\Phi_j}(u,1)$ be the resolvent of the following differential equation

$$\dot{\boldsymbol{\gamma}}_j \;=\; -\boldsymbol{A_j}(u)^T.\boldsymbol{\gamma_j}, \tag{C.1}$$

such that $\boldsymbol{\Phi_j}(1,1) = \boldsymbol{Id}$. Then, $\boldsymbol{\gamma_i}(u) = \boldsymbol{\Phi_i}(u,1)\boldsymbol{\gamma_j(1)}$ and

$$\begin{aligned}
b_i^j &= \int_0^1 \boldsymbol{\gamma_{i-1}}(u)^T \boldsymbol{b_{j-1}}(u)du \\
&= \int_0^1 \left(\boldsymbol{\Phi_{j-1}}(u,1)\boldsymbol{\Phi_j}(0,1)...\boldsymbol{\Phi_i}(0,1)\frac{\partial h_{i+1}}{\partial \boldsymbol{x}}(\overline{\boldsymbol{x}}(\overline{\theta}_{i+1}))^T \right)^T \boldsymbol{b_{j-1}}(u)du \\
&= \frac{\partial h_{i+1}}{\partial \boldsymbol{x}}(\overline{\boldsymbol{x}}(\overline{\theta}_{i+1})) \left(\prod_{k=j}^{i} \boldsymbol{\Phi_k}(0,1) \right)^T \int_0^1 \boldsymbol{\Phi_{j-1}}(u,1)^T \boldsymbol{b_{j-1}}(u)du \\
&= \frac{\partial h_{i+1}}{\partial \boldsymbol{x}}(\overline{\boldsymbol{x}}(\overline{\theta}_{i+1})) \left(\prod_{k=j}^{i} \boldsymbol{\Phi_k}(\overline{\theta}_k, \overline{\theta}_{k+1}) \right)^T \int_{\overline{\theta}_{j-1}}^{\overline{\theta}_j} \boldsymbol{\Phi_{j-1}}(\theta, \overline{\theta}_j)^T \boldsymbol{b_{j-1}} \frac{d\theta}{\overline{\theta}_j - \overline{\theta}_{j-1}}
\end{aligned} \tag{C.2}$$

with the convention $\prod_{k=j}^{i} \boldsymbol{\Phi_k} = \boldsymbol{\Phi_j}.\boldsymbol{\Phi_{j+1}}...\boldsymbol{\Phi_i}$. Similarly,

$$c_i^j = \frac{\partial h_{i+1}}{\partial \boldsymbol{x}}(\overline{\boldsymbol{x}}(\overline{\theta}_{i+1})) \left(\prod_{k=j}^{i} \boldsymbol{\Phi_k}(\overline{\theta}_k, \overline{\theta}_{k+1}) \right)^T \int_{\overline{\theta}_{j-1}}^{\overline{\theta}_j} \boldsymbol{\Phi_{j-1}}(\theta, \overline{\theta}_j)^T \boldsymbol{c_{j-1}}(\theta) \frac{d\theta}{\overline{\theta}_j - \overline{\theta}_{j-1}} \tag{C.3}$$

and

$$e_i = -\frac{\partial h_{i+1}}{\partial \boldsymbol{x}}(\overline{\boldsymbol{x}}(\overline{\theta}_{i+1})) \left(\prod_{k=0}^{i} \boldsymbol{\Phi_k}(\overline{\theta}_k, \overline{\theta}_{k+1}) \right)^T \frac{\partial \boldsymbol{g}}{\partial \boldsymbol{p_{ivc}}}(\overline{\boldsymbol{p}}_{\boldsymbol{ivc}})$$

C.1.2 Rewriting of the equations

The expression (C.2) and (C.3) can be simplified using Equations (2.15):

$$\begin{aligned}
&\frac{d}{d\theta}\left[\boldsymbol{\Phi_{j-1}}(\theta, \overline{\theta}_j)^T \cdot \boldsymbol{f_{j-1}}(\overline{\boldsymbol{x}}(\theta), \theta) \cdot (\theta - \overline{\theta}_{j-1}) \right] \\
&= \left(-\boldsymbol{A_{j-1}}^T \boldsymbol{\Phi_{j-1}}(\theta, \overline{\theta}_j) \right)^T \cdot \boldsymbol{f_{j-1}}(\overline{\boldsymbol{x}}(\theta), \theta) \cdot (\theta - \overline{\theta}_{j-1}) \\
&\quad + \boldsymbol{\Phi_{j-1}}(\theta, \overline{\theta}_j)^T \cdot \left(\frac{\partial \boldsymbol{f_{j-1}}}{\partial \theta}(\overline{\boldsymbol{x}}(\theta), \theta) + \frac{\partial \boldsymbol{f_{j-1}}}{\partial \boldsymbol{x}}(\overline{\boldsymbol{x}}(\theta), \theta) \frac{d\overline{\boldsymbol{x}}(\theta)}{d\theta} \right) \cdot (\theta - \overline{\theta}_{j-1}) \\
&\quad + \boldsymbol{\Phi_{j-1}}(\theta, \overline{\theta}_j)^T \cdot \boldsymbol{f_{j-1}}(\overline{\boldsymbol{x}}(\theta), \theta) \\
&= -\boldsymbol{\Phi_{j-1}}(\theta, \overline{\theta}_j)^T \boldsymbol{A_{j-1}} \boldsymbol{f_{j-1}}(\overline{\boldsymbol{x}}(\theta), \theta)(\theta - \overline{\theta}_{j-1}) \\
&\quad + \boldsymbol{\Phi_{j-1}}(\theta, \overline{\theta}_j)^T \frac{\partial \boldsymbol{f_{j-1}}}{\partial \theta}(\overline{\boldsymbol{x}}(\theta), \theta)(\theta - \overline{\theta}_{j-1}) \\
&\quad + \boldsymbol{\Phi_{j-1}}(\theta, \overline{\theta}_j)^T \boldsymbol{A_{j-1}} \boldsymbol{f_{j-1}}(\overline{\boldsymbol{x}}(\theta), \theta)(\theta - \overline{\theta}_{j-1}) + \boldsymbol{\Phi_{j-1}}(\theta, \overline{\theta}_j)^T \boldsymbol{f_{j-1}}(\overline{\boldsymbol{x}}(\theta), \theta) \\
&= \boldsymbol{\Phi_{j-1}}(\theta, \overline{\theta}_j)^T \boldsymbol{b_{j-1}}
\end{aligned}$$

And, thus

$$
\begin{aligned}
b_i^j &= \frac{\partial h_{i+1}}{\partial \boldsymbol{x}}(\overline{\boldsymbol{x}}(\overline{\theta}_{i+1}))\left(\prod_{k=j}^{i}\boldsymbol{\Phi_k}(\overline{\theta}_k,\overline{\theta}_{k+1})\right)^T\int_{\overline{\theta}_{j-1}}^{\overline{\theta}_j}\boldsymbol{\Phi_{j-1}}(\theta,\overline{\theta}_j)^T\boldsymbol{b_{j-1}}\frac{d\theta}{\overline{\theta}_j-\overline{\theta}_{j-1}}\\
&= \frac{\partial h_{i+1}}{\partial \boldsymbol{x}}(\overline{\boldsymbol{x}}(\overline{\theta}_{i+1}))\left(\prod_{k=j}^{i}\boldsymbol{\Phi_k}(\overline{\theta}_k,\overline{\theta}_{k+1})\right)^T\\
&\qquad\int_{\overline{\theta}_{j-1}}^{\overline{\theta}_j}\frac{d}{d\theta}\left[\boldsymbol{\Phi_{j-1}}(\theta,\overline{\theta}_j)^T\cdot\boldsymbol{f_{j-1}}(\overline{\boldsymbol{x}}(\theta),\theta)\cdot(\theta-\overline{\theta}_{j-1})\right]\frac{d\theta}{\overline{\theta}_j-\overline{\theta}_{j-1}}\\
&= \frac{\partial h_{i+1}}{\partial \boldsymbol{x}}(\overline{\boldsymbol{x}}(\overline{\theta}_{i+1}))\left(\prod_{k=j}^{i}\boldsymbol{\Phi_k}(\overline{\theta}_k,\overline{\theta}_{k+1})\right)^T\boldsymbol{\Phi_{j-1}}(\overline{\theta}_j,\overline{\theta}_j)^T\cdot\boldsymbol{f_{j-1}}(\overline{\boldsymbol{x}}(\overline{\theta}_j),\overline{\theta}_j)\\
&= \frac{\partial h_{i+1}}{\partial \boldsymbol{x}}(\overline{\boldsymbol{x}}(\overline{\theta}_{i+1}))\left(\prod_{k=j}^{i}\boldsymbol{\Phi_k}(\overline{\theta}_k,\overline{\theta}_{k+1})\right)^T\boldsymbol{f_{j-1}}(\overline{\boldsymbol{x}}(\overline{\theta}_j),\overline{\theta}_j)
\end{aligned}
$$

Similarly,

$$
\begin{aligned}
&\frac{d}{d\theta}\left[\boldsymbol{\Phi_{j-1}}(\theta,\overline{\theta}_j)^T\cdot\boldsymbol{f_{j-1}}(\overline{\boldsymbol{x}}(\theta),\theta)\cdot(\overline{\theta}_j-\theta)\right]\\
&=\boldsymbol{\Phi_{j-1}}(\theta,\overline{\theta}_j)^T\boldsymbol{c_{j-1}}
\end{aligned}
$$

and

$$
c_i^j = -\frac{\partial h_{i+1}}{\partial \boldsymbol{x}}(\overline{\boldsymbol{x}}(\overline{\theta}_{i+1}))\left(\prod_{k=j-1}^{i}\boldsymbol{\Phi_k}(\overline{\theta}_k,\overline{\theta}_{k+1})\right)^T\boldsymbol{f_{j-1}}(\overline{\boldsymbol{x}}(\overline{\theta}_{j-1}),\overline{\theta}_{j-1})
$$

C.1.3 Matrix coefficients

There, we give expressions for the matrices used in §2.4.3.

$$\boldsymbol{\Lambda} = \begin{pmatrix} \boldsymbol{h_2^x}{\boldsymbol{\Phi_1}}^T\boldsymbol{\Delta f_1} & \boldsymbol{h_2^x f_2^l} & 0 & 0 & 0 \\ \boldsymbol{h_3^x}{\boldsymbol{\Phi_2}}^T{\boldsymbol{\Phi_1}}^T\boldsymbol{\Delta f_1} & \boldsymbol{h_3^x}{\boldsymbol{\Phi_2}}^T\boldsymbol{\Delta f_2} & \boldsymbol{h_3^x f_3^l} & 0 & 0 \\ \vdots & \vdots & \ddots & \ddots & 0 \\ \boldsymbol{h_n^x}{\boldsymbol{\Phi_{n-1}}}^T..{\boldsymbol{\Phi_1}}^T\boldsymbol{\Delta f_1} & \boldsymbol{h_n^x}{\boldsymbol{\Phi_{n-1}}}^T..{\boldsymbol{\Phi_2}}^T\boldsymbol{\Delta f_2} & \dots & \boldsymbol{h_n^x}{\boldsymbol{\Phi_{n-1}}}^T\boldsymbol{\Delta f_{n-1}} & \boldsymbol{h_{n-1}^x f_n^l} \\ \boldsymbol{h_{n+1}^x}{\boldsymbol{\Phi_n}}^T..{\boldsymbol{\Phi_1}}^T\boldsymbol{\Delta f_1} & \boldsymbol{h_{n+1}^x}{\boldsymbol{\Phi_n}}^T..{\boldsymbol{\Phi_2}}^T\boldsymbol{\Delta f_2} & \dots & \boldsymbol{h_{n+1}^x}{\boldsymbol{\Phi_n}}^T{\boldsymbol{\Phi_{n-1}}}^T\boldsymbol{\Delta f_{n-1}} & \boldsymbol{h_{n+1}^x}{\boldsymbol{\Phi_n}}^T\boldsymbol{\Delta f_n} \end{pmatrix} \tag{C.4}$$

$$\boldsymbol{b} = \begin{pmatrix} 0 \\ 0 \\ \vdots \\ 0 \\ \boldsymbol{h_{n+1}^x f_{n+1}^l} \end{pmatrix},\ \boldsymbol{c} = \begin{pmatrix} -\boldsymbol{h_2^x}{\boldsymbol{\Phi_1}}^T{\boldsymbol{\Phi_0}}^T\boldsymbol{f_1^r} \\ -\boldsymbol{h_3^x}{\boldsymbol{\Phi_2}}^T..{\boldsymbol{\Phi_0}}^T\boldsymbol{f_1^r} \\ \vdots \\ -\boldsymbol{h_{n+1}^x}{\boldsymbol{\Phi_n}}^T..{\boldsymbol{\Phi_0}}^T\boldsymbol{f_1^r} \end{pmatrix},\ \boldsymbol{E} = \begin{pmatrix} 0 & 1 \\ -\boldsymbol{h_2^x}{\boldsymbol{\Phi_1}}^T{\boldsymbol{\Phi_0}}^T\boldsymbol{G} & 0 \\ -\boldsymbol{h_3^x}{\boldsymbol{\Phi_2}}^T..{\boldsymbol{\Phi_0}}^T\boldsymbol{G} & 0 \\ \vdots & \vdots \\ -\boldsymbol{h_{n+1}^x}{\boldsymbol{\Phi_n}}^T..{\boldsymbol{\Phi_0}}^T\boldsymbol{G} & 0 \\ 0 & 0 \end{pmatrix} \tag{C.5}$$

where

$$\begin{aligned} \boldsymbol{G} &= \frac{\partial \boldsymbol{g}}{\partial \boldsymbol{p_{ivc}}}(\overline{\boldsymbol{p}}_{\boldsymbol{ivc}}) \\ \boldsymbol{h_i^x} &= \frac{\partial h_i}{\partial \boldsymbol{x}}(\overline{\boldsymbol{x}}(\overline{\theta}_i)) \\ \boldsymbol{\Phi_i} &= \boldsymbol{\Phi_i}(\overline{\theta}_i, \overline{\theta}_{i+1}) \\ \boldsymbol{f_i^l} &= \boldsymbol{f_{i-1}}(\overline{\boldsymbol{x}}(\overline{\theta}_i), \overline{\theta}_i) \\ \boldsymbol{f_i^r} &= \boldsymbol{f_i}(\overline{\boldsymbol{x}}(\overline{\theta}_i), \overline{\theta}_i) \\ \boldsymbol{\Delta f_i} &= \boldsymbol{f_i^l} - \boldsymbol{f_i^r} \end{aligned} \tag{C.6}$$

C.2 Case study for the inversion of the matrix Λ

Here, we present two classes of examples, for which the invertibility assumption on the $\mathbf{\Lambda}$ matrix introduced in Chapter 2 can be investigated.

C.2.1 Scalar case (m=1)

In the case of a scalar state x, since every h_i^x, Δf_i, f_i^l, and Φ_i is also scalar, it is easy to show that the determinant of the matrix Λ can be factorized as follows

$$\det \mathbf{\Lambda} = (-1)^{n+1} \prod_{i=2}^{n+1} h_i^x \cdot \prod_{i=1}^{n} \Phi_i \cdot \Delta f_1 \cdot \prod_{i=2}^{n} f_i^r \tag{C.7}$$

By definition, the resolvents Φ_i are invertible. Then, in this scalar case, the non-invertibility of the matrix Λ arise out of one of the following:

- $\Delta f_1 = 0$. In fact, changing the time trigger does not affect the evolution of the whole differential system because the state x remains the same before and after the trigger. No compensation is possible.

- $h_i^x = 0$: to first order, an update of the state δx will not provide any change to the transition timing $(\frac{\partial h_i}{\partial x}(\overline{x}(\overline{\theta}_i))\delta x = 0$. The transition occurs at the same moment, regardless of any actions applied to the trigger. No compensation can thus be obtained (at first order).

- $f_i^r = 0$: the right-hand side of one of the differential systems vanishes at its beginning. In the case of an autonomous system, the solution is constant and, therefore, is not controllable. In the case of a non-autonomous system, the compensation is possible to obtain, but only at the second order.

C.2.2 Two-systems cases (n=2)

Let the number of differential systems be $n = 2$. Then, the matrix $\mathbf{\Lambda}$ is reduced to the scalar $\boldsymbol{h_2^x \Phi_1 \Delta f_1}$. This determinant may vanish when:

- $\boldsymbol{\Delta f_1} = 0$: see C.2.1.

- $\boldsymbol{h_2^x} = 0$: see C.2.1.

- the product $\boldsymbol{h_2^x \Phi_1 \Delta f_1}$ vanishes: the effect of a change of the trigger variable (represented by $\boldsymbol{\Delta f_1}$) has to be non-zero (as previously stated). However, if this effect, forwarded to the transition time ($\boldsymbol{\Phi_1 \Delta f_1}$), has an impact on the direction of the transition $\boldsymbol{h_2^x}$ which vanishes ($\boldsymbol{h_2^x \Phi_1 \Delta f_1} = 0$), then no

compensation can be obtained. This is certainly the case, for example, with the following problem: two linear systems, and a linear final transition.

$$\begin{aligned}\frac{d\boldsymbol{x}}{d\theta} &= \boldsymbol{A_0 x}\\ \frac{d\boldsymbol{x}}{d\theta} &= \boldsymbol{A_1 x} \qquad h_2(\boldsymbol{x}) = \boldsymbol{h_2 x},\end{aligned}$$

where $\boldsymbol{A_1} = \boldsymbol{A_0} + \boldsymbol{Id}$, ($\boldsymbol{Id}$: Identity). Indeed, in this case, one has (we follow notation of §C.1.3)

$$\begin{aligned}\boldsymbol{\Phi_1} &= e^{\boldsymbol{A_1}^T(\overline{\theta}_2-\overline{\theta}_1)}\\ \boldsymbol{h_2^x} &= \boldsymbol{h_2}\end{aligned}$$

and thus Λ is reduced to the scalar

$$\begin{aligned}\boldsymbol{\Lambda} &= \boldsymbol{h_2}\left(e^{\boldsymbol{A_1}^T(\overline{\theta}_2-\overline{\theta}_1)}\right)^T(\boldsymbol{A_1}-\boldsymbol{A_0})\overline{\boldsymbol{x}}(\overline{\theta}_1)\\ &= \boldsymbol{h_2}e^{\boldsymbol{A_1}(\overline{\theta}_2-\overline{\theta}_1)}\overline{\boldsymbol{x}}(\overline{\theta}_1)\\ &= \boldsymbol{h_2}\overline{\boldsymbol{x}}(\overline{\theta}_2)\end{aligned}$$

By definition of the transition equation, $\boldsymbol{\Lambda}$ vanishes.

Appendix D

Proof of the sensitivity theorem for $C^0 \cap C^1_{pc}$ functions

We recall that a $C^0 \cap C^1_{pc}$ function is a continuous function f for which there exists a partition $\mathcal{P}(\Omega)$ of its domain $\Omega \subset \mathbb{R}^n$ such that f is continuously differentiable on each $P \in \mathcal{P}(\Omega)$. Two consecutive subsets of the partition $\mathcal{P}(\Omega)$ are separated by a discontinuity hypersurface $\{\boldsymbol{x} \in \mathbb{R}^n | h(\boldsymbol{x}) = 0\}$.

In the following, the first theorem is a more complete form of Theorem 2.4.1 suitable for autonomous differential systems. Then, the three following theorems are theorems of increasing complexity suitable for $C^0 \cap C^1_{pc}$ functions. Theorem D.2.3 is the main theorem of this section, and is the one presented and used in Section 2.5.1.

D.1 C^0 or C^1 functions

Theorem D.1.1 (Sensitivity of an autonomous differential equation)**.** *Consider the following differential system*

$$\begin{cases} \dfrac{d}{dt}\boldsymbol{z}(t) = \boldsymbol{f}(\boldsymbol{z}(t), \boldsymbol{p_1}, t) \\ \quad \boldsymbol{z}(0) = \boldsymbol{p_2} \end{cases}$$

where $\boldsymbol{f} : \Omega \to \mathbb{R}^n$ is piecewise C^1 ($C^0 \cap C^1_{pc}$) with several continuously differentiable discontinuity hypersurfaces of the type $h(\boldsymbol{x}, \boldsymbol{p_1}, t) = 0$, and Ω is an open subset of $\mathbb{R}^n \times \mathbb{R}^k \times [0, 1]$. We denote by $\boldsymbol{z_p}$ the solution corresponding to the parameter $\boldsymbol{p} = (\boldsymbol{p_1}, \boldsymbol{p_2})$.

Let $\overline{\boldsymbol{p}}$ be such that the solution $\boldsymbol{z}_{\overline{\boldsymbol{p}}}$ crosses the discontinuity hypersurfaces in the following order: $h_1(\boldsymbol{x}, \boldsymbol{p_1}, t) = 0$ at $t = \overline{t}^s_1$, $h_2(\boldsymbol{x}, \boldsymbol{p_1}, t) = 0$ at $t = \overline{t}^s_2 > \overline{t}^s_1$, ..., $h_m(\boldsymbol{x}, \boldsymbol{p_1}, t) = 0$ at $t = \overline{t}^s_m > \overline{t}^s_{m-1}$. The preceding term "crosses" means that at time $\overline{t}^s_i$, one has

$$\frac{\partial h_i}{\partial \boldsymbol{x}}(\boldsymbol{z}_{\overline{\boldsymbol{p}}}(\overline{t}^s_i), \overline{\boldsymbol{p}}_{\boldsymbol{1}}, \overline{t}^s_i).\boldsymbol{f}(\boldsymbol{z}_{\overline{\boldsymbol{p}}}(\overline{t}^s_i), \overline{\boldsymbol{p}}_{\boldsymbol{1}}, \overline{t}^s_i) + \frac{\partial h_i}{\partial t}(\boldsymbol{z}_{\overline{\boldsymbol{p}}}(\overline{t}^s_i), \overline{\boldsymbol{p}}_{\boldsymbol{1}}, \overline{t}^s_i) \neq 0 \qquad \text{(D.1)}$$

This last expression can be assumed strictly positive without loss of generality.

Then,

- *there exists a neighborhood $\mathcal{V}(\overline{\boldsymbol{p}})$ of $\overline{\boldsymbol{p}}$ such that for every $\boldsymbol{p} \in \mathcal{V}(\overline{\boldsymbol{p}})$, the differential system has a unique solution $\boldsymbol{z_p}$ that crosses the discontinuity hypersurface in the exact same order as $\boldsymbol{z_{\overline{p}}}$ does.*

- *the application $\boldsymbol{\Gamma}$*

$$\begin{aligned} \boldsymbol{\Gamma} : \mathcal{V}(\overline{\boldsymbol{p}}) &\to ([0,1] \to \mathbb{R}^n) \\ \boldsymbol{p} &\mapsto \boldsymbol{z_p} \end{aligned}$$

  is differentiable and its derivative in $\overline{\boldsymbol{p}}$ is the application which maps $\boldsymbol{\delta p}$ to the solution of

$$\begin{cases} \dfrac{d}{dt}\boldsymbol{\delta z}(t) = \dfrac{\partial \boldsymbol{f}}{\partial \boldsymbol{z}}(\boldsymbol{z_{\overline{p}}}(t), \overline{\boldsymbol{p}}_{\boldsymbol{1}}, t).\boldsymbol{\delta z}(t) + \dfrac{\partial \boldsymbol{f}}{\partial \boldsymbol{p_1}}(\boldsymbol{z_{\overline{p}}}(t), \overline{\boldsymbol{p}}_{\boldsymbol{1}}, t).\boldsymbol{\delta p_1} \\ \boldsymbol{\delta z}(0) = \boldsymbol{\delta p_2} \end{cases}$$

Proof. see [20]. □

D.2 $C^0 \cap C^1_{pc}$ functions

Theorem D.2.1 (Sensitivity of an autonomous differential equation with $C^0 \cap C^1_{pc}$ right-hand side with 1 discontinuity)**.** *Consider the following differential system*

$$\begin{cases} \dfrac{d}{dt}\boldsymbol{z}(t) = f(\boldsymbol{z}(t)) \\ \boldsymbol{z}(0) = p \end{cases}$$

where $\boldsymbol{f} : \Omega \to \mathbb{R}^n$ is piecewise C^1 ($C^0 \cap C^1_{pc}$), and Ω is an open subset of $\mathbb{R}^n$. We denote by $\boldsymbol{z_p}$ the solution corresponding to the parameter $\boldsymbol{p}$.

Let $\overline{\boldsymbol{p}}$ be such that the solution $\boldsymbol{z_{\overline{p}}}$ crosses once and only once a discontinuity hypersurface $h(\boldsymbol{x}) = 0$ in time $\overline{t}_s \in]0,1[$. The term "crosses" means that at time $\overline{t}_s$, one has $\frac{\partial h}{\partial \boldsymbol{x}}(\boldsymbol{z_{\overline{p}}}(\overline{t}_s)).\boldsymbol{f}(\boldsymbol{z_{\overline{p}}}(\overline{t}_s)) \neq 0$, which can be supposed strictly positive without loss of generality).

Then,

- *there exists a neighborhood $\mathcal{V}(\overline{\boldsymbol{p}})$ of $\overline{\boldsymbol{p}}$ such that for every $p \in \mathcal{V}(\overline{\boldsymbol{p}})$, the differential system has a unique solution $\boldsymbol{z_p}$ that crosses the discontinuity hypersurface once in $[0,1]$.*

- *the application* $\mathbf{\Gamma}$

$$\begin{aligned} \mathbf{\Gamma} : \mathcal{V}(\overline{\boldsymbol{p}}) &\to ([0,1] \to \mathbb{R}^n) \\ \boldsymbol{p} &\mapsto \boldsymbol{z}_{\boldsymbol{p}} \end{aligned}$$

is differentiable and its derivative in $\overline{\boldsymbol{p}}$ *is the application which maps* $\boldsymbol{\delta p}$ *to the solution of*

$$\begin{cases} \dfrac{d}{dt}\boldsymbol{\delta z}(t) = \dfrac{\partial \boldsymbol{f}}{\partial \boldsymbol{z}}(\boldsymbol{z}_{\overline{\boldsymbol{p}}}(t)).\boldsymbol{\delta z}(t) \\ \boldsymbol{\delta z}(0) = \boldsymbol{\delta p} \end{cases} \tag{D.2}$$

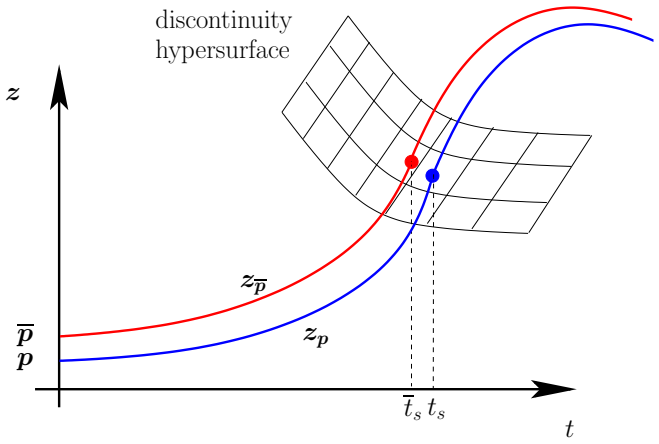

Figure D.1: *Two solutions of the differential system with 1 discontinuity.*

Proof of Theorem D.2.1. First note that the fact that the application $\mathbf{\Gamma}$ is well defined and continuous in this case follows from Theorem D.1.1 ($\boldsymbol{f} \in C^0 \cap C^1_{pc}$ is of course Lipschitz).

Let us prove the first point. Let Υ be the following application

$$\begin{aligned} \Upsilon : \mathbb{R} \times \mathbb{R} &\to \mathbb{R} \\ (\boldsymbol{p}, t) &\mapsto h(\boldsymbol{z}_{\boldsymbol{p}}(t)) \end{aligned}$$

The trajectory reaches the discontinuity hypersurface at a point defined by the zero of Υ. We want to use the implicit functions theorem to find a mapping between $\boldsymbol{p}$ and the discontinuity reaching time t_s. Since the applications $\boldsymbol{f}$, h, $\boldsymbol{p} \mapsto \boldsymbol{z}_{\boldsymbol{p}}$ (by Theorem D.1.1), and $t \mapsto \boldsymbol{z}_{\boldsymbol{p}}(t)$ are continuous, Υ is a continuous function. Secondly, since h and $t \mapsto \boldsymbol{z}_{\boldsymbol{p}}(t)$ are continuously differentiable functions, Υ is continuously differentiable with respect to t. Finally, since $\frac{\partial \Upsilon}{\partial t} = \frac{\partial h}{\partial \boldsymbol{x}}(\boldsymbol{z}_{\overline{\boldsymbol{p}}}(\overline{t}_s)).\boldsymbol{f}(\boldsymbol{z}_{\overline{\boldsymbol{p}}}(\overline{t}_s))$ is invertible in $(\overline{\boldsymbol{p}}, \overline{t}_s)$, from the implicit functions

theorem [60, thm 3.8.1], there exists two neighborhoods $\mathcal{V}_1(\overline{\boldsymbol{p}})$, and $\mathcal{W}_1(\overline{t}_s)$ on which the application ϕ mapping $\boldsymbol{p}$ to the solution of $\Upsilon(\boldsymbol{p}, \phi(\boldsymbol{p})) = 0$ is well-defined and continuously differentiable. Moreover, $\phi(\boldsymbol{p})$ is the *unique* solution of $\Upsilon(\boldsymbol{p}, \phi(\boldsymbol{p})) = 0$ in $\mathcal{W}_1(\overline{t}_s)$.

Since $0 < \overline{t}_s < 1$, the set $\mathcal{W}_2(t_s) = \mathcal{W}_1(t_s) \cap]0, 1[$ is a neighborhood of $\overline{t}_s$. From the continuity of ϕ, one gets that there exists a neighborhood $\mathcal{V}_2(\overline{\boldsymbol{p}})$ of $\overline{\boldsymbol{p}}$ such that

$$\forall \boldsymbol{p} \in \mathcal{V}_2(\overline{\boldsymbol{p}}), \quad \phi(\boldsymbol{p}) = t_s \in \mathcal{W}_2(\overline{t}_s) \tag{D.3}$$

Thus for all $\boldsymbol{p} \in \mathcal{V}_2(\overline{\boldsymbol{p}})$, $\boldsymbol{z_p}$ "reaches" once and only once the discontinuity hypersurface $h(\boldsymbol{x}) = 0$ (at time t_s).

To prove that $\boldsymbol{z_p}$ has the exact same behavior as $\boldsymbol{z_{\overline{p}}}$, we refine our neighborhood to have that $\boldsymbol{z_p}$, in fact, "crosses" (in the sense of the theorem statement) the discontinuity hypersurface $h(\boldsymbol{x}) = 0$ at time t_s, and that it does not reach any other discontinuity hypersurface in-between.

Since $\boldsymbol{p} \mapsto \frac{\partial \Upsilon}{\partial t}(\boldsymbol{p}, \phi(\boldsymbol{p}))$ is continuous and strictly positive at $\overline{\boldsymbol{p}}$, there exists a neighborhood $\mathcal{V}_3(\overline{\boldsymbol{p}})$ such that

$$\forall p \in \mathcal{V}_3(\overline{\boldsymbol{p}}), \quad \frac{\partial \Upsilon}{\partial t}(p, \phi(p)) > 0 \tag{D.4}$$

Then, for all $\boldsymbol{p}$ in $\mathcal{V}_3(\overline{\boldsymbol{p}})$, the trajectory $\boldsymbol{z_p}$ "crosses" the discontinuity hypersurface at a time t_s.

We wish to prove that there exists a neighborhood $\mathcal{V}_4(\overline{\boldsymbol{p}})$ such that, for all $\boldsymbol{p}$ in $\mathcal{V}_4(\overline{\boldsymbol{p}})$, the trajectory $\boldsymbol{z_p}$ does not reach any other discontinuity hypersurface than the one crossed by $\boldsymbol{z_{\overline{p}}}$. We proceed by contradiction. Assume that this statement is false. Then, one can construct a sequence $\{\boldsymbol{p_n}\}_{n \in \mathbb{N}}$ converging towards $\overline{\boldsymbol{p}}$ such that there exists a discontinuity hypersurface $\tilde{h}(\boldsymbol{x}) = 0$, and a sequence of times $0 \leq \theta_n \leq 1$ such that

$$\forall n, \quad \tilde{h}(\boldsymbol{z_{p_n}}(\theta_n)) = 0 \tag{D.5}$$

Since the sequence $0 \leq \theta_n \leq 1$ is bounded, there exists a converging subsequence $\theta_{\gamma(n)}$ converging towards θ. By continuity of the applications $\boldsymbol{p} \mapsto \boldsymbol{z_p}$, $\boldsymbol{z_p}$, and $\tilde{h}$, $\tilde{h}(\boldsymbol{z_{p_{\gamma(n)}}}(\theta_{\gamma(n)}))$ converges towards $\tilde{h}(\boldsymbol{z_{\overline{p}}}(\theta))$. Thus, $\tilde{h}(\boldsymbol{z_{\overline{p}}}(\theta)) = 0$, and $\boldsymbol{z_{\overline{p}}}$ reaches the discontinuity hypersurface $\tilde{h}(\boldsymbol{x}) = 0$. This proves the existence of $\mathcal{V}_4(\overline{\boldsymbol{p}})$.

Finally, consider $\mathcal{V}(\overline{\boldsymbol{p}}) = \mathcal{V}_2(\overline{\boldsymbol{p}}) \cap \mathcal{V}_3(\overline{\boldsymbol{p}}) \cap \mathcal{V}_4(\overline{\boldsymbol{p}})$. Since $\mathcal{V}(\overline{\boldsymbol{p}}) \subset \mathcal{V}_2(\overline{\boldsymbol{p}})$, then, for all $\boldsymbol{p}$ in $\mathcal{V}(\overline{\boldsymbol{p}})$, the trajectory $\boldsymbol{z_p}$ reaches the discontinuity hypersurface. Further, since $\mathcal{V}(\overline{\boldsymbol{p}}) \subset \mathcal{V}_4(\overline{\boldsymbol{p}})$, then, for all $\boldsymbol{p}$ in $\mathcal{V}(\overline{\boldsymbol{p}})$, the trajectory $\boldsymbol{z_p}$ does not reach any other discontinuity hypersurface than $h(\boldsymbol{x}) = 0$, and, finally, since $\mathcal{V}(\overline{\boldsymbol{p}}) \subset \mathcal{V}_3(\overline{\boldsymbol{p}})$, then, for all $\boldsymbol{p}$ in $\mathcal{V}(\overline{\boldsymbol{p}})$, the trajectory $\boldsymbol{z_p}$ in fact crosses the discontinuity hypersurfaces. This proves the first point of the theorem.

Now let us prove the second point. Let $p \in \mathcal{V}(\overline{\boldsymbol{p}})$. Since $\boldsymbol{z_p}$ and $\boldsymbol{z_{\overline{p}}}$ cross once and only once the discontinuity hypersurface, we note t_s and $\overline{t}_s$ the times at which they reach it. Without loss of generality, assume $\overline{t}_s < t_s$ (see Figure D.1).

From Theorem D.1.1, we get that Equation (D.2) has a solution on $[0, \overline{t}_s]$, and on $[\overline{t}_s, 1]$. Note $\boldsymbol{x}_{\overline{\boldsymbol{p}}}$ this solution on $[0, 1]$.

To prove the theorem, we have to prove that for all $t \in [0, 1]$, $\boldsymbol{z}_{\boldsymbol{p}}(t) - \boldsymbol{z}_{\overline{\boldsymbol{p}}}(t) = \boldsymbol{x}_{\overline{\boldsymbol{p}}}(t) + o(\boldsymbol{\delta p})$. We now prove it on three different intervals: $[0, \overline{t}_s]$, $[\overline{t}_s, t_s]$, and $[t_s, 1]$

1. From Theorem D.1.1, the latter equality holds everywhere in $[0, \overline{t}_s]$. In particular, $\boldsymbol{z}_{\boldsymbol{p}}(\overline{t}_s) - \boldsymbol{z}_{\overline{\boldsymbol{p}}}(\overline{t}_s) = \boldsymbol{x}_{\overline{\boldsymbol{p}}}(\overline{t}_s) + o(\boldsymbol{\delta p})$.

2. Around the discontinuity, we have

$$\begin{aligned}\boldsymbol{z}_{\overline{\boldsymbol{p}}}(t_s) &= \boldsymbol{z}_{\overline{\boldsymbol{p}}}(\overline{t}_s) + \boldsymbol{f}^+(\boldsymbol{z}_{\overline{\boldsymbol{p}}}(\overline{t}_s))(t_s - \overline{t}_s) + o(t_s - \overline{t}_s)\\ \boldsymbol{z}_{\boldsymbol{p}}(t_s) &= \boldsymbol{z}_{\boldsymbol{p}}(\overline{t}_s) + \boldsymbol{f}^-(\boldsymbol{z}_{\boldsymbol{p}}(t_s))(t_s - \overline{t}_s) + o(t_s - \overline{t}_s)\end{aligned}$$

   Then,

$$\begin{aligned}\boldsymbol{z}_{\boldsymbol{p}}(t_s) - \boldsymbol{z}_{\overline{\boldsymbol{p}}}(t_s) &= \boldsymbol{z}_{\boldsymbol{p}}(\overline{t}_s) - \boldsymbol{z}_{\overline{\boldsymbol{p}}}(\overline{t}_s) + \boldsymbol{f}^-(\boldsymbol{z}_{\boldsymbol{p}}(t_s))(t_s - \overline{t}_s)\\ &\quad - \boldsymbol{f}^+(\boldsymbol{z}_{\overline{\boldsymbol{p}}}(\overline{t}_s))(t_s - \overline{t}_s) + o(t_s - \overline{t}_s)\\ &= \boldsymbol{x}_{\overline{\boldsymbol{p}}}(\overline{t}_s) + o(\boldsymbol{\delta p}) + (\boldsymbol{f}^-(\boldsymbol{z}_{\boldsymbol{p}}(t_s)) - \boldsymbol{f}^+(\boldsymbol{z}_{\overline{\boldsymbol{p}}}(\overline{t}_s)))(t_s - \overline{t}_s)\\ &\quad + o(t_s - \overline{t}_s)\end{aligned} \tag{D.6}$$

   On the other hand, since $t_s = \phi(\boldsymbol{p})$ and because ϕ is continuous, one has

$$t_s - \overline{t}_s = O(\boldsymbol{\delta p}) \tag{D.7}$$

   Moreover, since $t \mapsto \boldsymbol{z}_{\boldsymbol{p}}(t)$, and $\boldsymbol{p} \mapsto \boldsymbol{z}_{\boldsymbol{p}}$ (Theorem D.1.1) are continuous, one has

$$\begin{aligned}\boldsymbol{z}_{\boldsymbol{p}}(t_s) - \boldsymbol{z}_{\overline{\boldsymbol{p}}}(\overline{t}_s) &= \boldsymbol{z}_{\boldsymbol{p}}(t_s) - \boldsymbol{z}_{\boldsymbol{p}}(\overline{t}_s) + \boldsymbol{z}_{\boldsymbol{p}}(\overline{t}_s) - \boldsymbol{z}_{\overline{\boldsymbol{p}}}(\overline{t}_s)\\ &= O(t_s - \overline{t}_s) + O(\boldsymbol{\delta p})\\ &= O(\boldsymbol{\delta p}) \qquad \text{(using Equation (D.7))}\end{aligned} \tag{D.8}$$

   Since $\boldsymbol{f}$ is continuous,

$$\begin{aligned}\boldsymbol{f}^-(\boldsymbol{z}_{\boldsymbol{p}}(t_s)) - \boldsymbol{f}^+(\boldsymbol{z}_{\overline{\boldsymbol{p}}}(\overline{t}_s)) &= O(\boldsymbol{z}_{\boldsymbol{p}}(t_s) - \boldsymbol{z}_{\overline{\boldsymbol{p}}}(\overline{t}_s))\\ &= O(\boldsymbol{\delta p}) \qquad \text{(using Equation (D.8))}\end{aligned} \tag{D.9}$$

   Finally, using Equations (D.6), (D.7), and (D.9), we have

$$\begin{aligned}\boldsymbol{z}_{\boldsymbol{p}}(t_s) - \boldsymbol{z}_{\overline{\boldsymbol{p}}}(t_s) &= \boldsymbol{x}_{\overline{\boldsymbol{p}}}(\overline{t}_s) + o(\boldsymbol{\delta p}) + O(t_s - \overline{t}_s)(t_s - \overline{t}_s) + o(t_s - \overline{t}_s)\\ &= \boldsymbol{x}_{\overline{\boldsymbol{p}}}(\overline{t}_s) + o(\boldsymbol{\delta p}) + o(t_s - \overline{t}_s)\\ &= \boldsymbol{x}_{\overline{\boldsymbol{p}}}(\overline{t}_s) + o(\boldsymbol{\delta p})\end{aligned} \tag{D.10}$$

3. Finally, using Theorem D.1.1 on the interval $[t_s, 1]$ about $\overline{\boldsymbol{q}} = \boldsymbol{z}_{\overline{\boldsymbol{p}}}(t_s)$ for $\boldsymbol{\delta q} = \boldsymbol{z}_{\boldsymbol{p}}(t_s) - \boldsymbol{z}_{\overline{\boldsymbol{p}}}(t_s)$, one has

$$\begin{aligned} \forall t \in [t_s, 1], \quad & \boldsymbol{z}_{\overline{\boldsymbol{q}}+\boldsymbol{\delta q}}(t - t_s) - \boldsymbol{z}_{\overline{\boldsymbol{q}}}(t - t_s) = \boldsymbol{x}_{\overline{\boldsymbol{q}}}(t - t_s) + o(\boldsymbol{\delta q}) \\ & \boldsymbol{z}_{\boldsymbol{z}_{\boldsymbol{p}}(\boldsymbol{t_s})}(t - t_s) - \boldsymbol{z}_{\boldsymbol{z}_{\overline{\boldsymbol{p}}}(\boldsymbol{t_s})}(t - t_s) = \boldsymbol{x}_{\boldsymbol{z}_{\overline{\boldsymbol{p}}}(\boldsymbol{t_s})}(t - t_s) + o(\boldsymbol{z}_{\boldsymbol{p}}(t_s) - \boldsymbol{z}_{\overline{\boldsymbol{p}}}(t_s)) \end{aligned} \tag{D.11}$$

By definition, $\boldsymbol{z}_{\boldsymbol{z}_{\overline{\boldsymbol{p}}}(\boldsymbol{t_s})}(t - t_s) = \boldsymbol{z}_{\overline{\boldsymbol{p}}}(t)$, $\boldsymbol{z}_{\boldsymbol{z}_{\boldsymbol{p}}(\boldsymbol{t_s})}(t - t_s) = \boldsymbol{z}_{\boldsymbol{p}}(t)$, and $\boldsymbol{x}_{\boldsymbol{z}_{\overline{\boldsymbol{p}}}(\boldsymbol{t_s})}(t - t_s) = \boldsymbol{x}_{\overline{\boldsymbol{p}}}(t)$. So, using Equations (D.10) and (D.11) we have

$$\begin{aligned} \forall t \in [t_s, 1], \quad \boldsymbol{z}_{\boldsymbol{p}}(t) - \boldsymbol{z}_{\overline{\boldsymbol{p}}}(t) &= \boldsymbol{x}_{\overline{\boldsymbol{p}}}(t) + o(\boldsymbol{x}_{\overline{\boldsymbol{p}}}(\overline{t}_s)) + o(\boldsymbol{\delta p}) \\ &= \boldsymbol{x}_{\overline{\boldsymbol{p}}}(t) + o(\boldsymbol{\delta p}) \end{aligned} \tag{D.12}$$

This ends the proof. □

Theorem D.2.2 (Sensitivity of an autonomous differential equation with $C^0 \cap C^1_{pc}$ right-hand side)**.** *Consider the following differential system*

$$\begin{cases} \dfrac{d}{dt}\boldsymbol{z}(t) = \boldsymbol{f}(\boldsymbol{z}(t)) \\ \quad \boldsymbol{z}(0) = \boldsymbol{p} \end{cases}$$

where $\boldsymbol{f} : \Omega \to \mathbb{R}^n$ is piecewise C^1 ($C^0 \cap C^1_{pc}$) with several continuously differentiable discontinuity hypersurfaces of the type $h(\boldsymbol{x}) = 0$, and Ω is an open subset of $\mathbb{R}^n$. We denote by $\boldsymbol{z}_{\boldsymbol{p}}$ the solution corresponding to the parameter $\boldsymbol{p}$.

Let $\overline{\boldsymbol{p}}$ be such that the solution $\boldsymbol{z}_{\overline{\boldsymbol{p}}}$ crosses the discontinuity hypersurfaces in the following order: $h_1(\boldsymbol{x}) = 0$ in $t = t_1^s$, $h_2(\boldsymbol{x}) = 0$ in $t = t_2^s > t_1^s$, ..., $h_m(\boldsymbol{x}) = 0$ in $t = t_m^s > t_{m-1}^s$. The term "crosses" means that at time $\overline{t}_i^s$, one has $\frac{\partial h_i}{\partial \boldsymbol{x}}(\boldsymbol{z}_{\overline{\boldsymbol{p}}}(\overline{t}_i^s)).\boldsymbol{f}(\boldsymbol{z}_{\overline{\boldsymbol{p}}}(\overline{t}_i^s)) \neq 0$, which can be supposed strictly positive without loss of generality).

Then,

- *there exists a neighborhood $\mathcal{V}(\overline{\boldsymbol{p}})$ of $\overline{\boldsymbol{p}}$ such that for every $\boldsymbol{p} \in \mathcal{V}(\overline{\boldsymbol{p}})$, the differential system has a unique solution $\boldsymbol{z}_{\boldsymbol{p}}$ that crosses the discontinuity hypersurface in the exact same order as $\boldsymbol{z}_{\overline{\boldsymbol{p}}}$.*
- *the application $\boldsymbol{\Gamma}$*

$$\begin{aligned} \boldsymbol{\Gamma} : \mathcal{V}(\overline{\boldsymbol{p}}) &\to ([0, 1] \to \mathbb{R}^n) \\ \boldsymbol{p} &\mapsto \boldsymbol{z}_{\boldsymbol{p}} \end{aligned}$$

is differentiable and its derivative in $\overline{\boldsymbol{p}}$ is the application which maps $\boldsymbol{\delta p}$ to the solution of

$$\begin{cases} \dfrac{d}{dt}\boldsymbol{\delta z}(t) = \dfrac{\partial \boldsymbol{f}}{\partial \boldsymbol{z}}(\boldsymbol{z}_{\overline{\boldsymbol{p}}}(t)).\boldsymbol{\delta z}(t) \\ \quad \boldsymbol{\delta z}(0) = \boldsymbol{\delta p} \end{cases} \tag{D.13}$$

Proof of Theorem D.2.2. First note that the fact that the application $\mathbf{\Gamma}$ is well defined and continuous in this case follows from Theorem D.1.1 ($\boldsymbol{f} \in C^0 \cap C^1_{pc}$ is of course Lipschitz).

Let us prove the first point Let $h_1(\boldsymbol{x}) = 0$, $h_2(\boldsymbol{x}) = 0$, ..., and $h_m(\boldsymbol{x}) = 0$, the discontinuity hypersurfaces in their order of crossing ($\boldsymbol{z_p}$ crosses h_1 at time t_1^s, then h_2 at time t_2^s, ...). Let Υ be the application

$$\begin{aligned} \mathbf{\Upsilon} : \mathbb{R} \times \mathbb{R}^m &\to \mathbb{R}^m \\ (\boldsymbol{p}, (t_1, t_2, ..., t_m)) &\mapsto (h_1(\boldsymbol{z_p}(t_1)), h_2(\boldsymbol{z_p}(t_2)), ..., h_m(\boldsymbol{z_p}(t_m))) \end{aligned}$$

Trajectory reaches the discontinuity hypersurfaces at times defined by the zeros of $\mathbf{\Upsilon}$. We want to use the implicit functions theorem to find a mapping between $\boldsymbol{p}$ and the discontinuity reaching times $(t_1, t_2, ..., t_m)$. Since the applications $\boldsymbol{f}$, h_i, $\boldsymbol{p} \mapsto \boldsymbol{z_p}$ (by Theorem D.1.1), and $t \mapsto \boldsymbol{z_p}(t)$ are continuous, $\mathbf{\Upsilon}$ is a continuous function. Then, because h_i and $t \mapsto \boldsymbol{z_p}(t)$ are continuously differentiable functions, $\mathbf{\Upsilon}$ is continuously differentiable with respect to its second component. Finally, since $\frac{\partial \mathbf{\Upsilon}}{\partial (t_1, t_2, ..., t_m)}$ is the following diagonal matrix

$$\frac{\partial \mathbf{\Upsilon}(\boldsymbol{p}, (t_1, t_2, ..., t_m))}{\partial (t_1, t_2, ..., t_m)} = \begin{pmatrix} \frac{\partial h_1}{\partial \boldsymbol{x}}(\boldsymbol{z_p}(t_1)).\boldsymbol{f}(\boldsymbol{z_p}(t_1)) & & \\ & \ddots & \\ & & \frac{\partial h_m}{\partial \boldsymbol{x}}(\boldsymbol{z_p}(t_m)).\boldsymbol{f}(\boldsymbol{z_p}(t_m)) \end{pmatrix} \tag{D.14}$$

it is invertible in $(\overline{\boldsymbol{p}}, (\overline{t}_1^s, \overline{t}_2^s, ..., \overline{t}_m^s))$. From the implicit functions theorem [60, thm 3.8.1], there exists two neighborhoods $\mathcal{V}_1(\overline{\boldsymbol{p}})$, and $\mathcal{W}_1(\overline{t}_1^s, \overline{t}_2^s, ..., \overline{t}_m^s)$ on which the application ϕ mapping $\boldsymbol{p}$ to the solution of $\mathbf{\Upsilon}(\boldsymbol{p}, \phi(\boldsymbol{p})) = 0$ is well defined and continuously differentiable. Moreover, $\phi(p)$ is the *unique* solution of $\mathbf{\Upsilon}(p, \phi(p)) = 0$ in $\mathcal{W}_1(\overline{t}_1^s, \overline{t}_2^s, ..., \overline{t}_m^s)$.

Since $0 < \overline{t}_1^s < \overline{t}_2^s < ... < \overline{t}_m^s < 1$. Let $(t_1, t_2, ...t_{m-1}) \in \mathbb{R}^{m-1}$, such that $0 < \overline{t}_1^s < t_1 < \overline{t}_2^s < t_2 < ...t_{m-1} < \overline{t}_m^s < 1$. Then, $\mathcal{W}_2$ defined as

$$\mathcal{W}_2(t_1^s, t_2^s, ..., t_m^s) = \mathcal{W}_1(t_1^s, t_2^s, ..., t_m^s) \cap]0, t_1[\times]t_1, t_2[\times ... \times]t_{m-1}, 1[\tag{D.15}$$

is a neighborhood of $(\overline{t}_1^s, \overline{t}_2^s, ..., \overline{t}_m^s)$.

From the continuity of ϕ, one gets that there exists a neighborhood $\mathcal{V}_2(\overline{\boldsymbol{p}})$ of $\overline{\boldsymbol{p}}$ such that

$$\forall \boldsymbol{p} \in \mathcal{V}_2(\overline{\boldsymbol{p}}), \quad \phi(\boldsymbol{p}) = (t_1^s, t_2^s, ..., t_m^s) \in \mathcal{W}_2(\overline{t}_1^s, \overline{t}_2^s, ..., \overline{t}_m^s) \tag{D.16}$$

Thus $\forall \boldsymbol{p} \in \mathcal{V}_2(\overline{\boldsymbol{p}})$, $\boldsymbol{z_p}$ "reaches" once and only once the discontinuity hypersurface $h_i(\boldsymbol{x}) = 0$ (at time t_i^s), and $t_{i-1} < t_i^s < t_i$[1].

To prove that $\boldsymbol{z_p}$ has the exact same behavior as $\boldsymbol{z_{\overline{p}}}$, we refine our neighborhood to guarantee that $\boldsymbol{z_p}$ "crosses" (in the sense of the theorem statement) the

[1] with the convention $t_0 = 0$, and $t_m = 1$

discontinuity hypersurfaces $h_i(\boldsymbol{x}) = 0$ at the times t_i^s, and that it does not reach any other discontinuity hypersurface in-between.

Since $\boldsymbol{p} \mapsto \frac{\partial \boldsymbol{\Upsilon}_i}{\partial t_i}(\boldsymbol{p}, \phi(\boldsymbol{p}))$ is continuous and strictly positive at $\overline{p}$, there exists a neighborhood $\mathcal{V}_3^i(\overline{\boldsymbol{p}})$ such that

$$\forall \boldsymbol{p} \in \mathcal{V}_3^i(\overline{\boldsymbol{p}}), \quad \frac{\partial \boldsymbol{\Upsilon}_i}{\partial t_i}(\boldsymbol{p}, \phi_i(\boldsymbol{p})) > 0. \tag{D.17}$$

Then, for all $\boldsymbol{p}$ in $\mathcal{V}_3^i(\overline{\boldsymbol{p}})$, the trajectory $\boldsymbol{z_p}$ "crosses" the discontinuity hypersurface at a time t_i^s. Now, consider $\mathcal{V}_3(\overline{\boldsymbol{p}}) = \cap_{1<i<m}\mathcal{V}_3^i(\overline{\boldsymbol{p}})$. $\mathcal{V}_3(\overline{\boldsymbol{p}})$, which clearly is a neighborhood of $\overline{\boldsymbol{p}}$.

We wish to prove that there exists a neighborhood $\mathcal{V}_4(\overline{\boldsymbol{p}})$ such that, for all $\boldsymbol{p}$ in $\mathcal{V}_4(\overline{\boldsymbol{p}})$, the trajectory $\boldsymbol{z_p}$ does not reach any other discontinuity hypersurface than the one crossed $\boldsymbol{z_{\overline{p}}}$. Again, we proceed by contradiction. Assume that it is false. Then, one can construct a sequence $\{\boldsymbol{p_n}\}_{n\in\mathbb{N}}$ converging towards $\overline{\boldsymbol{p}}$ such that there exists a discontinuity hypersurface $h(\boldsymbol{x}) = 0$ and a sequence of time $0 \leq \theta_n \leq 1$ such that

$$\forall n, \quad h(\boldsymbol{z_{p_n}}(\theta_n)) = 0. \tag{D.18}$$

Since the sequence $0 \leq \theta_n \leq 1$ is bounded, there exists a converging subsequence $\theta_{\gamma(n)}$ (converging towards θ). By continuity of the applications $\boldsymbol{p} \mapsto \boldsymbol{z_p}$, $\boldsymbol{z_p}$, and h, $h(\boldsymbol{z_{p_{\gamma(n)}}}(\theta_{\gamma(n)}))$ converges towards $h(\boldsymbol{z_{\overline{p}}}(\theta))$. Thus, $h(\boldsymbol{z_{\overline{p}}}(\theta)) = 0$, and $\boldsymbol{z_{\overline{p}}}$ reaches the discontinuity hypersurface $h(\boldsymbol{x}) = 0$. This proves the existence of $\mathcal{V}_4(\overline{\boldsymbol{p}})$.

Finally, consider $\mathcal{V}(\overline{\boldsymbol{p}}) = \mathcal{V}_2(\overline{\boldsymbol{p}}) \cap \mathcal{V}_3(\overline{\boldsymbol{p}}) \cap \mathcal{V}_4(\overline{\boldsymbol{p}})$. Since $\mathcal{V}(\overline{\boldsymbol{p}}) \subset \mathcal{V}_2(\overline{\boldsymbol{p}})$, then, for all $\boldsymbol{p}$ in $\mathcal{V}(\overline{\boldsymbol{p}})$, the trajectory $\boldsymbol{z_p}$ reaches the discontinuity hypersurfaces in the same order as $\boldsymbol{z_{\overline{p}}}$. Further, since $\mathcal{V}(\overline{\boldsymbol{p}}) \subset \mathcal{V}_4(\overline{\boldsymbol{p}})$, then, for all $\boldsymbol{p}$ in $\mathcal{V}(\overline{\boldsymbol{p}})$, the trajectory $\boldsymbol{z_p}$ does not reach any other discontinuity hypersurface than the one reached by $\boldsymbol{z_{\overline{p}}}$, and, finally, since $\mathcal{V}(\overline{\boldsymbol{p}}) \subset \mathcal{V}_3(\overline{\boldsymbol{p}})$, then, for all $\boldsymbol{p}$ in $\mathcal{V}(\overline{\boldsymbol{p}})$, the trajectory $\boldsymbol{z_p}$ crosses the discontinuity hypersurfaces. This prove the first point.

Now, let us prove the second point of the theorem. From theorem D.1.1, we get that the Equation (D.13) has a solution on $[0, \overline{t}_1^s]$, on $[\overline{t}_1^s, \overline{t}_2^s]$,..., and on $[\overline{t}_m^s, 1]$. Note $\boldsymbol{x_{\overline{p}}}$ this solution globally defined on $[0, 1]$. To prove the theorem, we have to prove that

$$\forall t \in [0,1], \boldsymbol{z_p}(t) - \boldsymbol{z_{\overline{p}}}(t) = \boldsymbol{x_{\overline{p}}}(t) + o(\boldsymbol{\delta p}).$$

We now prove it on by induction on m.

- From Theorem D.1.1, if $m = 0$, $\boldsymbol{f} \in C^1$, so that

$$\forall t \in [0,1], \boldsymbol{z_p}(t) - \boldsymbol{z_{\overline{p}}}(t) = \boldsymbol{x_{\overline{p}}}(t) + o(\boldsymbol{\delta p}) \tag{D.19}$$

- Assume it is true for $m-1$, then, on the fixed time interval $[0, t_m]$, one has

$$\forall t \in [0,t_m], \boldsymbol{z_p}(t) - \boldsymbol{z_{\overline{p}}}(t) = \boldsymbol{x_{\overline{p}}}(t) + o(\boldsymbol{\delta p}) \tag{D.20}$$

By definition of $\mathcal{V}(\overline{\boldsymbol{p}})$, on the fixed time interval $[t_m, 1]$, each solution $\boldsymbol{z_p}$ crosses the discontinuity hypersurface $h_m(\boldsymbol{x}) = 0$ once. Using Theorem D.2.1 about $\overline{\boldsymbol{q}} = \boldsymbol{z}_{\overline{\boldsymbol{p}}}(t_m)$ for $\boldsymbol{\delta q} = \boldsymbol{z_p}(t_m) - \boldsymbol{z}_{\overline{\boldsymbol{p}}}(t_m)$, we have

$$\begin{aligned} \forall t \in [t_m, 1], \quad \boldsymbol{z}_{\overline{\boldsymbol{q}}+\boldsymbol{\delta q}}(t - t_m) - \boldsymbol{z}_{\overline{\boldsymbol{q}}}(t - t_m) &= \boldsymbol{x}_{\overline{\boldsymbol{q}}}(t - t_m) + o(\boldsymbol{\delta q}) \\ \boldsymbol{z}_{\boldsymbol{z_p}(\boldsymbol{t_m})}(t - t_m) - \boldsymbol{z}_{\boldsymbol{z}_{\overline{\boldsymbol{p}}}(\boldsymbol{t_m})}(t - t_m) &= \boldsymbol{x}_{\boldsymbol{z}_{\overline{\boldsymbol{p}}}(\boldsymbol{t_m})}(t - t_m) + o(\boldsymbol{z_p}(t_m) - \boldsymbol{z}_{\overline{\boldsymbol{p}}}(t_m)) \end{aligned} \tag{D.21}$$

By definition, $\boldsymbol{z}_{\boldsymbol{z}_{\overline{\boldsymbol{p}}}(\boldsymbol{t_m})}(t-t_m) = \boldsymbol{z}_{\overline{\boldsymbol{p}}}(t)$, $\boldsymbol{z}_{\boldsymbol{z_p}(\boldsymbol{t_m})}(t-t_m) = \boldsymbol{z_p}(t)$, and $\boldsymbol{x}_{\boldsymbol{z}_{\overline{\boldsymbol{p}}}(\boldsymbol{t_m})}(t-t_m) = \boldsymbol{x}_{\overline{\boldsymbol{p}}}(t)$. So, using Equations (D.20) at time t_m in Equation (D.21) gives

$$\begin{aligned} \forall t \in [t_m, 1], \quad \boldsymbol{z_p}(t) - \boldsymbol{z}_{\overline{\boldsymbol{p}}}(t) &= \boldsymbol{x}_{\overline{\boldsymbol{p}}}(t) + o(\boldsymbol{x}_{\overline{\boldsymbol{p}}}(t_m)) + o(\boldsymbol{\delta p}) \\ &= \boldsymbol{x}_{\overline{\boldsymbol{p}}}(t) + o(\boldsymbol{\delta p}) \end{aligned} \tag{D.22}$$

Gathering Equations (D.19), and (D.22) one obtains the induction hypothesis at step m. Then one has

$$\forall t \in [0, 1], \quad \boldsymbol{z_p}(t) - \boldsymbol{z}_{\overline{\boldsymbol{p}}}(t) = \boldsymbol{x}_{\overline{\boldsymbol{p}}}(t) + o(\boldsymbol{\delta p})$$

This concludes the proof. □

Theorem D.2.3 (Sensitivity of a differential equation with $C^0 \cap C^1_{pc}$ right-hand side)**.** *Consider the following differential system*

$$\begin{cases} \dfrac{d}{dt}\boldsymbol{z}(t) = \boldsymbol{f}(\boldsymbol{z}(t), \boldsymbol{p_1}, t) \\ \quad \boldsymbol{z}(0) = \boldsymbol{p_2} \end{cases}$$

where $\boldsymbol{f} : \Omega \to \mathbb{R}^n$ is piecewise C^1 ($C^0 \cap C^1_{pc}$) with several continuously differentiable discontinuity hypersurfaces of the type $h(\boldsymbol{x}, \boldsymbol{p_1}, t) = 0$, and Ω is an open subset of $\mathbb{R}^n \times \mathbb{R}^k \times [0, 1]$. We denote by $\boldsymbol{z_p}$ the solution corresponding to the parameter $\boldsymbol{p} = (\boldsymbol{p_1}, \boldsymbol{p_2})$.

Let $\overline{\boldsymbol{p}}$ be such that the solution $\boldsymbol{z}_{\overline{\boldsymbol{p}}}$ crosses the discontinuity hypersurfaces in the following order: $h_1(\boldsymbol{x}, \boldsymbol{p_1}, t) = 0$ at $t = t_1^s$, $h_2(\boldsymbol{x}, \boldsymbol{p_1}, t) = 0$ at $t = t_2^s > t_1^s$, ..., $h_m(\boldsymbol{x}, \boldsymbol{p_1}, t) = 0$ at $t = t_m^s > t_{m-1}^s$. The preceding term "crosses" means that at time $\overline{t}_i^s$, one has

$$\frac{\partial h_i}{\partial \boldsymbol{x}}(\boldsymbol{z}_{\overline{\boldsymbol{p}}}(\overline{t}_i^s), \overline{\boldsymbol{p}}_{\boldsymbol{1}}, \overline{t}_i^s).\boldsymbol{f}(\boldsymbol{z}_{\overline{\boldsymbol{p}}}(\overline{t}_i^s), \overline{\boldsymbol{p}}_{\boldsymbol{1}}, \overline{t}_i^s) + \frac{\partial h_i}{\partial t}(\boldsymbol{z}_{\overline{\boldsymbol{p}}}(\overline{t}_i^s), \overline{\boldsymbol{p}}_{\boldsymbol{1}}, \overline{t}_i^s) \neq 0 \tag{D.23}$$

This last expression can be assumed strictly positive without loss of generality.

Then,

- *there exists a neighborhood $\mathcal{V}(\overline{\boldsymbol{p}})$ of $\overline{\boldsymbol{p}}$ such that for every $\boldsymbol{p} \in \mathcal{V}(\overline{\boldsymbol{p}})$, the differential system has a unique solution $\boldsymbol{z_p}$ that crosses the discontinuity hypersurface in the exact same order as $\boldsymbol{z}_{\overline{\boldsymbol{p}}}$.*

- *the application* $\mathbf{\Gamma}$

$$\begin{aligned} \mathbf{\Gamma} : \mathcal{V}(\overline{\boldsymbol{p}}) &\to ([0,1] \to \mathbb{R}^n) \\ \boldsymbol{p} &\mapsto \boldsymbol{z_p} \end{aligned}$$

is differentiable and its derivative in $\overline{\boldsymbol{p}}$ *is the application which maps* $\boldsymbol{\delta p}$ *to the solution of*

$$\begin{cases} \dfrac{d}{dt}\boldsymbol{\delta z}(t) = \dfrac{\partial \boldsymbol{f}}{\partial \boldsymbol{z}}(\boldsymbol{z}_{\overline{\boldsymbol{p}}}(t), \overline{\boldsymbol{p}}_{\boldsymbol{1}}, t).\boldsymbol{\delta z}(t) + \dfrac{\partial \boldsymbol{f}}{\partial \boldsymbol{p_1}}(\boldsymbol{z}_{\overline{\boldsymbol{p}}}(t), \overline{\boldsymbol{p}}_{\boldsymbol{1}}, t).\boldsymbol{\delta p_1} \\ \quad \boldsymbol{\delta z}(0) = \boldsymbol{\delta p_2} \end{cases} \tag{D.24}$$

Proof. We wish to use Theorem D.2.2. To this end, we extend the state $\boldsymbol{y} = (\boldsymbol{z}, \boldsymbol{p_1}, t)^T$. Then $\boldsymbol{y}$ satisfies the following system of differential equations

$$\begin{cases} \dfrac{d}{dt}\boldsymbol{y}(t) = (\boldsymbol{f}(\boldsymbol{y}(t)), 0, 1)^T \\ \quad \boldsymbol{y}(0) = (\boldsymbol{p_2}, \boldsymbol{p_1}, 0)^T \end{cases}$$

For $\overline{\boldsymbol{p}} = (\overline{\boldsymbol{p}}_{\boldsymbol{1}}, \overline{\boldsymbol{p}}_{\boldsymbol{2}})$, since the solution $\boldsymbol{z}_{\overline{\boldsymbol{p}}}$, "crosses" the discontinuity hypersurfaces $h_i(\boldsymbol{z}, \boldsymbol{p_1}, t) = 0$, and

$$\frac{\partial h_i}{\partial \boldsymbol{x}}(\boldsymbol{z}_{\overline{\boldsymbol{p}}}(\overline{t}_i^s), \overline{\boldsymbol{p}}_{\boldsymbol{1}}, \overline{t}_i^s).\boldsymbol{f}(\boldsymbol{z}_{\overline{\boldsymbol{p}}}(\overline{t}_i^s), \overline{\boldsymbol{p}}_{\boldsymbol{1}}, \overline{t}_i^s) + \frac{\partial h_i}{\partial t}(\boldsymbol{z}_{\overline{\boldsymbol{p}}}(\overline{t}_i^s), \overline{\boldsymbol{p}}_{\boldsymbol{1}}, \overline{t}_i^s) = \frac{\partial h_i}{\partial \boldsymbol{y}}(\boldsymbol{y}_{\overline{\boldsymbol{p}}}(\overline{t}_s)).(\boldsymbol{f}(\boldsymbol{y}_{\overline{\boldsymbol{p}}}(\overline{t}_i^s)), 0, 1)^T$$

then the solution $\boldsymbol{y}_{\overline{\boldsymbol{p}}}$ "crosses" the discontinuity hypersurfaces $h_i(\boldsymbol{y}) = 0$. Then, Theorem D.2.2 yields the existence of a neighborhood $\mathcal{V}(\overline{\boldsymbol{p}})$ on which the application $\mathbf{\Gamma}$ is differentiable and its derivative is the application which maps $\boldsymbol{\delta p} = (\boldsymbol{\delta p}_1, \boldsymbol{\delta p}_2)$ to the solution of

$$\begin{cases} \dfrac{d}{dt}\boldsymbol{\delta y}(t) = \dfrac{\partial(\boldsymbol{y} \mapsto (\boldsymbol{f}(\boldsymbol{y}), 0, 1)^T)}{\partial \boldsymbol{y}}(\boldsymbol{y}_{\overline{\boldsymbol{p}}}(t)).\boldsymbol{\delta y}(t) \\ \quad \boldsymbol{\delta y}(0) = (\boldsymbol{\delta p_2}, \boldsymbol{\delta p_1}, 0) \end{cases}$$

or equivalently

$$\begin{cases} \dfrac{d}{dt}\boldsymbol{\delta z}(t) = \dfrac{\partial \boldsymbol{f}}{\partial \boldsymbol{z}}(\boldsymbol{z}_{\overline{\boldsymbol{p}}}(t), \overline{\boldsymbol{p}}_{\boldsymbol{1}}, t).\boldsymbol{\delta z}(t) + \dfrac{\partial \boldsymbol{f}}{\partial \boldsymbol{p_1}}(\boldsymbol{z}_{\overline{\boldsymbol{p}}}(t), \overline{\boldsymbol{p}}_{\boldsymbol{1}}, t).\boldsymbol{\delta p}_1 \\ \quad \boldsymbol{\delta z}(0) = \boldsymbol{\delta p}_2 \end{cases}$$

this conclude the proof.

□

Appendix E

Analytic expression of the correction gain

In this appendix, we explain how to find an analytic expression to the combustion controller gain "α" in the case study developed in Section 4.1. We follow the frame of Algorithm 2.6.1 step by step.

1) The combustion model under consideration is expressed in §4.2.2 under the form of $n+1=2$ differential systems of dimensions $m=4$. We recall that the state is $\boldsymbol{x}=(P,T,X,\tau_{ai})$. The initial state of the first differential equation is

$$\boldsymbol{x_0}=\boldsymbol{G_0 p_{ivc}}=\begin{pmatrix}1&0&0\\0&1&0\\0&0&1\\0&0&0\end{pmatrix}\begin{pmatrix}P_{ivc}\\T_{ivc}\\X_{ivc}\end{pmatrix} \tag{E.1}$$

The evolution of the state during both phases is governed by

i)

$$\boldsymbol{f_0}(\boldsymbol{x},\theta)=\begin{pmatrix}-\gamma P\dfrac{dV(\theta)}{d\theta}\dfrac{1}{V(\theta)}\\-(\gamma-1)T\dfrac{dV(\theta)}{d\theta}\dfrac{1}{V(\theta)}\\0\\0\end{pmatrix} \tag{E.2}$$

ii)

$$\boldsymbol{f_1}(\boldsymbol{x},\theta) = \begin{pmatrix} -\gamma P \dfrac{dV(\theta)}{d\theta}\dfrac{1}{V(\theta)} \\ -(\gamma-1)T\dfrac{dV(\theta)}{d\theta}\dfrac{1}{V(\theta)} \\ 0 \\ A\dfrac{1+kM_f^{pilot}}{1+CX}P(\theta)^{n_1}\exp\left(-\dfrac{T_1}{T(\theta)}\right)\dfrac{1}{N_e} \end{pmatrix} \tag{E.3}$$

And the controlled combustion phasing is defined by the transition equation

$$\begin{aligned} & h_2(\boldsymbol{x}) = 0 \\ \Leftrightarrow & \boldsymbol{h_2 x} - 1 = 0 \end{aligned} \tag{E.4}$$

where $\boldsymbol{h_2} = \begin{pmatrix} 0 & 0 & 0 & 1 \end{pmatrix}$.

2) Both differential systems present decoupled dynamics. More precisely, the evolution of the pressure, temperature, and BGR is independent from the evolution of the state τ_{ai}. The reference first three components of the state (pressure, temperature and BGR) can thus be simply integrated in

$$\forall \theta \in [\overline{\theta}_{ivc}, \overline{\theta}_{soc}], \quad \begin{cases} \overline{P}(\theta) = \overline{P}_{ivc}\left(\dfrac{V(\overline{\theta}_{ivc})}{V(\theta)}\right)^{\gamma} \\ \overline{P}(\theta) = \overline{T}_{ivc}\left(\dfrac{V(\overline{\theta}_{ivc})}{V(\theta)}\right)^{\gamma-1} \\ \overline{X}(\theta) = \overline{X}_{ivc} \end{cases} \tag{E.5}$$

We do not integrate the last component of the state, because it will not be of any use in the following. The only thing to remark is that

$$\int_{\overline{\theta}_{inj}}^{\overline{\theta}_{soc}} A_{ai}(\overline{P}(\theta), \overline{T}(\theta), \overline{X}(\theta), M_f^{pilot})\frac{d\theta}{N_e} = 1 \tag{E.6}$$

3) We first compute the values of each of the variables used in the definition of $\boldsymbol{\Lambda}$, $\boldsymbol{b}$, $\boldsymbol{c}$, and $\boldsymbol{E}$ (see Equations (C.6) of §C.1.3).

- $\boldsymbol{G}$ and $\boldsymbol{h_2^x}$: From the definitions of the initial state of the first differential system, and of the transition equation, one simply has

$$\begin{aligned} \boldsymbol{G} &= \frac{\partial \boldsymbol{g}}{\partial \boldsymbol{p_{ivc}}}(\overline{\boldsymbol{p}}_{\boldsymbol{ivc}}) = \boldsymbol{G_0} \\ \boldsymbol{h_2^x} &= \frac{\partial h_2}{\partial \boldsymbol{x}}(\overline{\boldsymbol{x}}(\overline{\theta}_2)) = \boldsymbol{h_2} \end{aligned}$$

- the "$\boldsymbol{\Phi}$" variables: the adjoint equations corresponding to both systems are

$$\frac{d\boldsymbol{\gamma_0}}{d\theta} = -\boldsymbol{A_0}(\theta)^T\boldsymbol{\gamma_0} \quad , \quad \forall\theta \in [\overline{\theta}_{ivc}, \overline{\theta}_{inj}]$$
$$\frac{d\boldsymbol{\gamma_1}}{d\theta} = -\boldsymbol{A_1}(\theta)^T\boldsymbol{\gamma_1} \quad , \quad \forall\theta \in [\overline{\theta}_{inj}, \overline{\theta}_{soc}]$$

where

$$\boldsymbol{A_0}(\theta) = \begin{pmatrix} -\gamma\frac{dV(\theta)}{d\theta}\frac{1}{V(\theta)} & 0 & 0 & 0 \\ 0 & -(\gamma-1)\frac{dV(\theta)}{d\theta}\frac{1}{V(\theta)} & 0 & 0 \\ 0 & 0 & 0 & 0 \\ 0 & 0 & 0 & 0 \end{pmatrix}$$

and

$$\boldsymbol{A_1}(\theta) = \begin{pmatrix} -\gamma\frac{dV(\theta)}{d\theta}\frac{1}{V(\theta)} & 0 & 0 & 0 \\ 0 & -(\gamma-1)\frac{dV(\theta)}{d\theta}\frac{1}{V(\theta)} & 0 & 0 \\ 0 & 0 & 0 & 0 \\ \frac{1}{N_e}\frac{\partial A_{ai}}{\partial P}(\overline{P}(\theta), \overline{T}(\theta), \overline{X}(\theta), M_f^{pilot}) & \frac{1}{N_e}\frac{\partial A_{ai}}{\partial T} & \frac{1}{N_e}\frac{\partial A_{ai}}{\partial X} & 0 \end{pmatrix}$$

We integrate both equations to find their resolvents. Again, due to their particular form, integration can be carried out analytically:

$$\boldsymbol{\Phi_0}(\overline{\theta}_{ivc}, \overline{\theta}_{inj}) = \begin{pmatrix} \left(\frac{V(\overline{\theta}_{ivc})}{V(\overline{\theta}_{inj})}\right)^{\gamma} & 0 & 0 & 0 \\ 0 & \left(\frac{V(\overline{\theta}_{ivc})}{V(\overline{\theta}_{inj})}\right)^{\gamma-1} & 0 & 0 \\ 0 & 0 & 1 & 0 \\ 0 & 0 & 0 & 1 \end{pmatrix}$$

and

$$\boldsymbol{\Phi_1}(\overline{\theta}_{inj}, \overline{\theta}_{soc}) = \begin{pmatrix} \left(\frac{V(\overline{\theta}_{inj})}{V(\overline{\theta}_{soc})}\right)^{\gamma} & 0 & 0 & \Phi_1^{14} \\ 0 & \left(\frac{V(\overline{\theta}_{inj})}{V(\overline{\theta}_{soc})}\right)^{\gamma-1} & 0 & \Phi_1^{24} \\ 0 & 0 & 1 & \Phi_1^{34} \\ 0 & 0 & 0 & 1 \end{pmatrix}$$

where

$$\Phi_1^{14} = \int_{\overline{\theta}_{inj}}^{\overline{\theta}_{soc}} \frac{\partial A_{ai}}{\partial P}(\overline{P}(u), \overline{T}(u), \overline{X}(u), M_f^{pilot}) \left(\frac{V(\overline{\theta}_{inj})}{V(u)}\right)^{\gamma} \frac{du}{N_e}$$
$$\Phi_1^{24} = \int_{\overline{\theta}_{inj}}^{\overline{\theta}_{soc}} \frac{\partial A_{ai}}{\partial T}(\overline{P}(u), \overline{T}(u), \overline{X}(u), M_f^{pilot}) \left(\frac{V(\overline{\theta}_{inj})}{V(u)}\right)^{\gamma-1} \frac{du}{N_e}$$
$$\Phi_1^{34} = \int_{\overline{\theta}_{inj}}^{\overline{\theta}_{soc}} \frac{\partial A_{ai}}{\partial X}(\overline{P}(u), \overline{T}(u), \overline{X}(u), M_f^{pilot}) \frac{du}{N_e}$$

- Finally, the "$\boldsymbol{f}$" variables:

$$\boldsymbol{f_0^r} = \boldsymbol{f_0}(\overline{\boldsymbol{x}}(\overline{\theta}_0), \overline{\theta}_0) = \begin{pmatrix} -\gamma \overline{P}(\overline{\theta}_{ivc}) \dfrac{dV}{d\theta}(\overline{\theta}_{ivc}) \dfrac{1}{V(\overline{\theta}_{ivc})} \\ -(\gamma - 1)\overline{T}(\overline{\theta}_{ivc}) \dfrac{dV}{d\theta}(\overline{\theta}_{ivc}) \dfrac{1}{V(\overline{\theta}_{ivc})} \\ 0 \\ 0 \end{pmatrix}$$

$$\boldsymbol{f_1^l} = \boldsymbol{f_0}(\overline{\boldsymbol{x}}(\overline{\theta}_1), \overline{\theta}_1) = \begin{pmatrix} -\gamma \overline{P}(\overline{\theta}_{inj}) \dfrac{dV}{d\theta}(\overline{\theta}_{inj}) \dfrac{1}{V(\overline{\theta}_{inj})} \\ -(\gamma - 1)\overline{T}(\overline{\theta}_{inj}) \dfrac{dV}{d\theta}(\overline{\theta}_{inj}) \dfrac{1}{V(\overline{\theta}_{inj})} \\ 0 \\ 0 \end{pmatrix}$$

$$\boldsymbol{f_1^r} = \boldsymbol{f_1}(\overline{\boldsymbol{x}}(\overline{\theta}_1), \overline{\theta}_1) = \begin{pmatrix} -\gamma \overline{P}(\overline{\theta}_{inj}) \dfrac{dV}{d\theta}(\overline{\theta}_{inj}) \dfrac{1}{V(\overline{\theta}_{inj})} \\ -(\gamma - 1)\overline{T}(\overline{\theta}_{inj}) \dfrac{dV}{d\theta}(\overline{\theta}_{inj}) \dfrac{1}{V(\overline{\theta}_{inj})} \\ 0 \\ \dfrac{1}{N_e} A_{ai}(\overline{P}(\overline{\theta}_{inj}), \overline{T}(\overline{\theta}_{inj}), \overline{X}(\overline{\theta}_{inj}), M_f^{pilot}) \end{pmatrix}$$

$$\boldsymbol{f_2^l} = \boldsymbol{f_1}(\overline{\boldsymbol{x}}(\overline{\theta}_2), \overline{\theta}_2) = \begin{pmatrix} -\gamma \overline{P}(\overline{\theta}_{soc}) \dfrac{dV}{d\theta}(\overline{\theta}_{soc}) \dfrac{1}{V(\overline{\theta}_{soc})} \\ -(\gamma - 1)\overline{T}(\overline{\theta}_{soc}) \dfrac{dV}{d\theta}(\overline{\theta}_{soc}) \dfrac{1}{V(\overline{\theta}_{soc})} \\ 0 \\ \dfrac{1}{N_e} A_{ai}(\overline{P}(\overline{\theta}_{soc}), \overline{T}(\overline{\theta}_{soc}), \overline{X}(\overline{\theta}_{soc}), M_f^{pilot}) \end{pmatrix}$$

and

$$\Delta \boldsymbol{f_1} = \boldsymbol{f_1^l} - \boldsymbol{f_1^r} = \begin{pmatrix} 0 \\ 0 \\ 0 \\ -\dfrac{1}{N_e} A_{ai}(\overline{P}(\overline{\theta}_{inj}), \overline{T}(\overline{\theta}_{inj}), \overline{X}(\overline{\theta}_{inj}), M_f^{pilot}) \end{pmatrix}$$

From these variables, one can follow the definitions given in §C.1.3 to get matrices $\boldsymbol{\Lambda}$, $\boldsymbol{b}$, $\boldsymbol{c}$, and $\boldsymbol{E}$:

- $\boldsymbol{\Lambda}$:

$$\begin{aligned}\boldsymbol{\Lambda} &= \boldsymbol{h_2^x}\boldsymbol{\Phi_1}(\overline{\theta}_{inj},\overline{\theta}_{soc})^T\Delta\boldsymbol{f_1}\\ &= \begin{pmatrix}0 & 0 & 0 & 1\end{pmatrix}\begin{pmatrix}\left(\frac{V(\overline{\theta}_{ivc})}{V(\theta_{inj})}\right)^{\gamma} & 0 & 0 & 0\\ 0 & \left(\frac{V(\overline{\theta}_{ivc})}{V(\theta_{inj})}\right)^{\gamma-1} & 0 & 0\\ 0 & 0 & 1 & 0\\ \Phi_1^{14} & \Phi_1^{24} & \Phi_1^{34} & 1\end{pmatrix}\\ &\quad\begin{pmatrix}0\\0\\0\\\frac{1}{N_e}A_{ai}(\overline{P}(\overline{\theta}_{inj}),\overline{T}(\overline{\theta}_{inj}),\overline{X}(\overline{\theta}_{inj}),M_f^{pilot})\end{pmatrix}\\ &= \frac{1}{N_e}A_{ai}(\overline{P}(\overline{\theta}_{inj}),\overline{T}(\overline{\theta}_{inj}),\overline{X}(\overline{\theta}_{inj}),M_f^{pilot})\end{aligned}$$

- $\boldsymbol{E}$:

$$\boldsymbol{E} = \begin{pmatrix}0 & 1\\ E^{21} & 0\\ 0 & 0\end{pmatrix}$$

where

$$\begin{aligned}E^{21} &= -\boldsymbol{h_2^x}\boldsymbol{\Phi_1}^T\boldsymbol{\Phi_0}^T\boldsymbol{g}\\ &= -\begin{pmatrix}0 & 0 & 0 & 1\end{pmatrix}\boldsymbol{\Phi_1}^T\boldsymbol{\Phi_0}^T\begin{pmatrix}1 & 0 & 0\\ 0 & 1 & 0\\ 0 & 0 & 1\\ 0 & 0 & 0\end{pmatrix}\\ &= -\begin{pmatrix}\Phi_1^{14}\left(\frac{V(\overline{\theta}_{ivc})}{V(\overline{\theta}_{inj})}\right)^{\gamma} & \Phi_1^{24}\left(\frac{V(\overline{\theta}_{ivc})}{V(\overline{\theta}_{inj})}\right)^{\gamma-1} & \Phi_1^{34}\end{pmatrix}\\ &= -\begin{pmatrix}\int_{\overline{\theta}_{inj}}^{\overline{\theta}_{soc}}\frac{\partial A_{ai}}{\partial P}(\overline{P}(u),\overline{T}(u),\overline{X}(u),M_f^{pilot})\left(\frac{V(\overline{\theta}_{ivc})}{V(u)}\right)^{\gamma}\frac{du}{N_e}\\ \int_{\overline{\theta}_{inj}}^{\overline{\theta}_{soc}}\frac{\partial A_{ai}}{\partial T}(\overline{P}(u),\overline{T}(u),\overline{X}(u),M_f^{pilot})\left(\frac{V(\overline{\theta}_{ivc})}{V(u)}\right)^{\gamma-1}\frac{du}{N_e}\\ \int_{\overline{\theta}_{inj}}^{\overline{\theta}_{soc}}\frac{\partial A_{ai}}{\partial X}(\overline{P}(u),\overline{T}(u),\overline{X}(u),M_f^{pilot})\frac{du}{N_e}\end{pmatrix}^T\end{aligned}$$

- vectors $\boldsymbol{b}$ and $\boldsymbol{c}$: due to the particular form of the model, these vectors are of no use in the following, we do not get into their calculation.

4) Because the matrix $\boldsymbol{\Lambda}$ is a scalar, the matrix $\boldsymbol{\Xi}$ is invertible if and only if

$$A_{ai}(\overline{P}(\overline{\theta}_{inj}),\overline{T}(\overline{\theta}_{inj}),\overline{X}(\overline{\theta}_{inj}),M_f^{pilot}) \neq 0$$

5) The gain "α" is thus given by (see Equation (2.26))

$$\begin{aligned}\boldsymbol{\alpha}(P_{ivc},T_{ivc},X_{ivc}) &= \begin{pmatrix}0 & 1 & 0 & ... & 0\end{pmatrix}\cdot\boldsymbol{\Xi}^{-1}\boldsymbol{E}\\ &= \boldsymbol{\Lambda}^{-1}E^{21}\\ &= N_e\frac{\begin{pmatrix}\int_{\overline{\theta}_{inj}}^{\overline{\theta}_{soc}}\frac{\partial A_{ai}}{\partial P}(\overline{P}(u),\overline{T}(u),\overline{X}(u),M_f^{pilot})\left(\frac{V(\overline{\theta}_{ivc})}{V(u)}\right)^{\gamma}\frac{du}{N_e}\\ \int_{\overline{\theta}_{inj}}^{\overline{\theta}_{soc}}\frac{\partial A_{ai}}{\partial T}(\overline{P}(u),\overline{T}(u),\overline{X}(u),M_f^{pilot})\left(\frac{V(\overline{\theta}_{ivc})}{V(u)}\right)^{\gamma-1}\frac{du}{N_e}\\ \int_{\overline{\theta}_{inj}}^{\overline{\theta}_{soc}}\frac{\partial A_{ai}}{\partial X}(\overline{P}(u),\overline{T}(u),\overline{X}(u),M_f^{pilot})\frac{du}{N_e}\end{pmatrix}^T}{A_{ai}(\overline{P}(\overline{\theta}_{inj}),\overline{T}(\overline{\theta}_{inj}),\overline{X}(\overline{\theta}_{inj}),M_f^{pilot})}\end{aligned}$$

The particular form of A_{ai} (see Equation (4.3)) leads to

$$\begin{aligned}\frac{\partial A_{ai}}{\partial P}(P,T,X,M_f^{pilot}) &= n\frac{A_{ai}(P,T,X,M_f^{pilot})}{P}\\ \frac{\partial A_{ai}}{\partial T}(P,T,X,M_f^{pilot}) &= \frac{T_A}{T^2}A_{ai}(P,T,X,M_f^{pilot})\\ \frac{\partial A_{ai}}{\partial X}(P,T,X,M_f^{pilot}) &= -C\frac{A_{ai}(P,T,X,M_f^{pilot})}{1+CX}\end{aligned}\qquad\text{(E.7)}$$

one can further simplify the expression of "α" using Equations (E.5), (E.6) and (E.7)

$$\boldsymbol{\alpha}(P_{ivc},T_{ivc},X_{ivc}) = N_e\frac{\begin{pmatrix}\frac{n}{P_{ivc}} & T_A\int_{\overline{\theta}_{inj}}^{\overline{\theta}_{soc}}\frac{A_{ai}(\overline{P}(u),\overline{T}(u),\overline{X}(u),M_f^{pilot})}{\overline{T}(\theta)^2}\frac{du}{N_e} & -\frac{C}{1+CX_{ivc}}\end{pmatrix}}{A_{ai}(P_{ivc}\left(\frac{V_{ivc}}{V(\overline{\theta}_{inj})}\right)^{\gamma},T_{ivc}\left(\frac{V_{ivc}}{V(\overline{\theta}_{inj})}\right)^{\gamma-1},\overline{X}_{ivc},M_f^{pilot})}$$

This expression can be obtained in a more simple way exploiting the particular form of the model and the adiabatic assumption. The interested reader can refer to [31].

Appendix F

Publications

F.1 Conference paper

[24] M. Hillion, H. Buhlbuck, J. Chauvin, and N. Petit. Combustion control of diesel engines using injection timing. In *Proc. of the Society of Automotive Engineering World Congress*, number 2009-01-0367, 2009

[28] M. Hillion, J. Chauvin, O. Grondin, and N. Petit. Active combustion control of Diesel HCCI engine: Combustion timing. In *Proc. of the Society of Automotive Engineering World Congress*, number 2008-01-0984, 2008

[29] M. Hillion, J. Chauvin, and N. Petit. Controlling the start of combustion on an HCCI Diesel engine. In *Proc. of the American Control Conference*, 2008

[30] M. Hillion, J. Chauvin, and N. Petit. Open-loop combustion timing control of a spark-ignited engine. In *Proc. of the 47th IEEE Conference on Decision and Control*, 2008

[31] M. Hillion, J. Chauvin, and N. Petit. Combustion control of an HCCI diesel engine with cool flame phenomenon. In *Proc. of the European Conference on Control*, 2009

F.2 Journal contribution

[32] M. Hillion, J. Chauvin, and N. Petit. Combustion control in internal combustion engines. In *IEEE Control Sytem Technology*, (submitted, under review)

[33] M. Hillion, J. Chauvin, and N. Petit. Control of highly diluted combustion in diesel engines. In *Control Engineering Practice*, (submitted, under review)

F.3 Patents

[26] M. Hillion and J. Chauvin. Méthode de contrôle actif de la combustion d'un moteur à allumage par compression, Patent 08/06.058 (France Application Number), 2008

[25] M. Hillion and J. Chauvin. Méthode de contrôle actif de la combustion d'un moteur à allumage commandé, Patent 08/04.641 (France Application Number), 12/542.827 (US Application Number), 2008

[27] M. Hillion and J. Chauvin. Procédé de contrôle de combustion d'un moteur Diesel, Patent FR2915242 (France), WO/2008/142261 (World Extension), 2008

Bibliography

[1] F. Agrell, H.-E. Angström, B. Eriksson, J. Wikander, and J. Linderyd. Transient control of HCCI through combined intake and exhaust valve actuation. In *Proc. of the Society of Automotive Engineering World Congress*, number 2003-01-3172, 2003.

[2] A. Aldawood, S. Mosbach, and M. Kraft. HCCI combustion phasing transient control by hydrogen-rich gas: Insvestigation using a fast detailed-chemistry full-cycle model. In *Proc. of the Society of Automotive Engineering World Congress*, number 2009-01-1134, 2009.

[3] I. Andersson, T. McKelvey, and M. Thor. Evaluation of a closec loop spark advance controller based on a torque sensor. In *Proc. of the Society of Automotive Engineering World Congress*, number 2008-01-0987, 2008.

[4] P. Andersson. *Air Charge Estimation in Turbocharged Spark Ignition Engines*. PhD thesis, Linköpings Universitet, dec 2005.

[5] W. J. D. Annand and T. H. Ma. Instantaneous heat transfer rates to the cylinder head surface of a small compression ignition engine. In *Institution of Mechanical Engineering*, 1970-1971.

[6] C. Barba, C. Burkhardt, K. Boulouchos, and M. Bargende. A phenomenological combustion model for heat release rate prediction in high-speed DI Diesel engines with common rail injection. In *Proc. of the Society of Automotive Engineering World Congress*, number 2000-01-2933, 2000.

[7] D. Brand, C. H. Onder, and L. Guzzella. Estimation of the instantaneous in-cylinder pressure for control purposes using crankshaft angular velocity. In *Proc. of the Society of Automotive Engineering World Congress*, 2005.

[8] K. Chang, G. A. Lavoie, and A. Babajimopoulos. Control of a multi-cylinder HCCI engine during transient operation by modulating residual gas fraction to compensate for wall temperature effects. In *Proc. of the Society of Automotive Engineering World Congress*, number 2007-01-0204, 2007.

[9] J. Chauvin, G. Corde, and N. Petit. Transient control of a Diesel engine airpath. In *Proc. of American Control Conference*, 2007.

[10] C. J. Chiang, A. G. Stefanopoulou, and M. Jankovic. Nonlinear observer-based control of load transitions in Homogeneous Charge Compression Ignition engines. In *IEEE Transaction on Control System Technology*, volume 15, number 3, pages 438–448, 2007.

[11] F. G. Chmela and G. C. Orthaber. Rate of heat release prediction for direct injection Diesel engines based on purely mixing controlled conditions. In *Proc. of the Society of Automotive Engineering World Congress*, number 1999-01-0186, 1999.

[12] J. S. Citron, J. E. O'Higgins, and L. Y. Chen. Cylinder by cylinder engine pressure and pressure torque waveform determination utilizing speed fluctuations. In *Proc. of the Society of Automotive Engineering World Congress*, Technical paper 890486, 1989.

[13] J. Damitz, R. Fehrmann, M. Schueler, M. Kessler, M. Youssef, and V. Dautel. Method and device for contolling an internal combustion engine, US Patent, n°2006/008511901, 2006.

[14] C. F. Daniels, G. G. Zhu, and J. Winkelman. Inaudible knock and partial-burn detection using in-cylinder ionization signal. In *Proc. of the Society of Automotive Engineering World Congress*, number 2003-01-3149, 2003.

[15] L. Eriksson. Spark advance for optimal efficiency. In *Proc. of the Society of Automotive Engineering World Congress*, number 1999-01-0548, 1999.

[16] L. Eriksson, L. Nielsen, and M. Glavenius. Closed loop ignition control by ionization current interpretation. In *Proc. of the Society of Automotive Engineering World Congress*, volume 106, pages 1216–1223, 1997.

[17] European Parliament. `http://www.europarl.europa.eu/commonpositions/1999/pdf/c5-0028-99_en.pdf`.

[18] J. M. Frias, C. M. Aceves, D. Flowers, and J. R. Smith. HCCI engine control by thermal management. In *Proc. of the Society of Automotive Engineering World Congress*, number 2000-01-2869, 2000.

[19] L. Guzzella, M. Simons, and H. P. Geering. Feedback linearizing air/fuel-ratio controller. In *Control Eng. Practice*, volume 5, number 8, pages 1101–1105, 1997.

[20] J. K. Hale. *Ordinary Differential Equation*. Krieger Publish Compagny, 2nd edition, 1980.

[21] G. Haraldsson, P. Tunestål, B. Johansson, and J. Hyvonen. HCCI combustion phasing with closed-loop combustion control using variable compression

ratio in a multi cylinder engine. In *Proc. of the Society of Automotive Engineering World Congress*, number 2003-01-1830, 2003.

[22] G. Haraldsson, P. Tunestål, B. Johansson, and J. Hyvonen. HCCI closed-loop combustion control using fast thermal management. In *Proc. of the Society of Automotive Engineering World Congress*, number 2004-01-0943, 2004.

[23] J. Heywood. *Internal combustion engine fundamental*. Mc Graw-Hill, Inc, 1988.

[24] M. Hillion, H. Buhlbuck, J. Chauvin, and N. Petit. Combustion control of diesel engines using injection timing. In *Proc. of the Society of Automotive Engineering World Congress*, number 2009-01-0367, 2009.

[25] M. Hillion and J. Chauvin. Méthode de contrôle actif de la combustion d'un moteur à allumage commandé, Patent 08/04.641 (France Application Number), 12/542.827 (US Application Number), 2008.

[26] M. Hillion and J. Chauvin. Méthode de contrôle actif de la combustion d'un moteur à allumage par compression, Patent 08/06.058 (France Application Number), 2008.

[27] M. Hillion and J. Chauvin. Procédé de contrôle de combustion d'un moteur Diesel, Patent FR2915242 (France), WO/2008/142261 (World Extension), 2008.

[28] M. Hillion, J. Chauvin, O. Grondin, and N. Petit. Active combustion control of Diesel HCCI engine: Combustion timing. In *Proc. of the Society of Automotive Engineering World Congress*, number 2008-01-0984, 2008.

[29] M. Hillion, J. Chauvin, and N. Petit. Controlling the start of combustion on an HCCI Diesel engine. In *Proc. of the American Control Conference*, 2008.

[30] M. Hillion, J. Chauvin, and N. Petit. Open-loop combustion timing control of a spark-ignited engine. In *Proc. of the 47th IEEE Conference on Decision and Control*, 2008.

[31] M. Hillion, J. Chauvin, and N. Petit. Combustion control of an HCCI diesel engine with cool flame phenomenon. In *Proc. of the European Conference on Control*, 2009.

[32] M. Hillion, J. Chauvin, and N. Petit. Combustion control in internal combustion engines. In *IEEE Control Sytem Technology*, (submitted, under review).

[33] M. Hillion, J. Chauvin, and N. Petit. Control of highly diluted combustion in diesel engines. In *Control Engineering Practice*, (submitted, under review).

[34] P. Hochstrasser, C. Sauer, G. Esteghlal, J. Schlemann, G. Mallebrein, and E. Klein. Method, device and computer programme for controlling an internal combustion engine, US Patent n°01944758 A1, 2004.

[35] G. F. Hohenberg. Acdvanced approaches for heat transfer calculation. In *Society of Automotive Engineering*, number 790825, 1979.

[36] L. IMAGINE. `http://www.lmsintl.com/imagine`.

[37] M. Jankovic, F. Frischmuth, A. Stefanopoulou, and J. Cook. Torque management of engines with variable cam timing. In *Control Systems Magazine, IEEE*, volume 18, pages 34–42, 1998.

[38] M. Järgenstedt. *Detection of the start of combustion using knock sensor signals*. PhD thesis, Linköpings University, Vehicular Systems Dept. of Electrical Engineering, 2000.

[39] T. Kailath. *Linear systems*. Prentice-Hall, Inc., 1980.

[40] F.-A. Lafossas, O. Colin, F. L. Berr, and P. Menegazzi. Application of a new 1d combustion model to gasoline transient engine operation. In *Proc. of the Society of Automotive Engineering World Congress*, number 2005-01-2107, 2005.

[41] F.-A. Lafossas, M. Marbaix, and P. Menegazzi. Development and application of a 0D D.I. Diesel combustion model for emissions prediction. In *Proc. of the Society of Automotive Engineering World Congress*, number 2007-01-1841, 2007.

[42] F. Le Berr, M. Miche, G. Le Solliec, F.-A. Lafossas, and G. Colin. Modelling of a turbocharged SI engine with variable camshaft timing for engine control purposes. In *Proc. of the Society of Automotive Engineering World Congress*, number 2006-01-3264, 2006.

[43] B. Lecointe and G. Monnier. Downsizing a gasoline engine using turbocharging with direct injection. In *Proc. of the Society of Automotive Engineering World Congress*, number 2003-01-0542, 2003.

[44] O. Lepreux. *Model-based temperature control of a Diesel Oxidation Catalyst*. PhD thesis, MinesParisTech, 2009.

[45] T. Leroy, G. Alix, A. Duparchy, and F. Le Berr. Modeling fresh air charge and residual gas fraction on a dual independant variable valve timing SI engine. In *Proc. of the Society of Automotive Engineering World Congress*, number 2008-01-0983, 2008.

[46] T. Leroy, M. Bitauld, J. Chauvin, and N. Petit. In-cylinder Burned Gas Rate Estimation and Control on VVA Diesel Engines. In *Proc. of Society of Automotive Engineering Conference*, number 2009-01-0366, 2009.

[47] T. Leroy, J. Chauvin, and N. Petit. Controlling air and burned gas masses of turbocharged VVT SI engines. In *Proc. of Conference on Decision and Control*, 2008.

[48] T. Leroy, J. Chauvin, N. Petit, and G. Corde. Motion planning control of the airpath of a S.I. engine with valve timing actuators. In *Proc. of the* 5^{th} *IFAC symposium on Advances in Automotive Control*, 2007.

[49] J. Livengood and P. Wu. Correlation of auto-ignition phenomena in internal combustion engines and rapid compression machine. In *Fifth International Symposium on Combustion*, pages 347–356, 1955.

[50] S. Magand, E. Watel, M. Castagné, D. Soleri, O. Grondin, S. Devismes, and S. Moroz. Optimization of a low NOx emission HCCI Diesel prototype vehicle. In *Thiesel, Conference on Thermo- and Fluid Dynamic Processes in Diesel Engines*, 2008.

[51] M. Metghalchi and J. C. Keck. Burning velocities of mixture of air with methanol iso-octane and indolene at high pressure and temperature. In *Combust. Flame*, volume 48, pages 191–210, 1982.

[52] S. Nakayama, T. Ibuki, H. Hosaki, and H. Tominaga. An application to model based combustion control to transient cycle-by-cycle diesel combustion. In *Proc. of the Society of Automotive Engineering World Congress*, number 2008-01-1311, 2008.

[53] E. Nguyen, L. Duval, O. Grondin, and J. Antoni. Engine combustion indicators from block vibrations using bayesian inference. In *International Conference on Noise & Vibration Engineering*, 2008.

[54] J.-O. Olsson, P. Tunestål, and B. Johansson. Closed-loop control of an HCCI engine. In *Proc. of the Society of Automotive Engineering World Congress*, number 2001-01-1031, 2001.

[55] J. Popp and C. Rutland. Model-based feed-forward control of Diesel HCCI en transients. In *Proc. of the Society of Automotive Engineering World Congress*, number 2009-01-0599, 2009.

[56] D. J. Powell. Engine control using cylinder pressure: past, present, and future. In *Journal of Dynamic Systems, Measurement, and Control.*, volume 115, pages 343–350, 1993.

[57] N. Ravi, M. J. Roelle, A. F. Jungkunz, and J. C. Gerdes. Model based control of exhaust recompression HCCI. In *the Fifth IFAC Symposium on Advances in Automotive Control*, number AAC07-084, pages 295–310, 2007.

[58] B. Reveille, M. Miche, S. Jay, and S. Henriot. Contribution of 3D CFD tools to the development and understanding of Diesel engines: improving today's engines and designing tomorrow's power unit. In *Congrès le Diesel, Ecole Centrale Lyon.*, 2004.

[59] D. Schiefer, R. Maennel, and W. Nardoni. Advantages of Diesel engine control using in-cylinder pressure information for closed loop control. In *Proc. of the Society of Automotive Engineering World Congress*, number 2003-01-0364, 2003.

[60] L. Schwartz. *Calcul différentiel et équations différentielles*. 1997.

[61] M. C. Sellnau, F. A. Matekunas, P. A. Battiston, C.-F. Chang, and D. R. Lancaster. Cylinder pressure-based engine control using pressure ratio management and low cost non intrusive cylinder pressure sensor. In *Proc. of the Society of Automotive Engineering World Congress*, number 2000-01-0932, 2000.

[62] A. Stefanopoulou and I. Kolmanovsky. Analysis and control of transient torque response in engines with internal exhaust gas recirculation. *IEEE Transactions on Control Systems Technology*, 7(5):555–566, 1999.

[63] K. Swan, M. Shahbakhti, and C. R. Koch. Predicting start of combustion using a modified knock integral method for an HCCI engine. In *Proc. of the Society of Automotive Engineering World Congress*, number 2006-01-1086, 2006.

[64] A. Torregrosa, P. Olmeda, B. Degraeuwe, and M. Reyes. A concise wall temperature model for DI diesel engines. In *Journal of Applied Thermal Engineering*, number 26, pages 1320–1327, 2006.

[65] T.-C. Tseng and W. K. Cheng. An adaptive air/fuel ratio controller for SI engine throttle transients. In *Proc. of the Society of Automotive Engineering World Congress*, number 1999-01-0552, 1999.

[66] US Environmental Protection Agency. `http://www.epa.gov/OMS/sftp.htm`.

[67] M. J. Van Nieuwstadt, I. Kolmanovsky, P. Moraal, A. G. Stefanopoulou, and M. Jankovic. EGR-VGT control schemes: Experimental comparison for a high-speed Diesel engine. In *Control System Magazine*, volume 20, pages 63–79, june 2000.

[68] B. Walter and B. Gatellier. Near zero NOx emissions and high fuel efficiency Diesel engine: the NADI^{TM} concept using dual mode combustion. In *Oil and Gas Science and Technology*, volume 58, pages 101–114, 2003.

[69] A. Widd, K. Ekholm, P. Tunestål, and R. Johansson. Experimental evaluation of predictive combustion phasing control in an HCCI engine using fast thermal management and VVA. In *2009 IEEE Multi Conference on Systems and Control*, 2009.

[70] I. I. Wiebe. Brennverlauf und kreisprozessrechnung von verbrennungsmotoren. In *VEB Verlag Technik Berlin*, 1970.

[71] C. Wilhelmsson, A. Vressner, P. Tunestål, B. Johansson, G. Särner, and M. Aldèn. In chamber wall temperature measurement and modeling during transient HCCI operation. In *Proc. of the Society of Automotive Engineering World Congress*, number 2005-01-3731, 2005.

[72] G. Woschni. A universally applicable equation for the instantaneous heat transfer coefficient in the internal combustion engine. In *Society of Automotive Engineering*, number 670931, 1967.

[73] P. Yoon, S. Park, M. Sunwoo, I. Ohm, and K. J. Yoon. Closed-loop control of spark advance and air-fuel ratio in SI engines using cylinder pressure. In *Proc. of the Society of Automotive Engineering World Congress*, number 2000-01-0933, 2000.

[74] G. G. Zhu, C. F. Daniels, and J. Winkelman. MBT timing detection and its closed-loop control using in-cylinder pressure signal. In *Proc. of the Society of Automotive Engineering World Congress*, number 2003-01-3266, 2003.